THERMAL MANAGEMENT OF BATTERIES

FOR

ELECTRIC AND HYBRID VEHICLES

THESIS SUBMITTED IN PARTIAL FULFILMENTS OF THE REQUIREMENT FOR THE DEGREE OF MASTER OF ENGINEERING IN AUTOMOBILE ENGINEERING UNDER FACULTY OF ENGINEERING AND TECHNOLOGY

Submitted by

DIPANKAR PAUL

Class Roll Number: 002111204001

Registration Number: 160296 of 202-22

Examination Roll Number: M4AUT23006

Academic Session: 2021-2023

Under the guidance of

Prof. Achintya Mukhopadhyay

And

Dr. Sourav Sarkar

Department of Mechanical Engineering

Jadavpur University

188, Raja S.C. Mullick Road,

Kolkata – 700032

DECLARATION OF ORIGINALITY AND COMPLIANCE OF ACADEMIC ETHICS

I hereby declare that the thesis entitled "**THERMAL MANAGEMENT OF BATTERIES FOR ELECTRIC AND HYBRID VAHICLES**" contains literature survey and original research work by the undersigned candidate, as a part of his *MASTER OF ENGINEERING IN AUTOMOBILE ENGINEERING under the DEPARTMENT OF MECHANICAL ENGINNERING*, studies during academic session 2020-2022.

All information in this document have been obtained and presented in accordance with the academic rules and ethical conduct.

I also declare that, as required by these rules of conduct, I have fully cited and referenced all the material and results that are not original to this work.

Name: **DIPANKAR PAUL**

Class Roll Number: **002111204001**

University Registration No: **160296 of 2021-22**

Examination Roll No: **M4AUT23006**

Date:

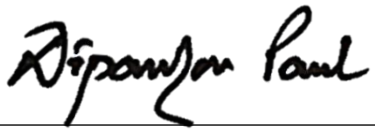

Signature of Candidate

FACULTY OF ENGINEERING & TECHNOLOGY

DEPARTMENT OF MECHANICAL ENGINEERING

JADAVPUR UNIVERSITY

KOLKATA

CERTIFICATE OF RECOMMENDATION

This is to certify that the thesis entitled "**THERMAL MANAGEMENT OF BATTERIES FOR ELECTRIC AND HYBRID VEHICLES**" is a bonafide work carried out by DIPANKAR PAUL under our supervision and guidance in partial fulfilment of the requirements for awarding the degree of Master of Engineering in Automobile Engineering under Department of Mechanical Engineering, Jadavpur University during the academic session 2021-2023.

THESIS SUPERVISOR
Prof. Achintya Mukhopadhyay
Department of Mechanical Engineering
Jadavpur University, Kolkata

THESIS SUPERVISOR
Dr. Sourav Sarkar
Department of Mechanical Engineering
Jadavpur University, Kolkata

Prof. Saswati Mazumdar
Dean
Faculty of Engineering and Technology
Jadavpur University, Kolkata

Prof. Amit Karmakar
Head of the department
Department of Mechanical Engineering
Jadavpur University, Kolkata

FACULTY OF ENGINEERING & TECHNOLOGY

DEPARTMENT OF MECHANICAL ENGINEERING

JADAVPUR UNIVERSITY

KOLKATA

CERTIFICATE OF APPROVAL

The foregoing thesis, entitled "**THEMAL MANAGEMENT OF BATTERIES FOR ELECTRIC AND HYBRID VEHICELS**" is hereby approved as a creditable study in the area of Automobile Engineering carried out and presented by DIPANKAR PAUL in a satisfactory manner to warrant its acceptance as a prerequisite to the degree for which it has been submitted. It is notified to be understood that by this approval, the undersigned do not necessarily endorse or approve any statement made, opinion expressed and conclusion drawn therein but approve the thesis only for the purpose for which it has been submitted.

Committee of final evaluation of thesis:

_____

_____

_____

ACKNOWLEDGEMENT

I am very thankful to my respected thesis supervisor **Prof. Achintya Mukhopadhyay**, Professor, and **Dr. Sourav Sarkar,** Assistant Professor, Department of Mechanical Engineering, Jadavpur University for his excellent and resourceful guidance, which helped me a lot in the completion of this thesis. Without their supervision and constant encouragement, it would not be possible to prepare such a thesis compactly. I do convey my best regards and gratitude to them.

The regular discussions and idea-sharing with my thesis supervisors really helped me to improve my knowledge day by day in my research related problems. They were always available for me for any query, whether it was a telephonic or a face to face discussion. Their appreciation and encouragement in this project work really helped me to realize my aspirations towards research work. They were the key persons in my project work and their guidance, supervision as well as providing necessary information in completing my master's thesis is immense.

I am highly indebted to all my professors, their guidance and supervision as well as for providing necessary information regarding thesis and also for their support in completing my master's thesis.

I would like to thank **Mr Saumendra Nath Mishra** PhD scholars, for giving me valuable suggestions and allowing me to access their systems whenever needed.

I would like to express my gratitude towards my parents and my younger brother for their kind cooperation and encouragement which helped me in the completion of my master's thesis.

Finally, my thanks and appreciations also go to my dear friends in developing my master's project and people who have willingly helped me out with their abilities.

DIPANKAR PAUL

M.E ("Automobile Engineering")

2nd Year, Final Semester

Department of Mechanical Engineering

Jadavpur University, Kolkata

TABLE OF CONTENTS

3. Numerical modelling

Nomenclature

LIB	Lithium-Ion battery
BTMS	Battery Thermal Management System
TR	Thermal Runaway
EV	Electric Vehicles
PCM	Phase Change Material
Li	Lithium
IC	Internal combustion
1-D	One dimensional
2-D	Two Dimensional
3-D	Three Dimensional
$LiCoO_2$	Lithium Cobalt Oxide
CoO_2	Cobalt Oxide
SEI	Solid Electrolyte Interface
CFD	Computational Fluid Dynamics
SoC	State of Charge
ISC	Internal Short Circuit
UDF	User Defined Function
v	Volume
ρ	Density
C_p	Specific heat
T	Temperature
K	Thermal Conductivity
A_{mush}	Mushy Zone Parameter

T_l	Liquidus Temperature
T_s	Solidus Temperature
T_m	Melting Temperature
μ	Dynamic Viscosity
β	Liquid fraction
L_f	Latent heat of fusion
ne	Negative electrode
pe	Positive electrode
t	time
α	Degree of conversion at positive electrode
ISCD	Internal Short Circuit Device
h	Heat transfer coefficient
ε	Emissivity
Q_{heater}	Heat from heater
x	Concentration of Species
x_0	Initial Concentration
A	Frequency Factor
E	Activation energy
Kb	Boltzmann Constant
m	Mass of material at electrode
H	Enthalpy
jr	Jelly roll
V	Voltage
C	Ampere hour
Q_{flux}	Heat flux

List of Figures

List of Tables

Chapter 1

1. Introduction

The Internal Combustion (IC) Engine has been at the forefront of the automotive industry from the very beginning. The primary source of energy for such engines comes from fossil fuels such as gasoline and diesel fuel. The passage of time brings with it a rise in the use of those fossil fuels on a day-to-day basis. We are already aware that the amount of fossil fuels that may be reserved is finite and continues to decrease on a daily basis. The fact that we will have a harder time extracting these fossil fuels is perhaps the most significant aspect. As a direct result of the combustion of fossil fuels, the quality of the air continues to deteriorate, and the surrounding environment will ultimately become contaminated. There are a variety of dangers to our health that we must face. Because of this, we are rapidly approaching the realization that the next generation of automobiles should be electric vehicles (EVs). It is capable of overcoming the limitations of internal combustion engines. Aside from the fact that electric vehicles are better for the environment, they also have other benefits, such as a more pleasurable driving experience, cheaper maintenance costs, better gas mileage, and lower overall costs of operation. Electric vehicles come in a variety of forms, including Plug-in Hybrid Electric Vehicles (PHEVs), Hybrid Electric Vehicles (HEVs), and Battery Electric Vehicles (BEVs), amongst others.

Battery electric vehicles are a well-known kind of the electric vehicles that are now available. The lithium-ion battery, often known as a LIB, is the primary source of power in BEVs. The battery pack is made up of several separate battery cells, each of which may be thought of as a chemical energy storage device for the device's electrical energy. The battery pack of an electric car is the source of the energy that is required to power the electric motor and other electrical components of the vehicle. An electric motor that functions according to the concept of electromagnetic induction is referred to as an induction motor. This kind of motor is also referred to as an asynchronous motor. It takes the vehicle's electrical energy and transforms it into the mechanical energy needed

to turn the wheels. Because of their dependability and high level of efficiency, induction motors are often used in electric cars. In order to get the induction motor to work, the DC output power of the battery pack is converted into AC power by the inverter. The ability of electric cars to adjust the driving wheel speed by changing frequency is the primary benefit that electric vehicles have over internal combustion engines. Internal combustion engines can only create torque and power out within a restricted speed range. On the other hand, the power-to-weight ratio of an induction motor is much greater.

At the current time, lithium-ion batteries are recognized as one of the most powerful batteries that also serve as an appealing energy storage technology. The energy density is high, the specific power is high, the self-discharge rates are low, the recyclability is high, the cycle life is outstanding, there is no mercy effect, and the weight is low. Because of this, nickel-cadmium (Ni-Cd) and nickel-metal hydride (Ni-MH) batteries are being phased out in favour of lead-acid, nickel-cadmium, and nickel-metal hydride batteries in electric vehicles. The impact of the rising temperature on the LIBs' operations is an essential problem that we need to concentrate on. Managing the increase in temperature, also known as thermal management, is an essential part of keeping lithium-ion batteries (LIBs) safe, maximizing their performance, and extending their lifespan. Internal resistance, chemical interactions, and other variables may contribute to the production of heat by LIBs when they are being charged, discharged, or even while they are being stored. An excessive amount of heat may result in a decline in performance, a shortening of the cycle life, and even potential safety issues like thermal runaway or fires. Because of these factors, the thermal stability of these batteries must always be maintained, even being subjected to a variety of abuses like as being exposed to heat, having an external short circuit, having a nail penetrate them, or being crushed. Because of this, a good battery thermal management system (BTMS) has to be created in order to safeguard the batteries from the dangerous increase in temperature. If this is not done, it may result in Thermal Runaway (TR), which poses a risk of explosion as well as a potential fire hazard. Thermal runaway, also known as TR, is a process in which there is an uncontrolled and self-sustaining rise in temperature even higher. When there is a circumstance in which the quantity of heat generated

within the battery is greater than the amount of heat dissipated to its surroundings, then thermal runaway (TR) occurs.

There are two basic variations of BTMS that may be distinguished from one another. The first kind of system is active systems, while the second type is passive systems. In active systems, the temperature of the battery is controlled by an external mechanism that involves the forced circulation of a certain coolant. This coolant might be air or water. On the other hand, a passive system is one that does not utilize any external components, such as heat pipes, hydrogels, or phase change materials (PCM), in order to transmit heat. As a result, this kind of system does not spend any energy, which leads to an increase in the vehicle's overall net efficiency.

Maintain the LIB's ideal working temperature between 20-50º C, with a maximum battery pack temperature change of 5º C. Battery pack temperature exceeds the safety limit of 60º C while running continuously. Above 50º C, battery longevity is under danger, and even a single cell's early degradation may impact performance and efficiency. BTMS's main goal is to manage battery cell temperature to improve battery life.

In order to have a better grasp on the process of TR, we will begin by investigating the chemistry behind LIB. In the chemistry portion of LIB, we are going to take a cursory look at the many different components of LIB in order to get an understanding of how it operates, including charging and discharging.

1.1 Battery overview

Batteries are devices that, via a process called electrolysis, turn the chemical energy that has been stored into electrical energy, and vice versa. Secondary batteries are so named because of the reversible nature of the electrode, which allows the battery to be recharged several times. The lead-acetate battery, the lithium-ion battery, the nickel-metal hydride battery, the nickel-cadmium battery, and many more are examples of popular secondary battery types. Electrochemical potential is a fascinating notion that is connected to metals, and it is the basis for how Lib's work. The propensity of a metal to give off electrons is referred to as its electrochemical potential. According to the electrochemical series, Li has the greatest propensity out of all the elements to lose electrons; as a result, Li is an excellent conductor of both heat and electricity

The LIB consists of an anode (the negative electrode), a cathode (the positive electrode), an electrolyte, and a separator. The purpose of the separator is to prevent the anode and cathode from coming into contact with one another. Electrodes are composed of current collectors as well as active material. The active material is adhered to the current collector in this configuration. The Red-ox process requires the presence of active material, and the current collector acts as the electron conducting medium in this reaction. Copper is used as a current collector at the anode, while Aluminium is utilized at the cathode of the battery. It is necessary to make use of binders in order to adhere the active material to the current collectors.

The majority of the active material that is used at the cathode is metal oxide, which creates a habitat for the lithium ions. Li-ions are inserted into the spaces in between the stratified structures of the metal oxides, which are known as the interstitial sites. In order to be suitable for use as a cathode, metal oxides should have a high capacity for storing lithium, a high thermal conductivity, and a high diffusivity. The capacity of the battery as well as its average voltage are both determined by the cathode. If there is a significant quantity of Li-ion intercalated in the cathode, then there will also be a significant amount of potential difference between the anode and the cathode. Because of this, the capacity of the battery as well as its average voltage will both be high. The nomenclature given to the different LIBs is determined by the types of metal oxides that

are used at the cathode. For instance, in lithium cobalt oxide ($LiCoO_2$) batteries (also known as Li-Cobalt batteries), lithium ions are intercalated in between the layers of cobalt oxide (CoO_2). Similar to this, some additional varieties of LIBs include $LiFePO_4$ (Li-Iron Phosphate), $LiMn_2O_4$ (Li-Manganese Oxide), $LiNiMnCoO_2$ (Li-Nickel Manganese Cobalt Oxide), $LiNiCoAlO_2$ (Li-Nickel Cobalt Aluminium Oxide), $Li_4Ti_5O_{12}$ (Li-Titanate), etc.

At the anode, active material is likewise used, just as it is at the cathode. Graphite is the active substance that is used at the anode in the majority of instances. Graphite is characterized by having a layered structure. Because these layers are very weakly connected to one another, it is relatively simple for the Li+ ions to be stored or intercalated between them. Because of its excellent thermal and electrical conductivity as well as its low electrochemical reactivity, graphite is often utilized as the active material in an anode.

The electrolyte is a solution that is based on lithium salts and functions as a medium for the transport of lithium ions between the cathode and the anode. In order to generate electricity, it is necessary for the electrons and the lithium ions to go in separate directions. An electrolyte is a chemical that does not allow electrons to travel through it but does allow Li+ ions to pass through it. As a result, the movement of electrons across the external circuit results in the production of electricity. A good electrolyte will have desirable chemical and electrochemical stability, a high capacity for transporting lithium ions, superior electronic insulating performance, and other desirable characteristics. Some examples of materials that are utilized as electrolytes are $LiPF_6$, $LiClO_4$, $LiAsF_6$, and others.

An insulating layer termed a separator is put between the anode and the cathode to prevent a short circuit from occurring as a result of temperature increase. Due to the tiny porosity of the separator, Li-ions may easily pass through it. The LIB is susceptible to TR if the temperature goes over a certain point, at which point the electrolyte may melt away. As such, the separator serves as a protective partition. Commercially, polypropylene (PP) and polyethylene (PE) are often employed as separators.

If the electrons come into touch with the electrolyte, the electrolyte's quality will deteriorate. However, as a result of the solid electrolyte interface (SEI), the electrons are prevented from ever making physical contact with the electrolyte. During the first time that we charge the cell, the Li-ions will travel through the electrolyte. As they do so, the solvent molecules that are present in the electrolyte will cover the Li-ions. When they get to the graphite layer, the Li-ions combine with the molecules of the solvent to produce a layer that is referred to as the SEI layer. The development of this SEI layer turned out to be a fortunate event in disguise. It prevents any direct contact between the electrons and the electrolyte, which stops any deterioration of the electrolyte that may otherwise occur. The development of the SEI layer uses up 5% of the lithium, while the remaining 95% of the lithium is contributed to the primary operation of the battery. Because the SEI layer permanently consumes both Li and the electrolyte, this results in a reduction in the total amount of Li, which in turn results in a reduction in the maximum capacity of our battery.

1.2 Working of LIB

If the electrons come into contact with the electrolyte, the quality of the electrolyte will suffer as a result. On the other hand, because of something called the solid electrolyte interface (SEI), the electrons are never allowed to come into direct physical contact with the electrolyte. When we charge the cell for the first time, the lithium ions will move through the electrolyte as they are being added. As a result of this process, the molecules of the solvent that are present in the electrolyte will cover the ions of lithium that are there. When the Li-ions reach the graphite layer, they interact with the molecules of the solvent to form a layer that is known as the SEI layer. This layer is produced when the Li-ions reach the graphite layer. It turned out that a misfortune was really a blessing in disguise when this SEI layer was developed. It prevents any direct contact between the electrons and the electrolyte, which inhibits any degradation of the electrolyte that would otherwise occur as a result of the potential for direct contact between the electrons and the electrolyte. The formation of the SEI layer consumes 5% of the lithium, while the principal functioning of the battery makes use of the remaining 95%

of the lithium. Because the SEI layer perpetually consumes both Li and the electrolyte, this leads in a drop in the overall quantity of Li, which in turn results in a reduction in the maximum capacity of our battery. This is a consequence of the fact that the SEI layer continuously consumes both.

1.2.1 Charging of LIB

When we charge the battery by connecting our power source to the metal oxide section (cathode), a greater force is applied to the flow of electrons. The positive side of the power source will, of course, attract and remove electrons from the Li-ions contained in the metal oxide. In the case of a LiCoO2 battery, the cobalt atoms are left in a state with a charge of +4 after their electrons are extracted. Since these electrons are unable to go through the electrolyte and reach the graphite layer, they are forced to travel via the external circuit instead. Meanwhile, positively charged Li-ions will be drawn to the negative terminal. They will then flow through the electrolyte back to the graphite layers, where they will get trapped due to the presence of the graphite layers. When all of the Li-ions have arrived to the graphite sheet, the cell will have reached its maximum charge.

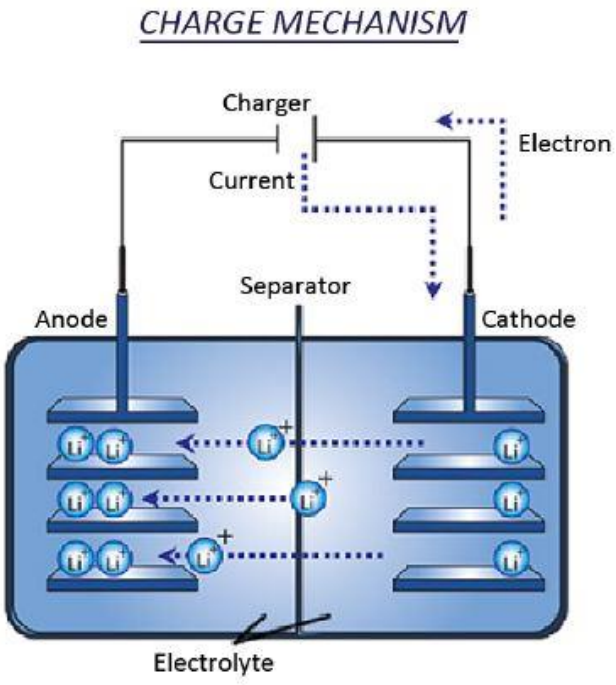

The steps involved in this procedure are shown in **Fig. 1**.

Figure 1: Charging of LIB

Various electrochemical reactions that take place while operation of LIB at the cathode and anode during charging**:**

During Charging

At cathode: $LiCoO_2 \rightarrow xLi^+ + Li_{1-x}CoO_2 + e^-$

At anode: $xLi^+ + e^- + 6C \rightarrow Li_xC_6$

Overall equation: $LiCoO_2 + 6C \rightarrow Li_{1-x}CoO_2 + Li_xC_6$

This whole thing was about the mechanics and chemistry that went into the functioning of LIB. Next, we will investigate the TR component, which is a significant source of concern for LIBs, as well as the factors that contribute to its development.

1.2.2 Discharging Of LIB

When the process of charging the battery is complete, it enters a condition that is unstable. After the power source is turned off and the load is connected, the lithium ions will attempt to revert to their stable condition as a component of the metal oxide. Because of this propensity, the lithium ions flow through the electrolyte and the load to the cobalt side, which wants to gain back in electrons. This occurs when the electrons pass through the load. Because electrons are moving about in the external circuit, we experience a flow of electrical current. It is versatile and may be put to a number of different uses. When lithium ions go to the cobalt side, they once again wedge themselves and intercalate with the cobalt and oxygen to form

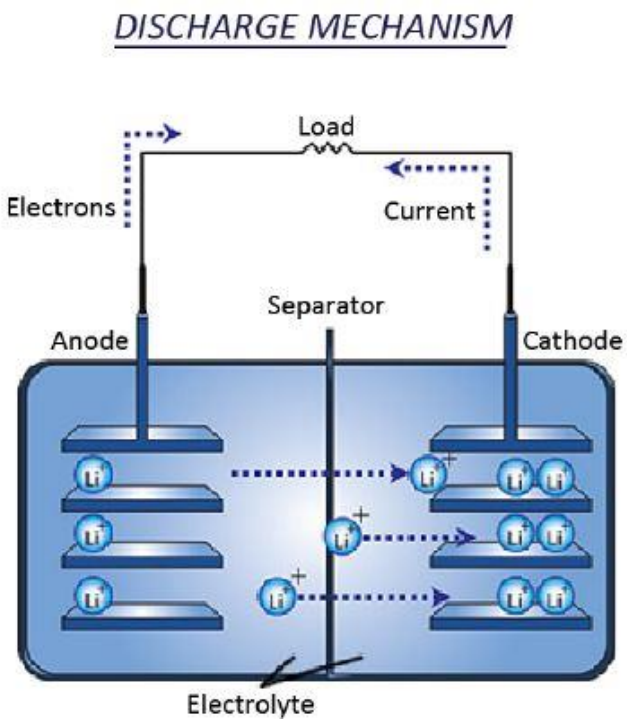

Figure 2: Discharging of LIB

LiCoO2, which is a stable compound. The steps involved in this procedure are shown in **Fig 2**.

Various electrochemical reactions that take place while operation of LIB at the cathode and anode during discharging:

During Discharging

At cathode: $xLi^+ + Li_{1-x}CoO_2 + e^- \rightarrow LiCoO_2$

At anode: $Li_xC_6 \rightarrow xLi^+ + e^- + 6C$

Overall equation: $Li_{1-x}CoO_2 + Li_xC_6 \rightarrow LiCoO_2 + 6C$

At the cathode, the reduction reaction takes place. At that location, cobalt oxide (CoO_2) interacts with lithium ions to generate lithium cobalt oxide ($LiCoO_2$). The process of oxidation takes place at the anode. At that location, graphite and Li-ions are formed from the intercalated graphite and Li combination LiC_6.

1.3 Thermal Runaway of Lithium-ion Battery

The TR is a significant contributor to the downfall of LIB. It all begins when one of them of the batteries develops a condition indicative of abusive battery use. These threatening situations could be of the electrical, thermal, or mechanical variety. When a battery is overcharged or over discharged, it is considered to be abusive to the electrical system. A high C-rate is another possible cause of this condition. The both the charging and discharging rates of a battery are both controlled by the C-rate. The C-rate is a measurement that determines how quickly a battery depletes itself in comparison to its full capacity. Thermal abuse happens when the battery reaches an unsafe temperature, while mechanical abuse happens when the vehicle is involved in a collision

or other type of mishap. Because of all of these factors, the battery goes through the TR process.

The thermal runaway starts off with an individual cell of the battery overheating and bursting into flame, which then gradually spreads to the other cells of the battery and consumes the entire battery pack. This process is known as thermal propagation. In general, an electric vehicle's battery pack will consist of more than one of battery modules, and each of these modules will have a large number of cells that are packed into a relatively compact area. Heat is produced inside the battery as a result of a number of exothermic chemical reactions that take place within the battery as well as resistance heating, also known as Joule heating. This heat is contained within the battery and is unable to escape the battery pack. If there is no way for the battery pack's heat to be removed from the battery pack using an external means, the battery pack will generate heat and remain to get warmer which will result in the battery losing its rated capacity. As a result, the state of degeneration of the battery becomes increasingly severe. Therefore, the use of external cooling is absolutely necessary in order to keep the batteries within the temperature range that is optimal for their performance.

The process starts off with an initial stage of consistent heating. In the event that the temperature within the LIB reaches 80-90°C, the exothermic degradation of the SEI layer will start. The LIB then transitions from a stage in which it is being heated continuously to a one in which it is heating itself. At this point, potentially hazardous substances including carbon monoxide and carbon dioxide are released. If monitoring is not paid during this stage, the temperature will continue to rise. Due to the fact that the SEI layer has broken down, the electrolyte is now in touch with the anode. This causes the reaction between the electrolyte and the lithiated graphite surface to take place, which in turn causes the reaction at the anode to speed up. When temperatures approach roughly 1300 degrees Celsius, the separator begins to contract. It causes a short circuit to form between the electrodes, which in turn initiates a reaction that is more intense between the metal oxide at the cathode and the electrolyte. As a consequence of this, oxygen is liberated, which further catalyses the reaction, so turning

the process into an exothermic one. All of these activities happen at the same time, which results in the emission of a significant amount of heat and gases. Because of these factors, the heat and fumes that are emitted start the combustion process and cause the LIB pack to catch fire. This puts people in potentially dangerous circumstances. The TR of LIB describes this kind of occurrence. **Figure 3** illustrates this particular stage of the TR process.

Therefore, the use of an external cooling system is required in order to keep the temperature of the battery pack within the appropriate range so that an electric vehicle can be driven safely and effectively. If this happens, the LIB pack will be able to maintain its safe condition since the rate of internal heat creation and the rate of heat loss to ambient will be equalized. In order to alleviate the thermal issues, an appropriate BTMS needs to be created to keep the temperature of the battery pack as well as the temperature of the cells within the optimal range.

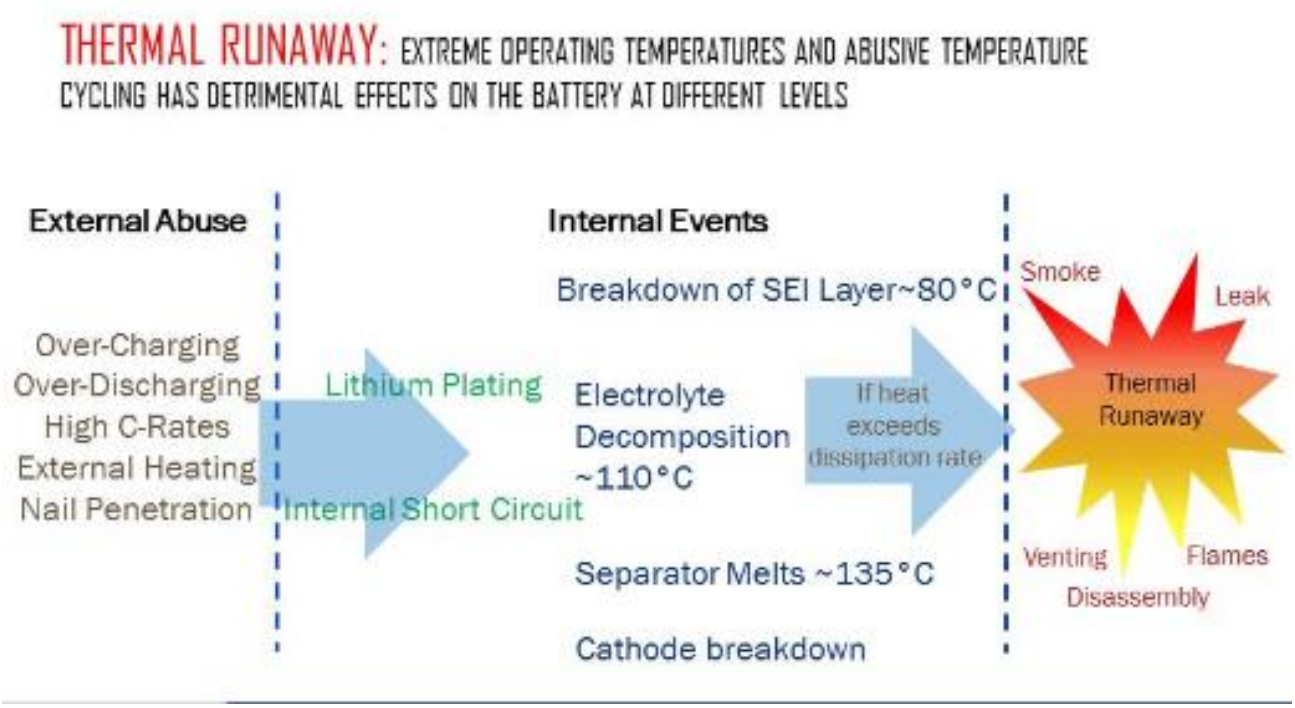

Figure 3: Representation of occurrence of TR in LIB

Chapter 2

2. Literature review and objective

2.1 Literature Review on Battery modelling

A prediction model for oven exposed testing was created by Hatchard et al. [1] by considering the thermal characteristics of the cells and the reaction kinetics for the materials used in the electrodes while the electrolyte was exposed to high temperatures. Before regulatory organizations will give LIBs the green light to be on the market, they need to demonstrate that they can withstand the heat of an oven. This model can predict how materials for electrodes and new battery capacities will respond to oven expose testing without having to actually create any cells. In addition to this, it would make it possible to test brand novel electrolytes as well as additives. Nevertheless, the ratio of electrolyte to electrode material is something that must be carefully observed and monitored. The model can be utilized to anticipate the outcomes of a number of different scenarios, including moving to a cathode with a higher reactive potential, altering the surface area of the carbon anode, and using different labels.

Kim et al. [2] have expanded the one-dimensional formulation that was created by hatchard et al. [1] to three dimensions (3-D). This model was constructed so that the geometrical considerations, which are extremely important for the big cells that are utilized in automotive applications, could be taken into account. The three-dimensional in nature model, which is used to simulate oven tests and determine how a local hot spot can expand across the cell, captures the form and dimensions of the cell components in addition to the geographic distribution of temperatures and materials. This model is used to determine how a local hot spot may expand across the cell. When comparing the lumped model to the oven mistreatment simulation experimentation of cells with a CoO_2 cathode, graphite anode, and conventional $LiPF_6$ electrolyte, the 3-D model forecasts that the TR will happen sooner or later based on the size of the cell. However, the timing of the TR is dependent on the lumped model. According to the findings of

this research, tiny cells are able to rid themselves of heat more quickly than larger cells. Consequently, the utilization of tiny cells is preferable for the prevention of TR under the same abusive conditions. According to the findings of this study, the first spread of hot spots within big cells occurs in both the longitudinally and azimuthal directions.

An 18650 LCO/Graphite cell using a Dimethyl Carbonate (DMC) electrolyte can have its gas production and temperature-pressure behaviour predicted by a mathematical model developed by Coman et al. [3]. The analysis was performed at intervals that were somewhat near to the venting event, and a cell was modelled utilizing the heating conditions of an oven. Establishing the balance of energy for a controlling volume with unsteady flow and making use of an isentropic process flow equations that connect to gas venting were both necessary steps in the process of developing the model. The results reveal that when there is no gas generation occurring within, the model fails to anticipate the pressure in the same way that it is observed experimentally. When the gas generation that is caused by pre-venting processes is factored into the model, it is able to replicate the pressure profile that is observed when the real measurements are carried out.

In this piece of study conducted by Parekh et al. [4], a mathematical model is used to make predictions regarding temporary temperature and voltage distributions of 18650 cylindrical LIBs at a variety of discharge rates. In order to offer quantitative data regarding the thermal behaviour of LIBs, the 18650 cylindrical LIBs are tested within the lab using air-cooling. This is done in order to ensure that the results are accurate. On the surface of the battery were installed four thermocouples, which were then subjected to one of four uniform current discharge rates: **1C**, **2C**, **3C**, and **4C**. The highest temperature that can be modelled is 46.86 degrees Celsius, and it occurs at a discharge rate of **4C**. The data also show that greater C-rates cause an increase in the outside temperature of the surface of the main part of the battery.

The internal short circuit (ISC) device that was implanted in Li-ion battery cells was utilized in the research paper that was written by Coman and his colleagues [5]. This is a novel approach to analyzing Thermal Runaway in those cells. The Arrhenius formulations are used to represent both the self-warming chemical processes and the

State of Charge (SoC) in the model. A local short circuit is caused by a short circuit in the internal device in the battery windings (jelly roll), and this is something that is modelled and accounted for in the model. During the process of modelling the short circuit, the total quantity of electric power that is available has an efficiency factor that is added to it to account for the conversion of electrical power into thermal energy. The efficiency factor takes into account the amount of energy that is released by the cell. It was determined that the amount of energy that flows out by a battery cell that has an ISCD is nearly comparable to the amount of energy that is sent out by a battery cell that undergoes TR as a consequence of overheating. They found that TR is responsible for releasing 28% of the 2.4 Ah of electrical energy produced by the 18650.

2.2 Literature Review on Thermal-Runaway

This work by Lopez et al. [6] focuses on testing demonstration as well as analysis of different LIB module combinations in order to characterize the thermal behaviour and provide safe methods. This was done in order to fulfil both of those goals. During the abuse test's heat-to-vent setting, one of the cells in a module will enter TR as a result of being heated by a heating source. The mechanism that underlies the spread of thermal runaway from one cell to the next has been identified. According to the findings, a significant reduction in the chance of TR spread in a module consisting of cylindrical cells can be achieved by increasing the space between the cells. Additionally, it lowers the temperatures of the cells, stops the loss of voltage in the cells, and mitigates the damage done to the cells in the surrounding area. Given these findings, it is recommended that precautions be taken to lessen the possibility of TR spread and module damage. In addition, the testing found that branching tabs, as opposed to serpentine tabs, are superior in terms of their ability to optimize the voltage retention and safety of the modules. This is because branching tabs are able to better electrically isolate the shorted trigger cell from the remainder of the module. In conclusion, the chance of TR propagation should be lowered by employing a variety of strategies, which vary according to the type of cell and the configuration of the module(s).

A method for the early identification of LIB TR that is based on gas sensing is described in Cai et al. [7]. By detecting levels of CO_2, which are produced at the very start of battery TR, it is possible to identify failing cells in their early stages before they completely fail. The simulation reveals that the reply time for sensing gases is substantially faster as compared to the conventional method of sensing the surface temperature. In contrary to the outside temperature measurement strategy, which is unable to recognize TR in its early stages when it spreads to neighbouring cells, the gas detecting approach can accurately forecast the occurrence of the event before it becomes a TR. The findings suggest that after neighbouring cells will initiate a TR, and this window of time is recognized as the critical window for TR propagation. Early detection carried out prior to the critical period of TR propagation is necessary in order to avert any further dangers posed by this phenomenon. If you measure the temperature of the drum's surface, you won't be able to identify TR before 710 seconds. It can be done to recognize TR 85 seconds sooner than the spreading critical time if gas sensors are used instead of the conventional sensors. According to the findings, using the gas sensor technology that was proposed in this study will make it possible to detect TR early on, however measuring the temperature of the drum's surface will take too long to be useful for TR detection.

The commercially available LIB for electric EVs' TR process is analysed in depth by Feng et al. [8], who provide a complete overview of the topic. A further clarification of the connection among the ISC and the TR can be achieved by the utilization of the energy release diagram, which is accompanied by two instances. To assist in the process of reducing the risk posed by TR, one strategy that offers protection on three different levels is offered. The three-level safety can be attained by providing passive defence and early indication before an incident of TR, enhancing the materials' inherent thermal stability, and minimizing secondary dangers such as TR propagation. These are the methods by which the protection can be provided. The ISC is the element that appears in every example of abuse, on average. to be the most difficult obstacle to conquer. Different types of ISC relate to different abuse scenarios. There are three stages of ISC when both the rate at which the self-discharge occurs and the formation of alien heat are taken into consideration. Before the ISC can move on toward the third level, often

known as TR, detection immediately needs to begin functioning properly. A brand-new energy release diagram is offered here in order to facilitate the measurement of the reaction kinetics for all of the constituent components found within the cell during TR. The energy released by chemical processes, as well as those involving combustion and ISC, is quantified by the energy release diagram that has been suggested. The proposed diagram of energy release provides a detailed explanation of the chain activities that occur during TR. In the case of a collision, the passenger will have sufficient time to exit the EV as a result of this design feature.

It was shown by Wang et al. [9] that different types of electrode materials, electrolytes, and cell types all exhibit different TR behaviours. Currently, researchers are trying to figure out exactly how these reactions alter based on the materials that are utilized for the cathode, anode, and electrolyte components of the battery. The state of charge and the rate of discharging also have a significant impact on the reactions. The finite element method (FEM) and related techniques have been utilized in the construction and simulation of thermal models ranging from one dimension to three dimensions. At the present time, one of the most successful ways to prevent explosions caused by batteries is to combine the use of a number of safety devices with the built-in security strategy. In subsequent research, it will be important to consider into account extreme circumstances, such as those in which the vehicle's engine will start but the battery will produce a high discharge rate.

2.3 Literature Review on cooling methods

The functionality of LIB as well as its longevity are both significantly influenced by temperature. The battery ought to be kept in a place where the temperature is adequately controlled and there is no danger of TR. This will ensure the battery's safety as well as its performance capacity and its longevity. As stated by Pesaran et al [10], BTMS is required to carry out four responsibilities in order to maintain the pack of batteries in the best possible condition. These include ventilation, heating, air conditioning, and insulation. Both power and heat are created when a battery cell is operating. To maintain

ideal conditions, we must dissipate this heat to ambient in advance. BTMS must therefore use a cooling technology.

When the temperature of the battery pack goes to a level that is even below than the lowest recommended temperature limit, the situation is considered to be unfavourable for batteries. Because of this, we need a heating device, like a Positive Temperature co-efficient (PTC) heating system, that can rapidly bring the temperature of the battery up to its optimal working range.

The difference in temperature between the inside of the battery cell and the outside atmosphere is bigger in conditions that are either extremely hot or extremely cold. Thus, it is a possibility that the temperature may drop or raise outside of its suitable range for temperature in such a circumstance when the battery isn't in use, for example while the car is idle. This is due to the fact that there is a possibility that the temperature may rise out of the appropriate temperature range. As a direct consequence of this, it is not an easy task of getting the battery functioning properly in a short period of time. As a result, the battery pack must have sufficient protection against the elements.

There is a possibility that the internal chemical reactions of a battery pack will produce gas, which will then need to be vented to the environment outside of the battery pack. Therefore, there must be ventilation.

The primary goal of BTMS is to keep a temperature curve, which can lead to identical heating among the battery cells in the LIB pack, while simultaneously minimizing the greatest temperature achieved and the temperature differential among batteries in a LIB pack. This can be accomplished by maintaining temperature gradient.

Additionally, the BTMS needs to be as lightweight as possible, in addition to being inexpensive, easy to maintain, and exceptionally dependable.

Vima Mali [11] researched the use of direct and indirect cooling methods for BTMS, revealing ways to reduce thermal load on Li-ion batteries and reduce the cost and weight

of BTMS for energy-efficient electric vehicles. Design parameters for basic BTMS by mathematical/numerical modelling and simulation.

Design optimization is necessary for an effective BTMS in an electric car. Air-based thermal management methods, such natural or forced-air cooling, reduce battery heat loss due to poor thermal conductivity and efficiency. Heat pipe or fluid cooling systems require sophisticated constructions and are costly. Leakage can cause short circuits and cause thermal runaway issues for battery modules. Thermal management systems using phase change materials increase battery module weight and cost, while achieving fast heat dispersion is problematic.

The thermoelectric generator-based heat management system (TEG) requires significant energy for EV driving.

The thermal runaway of Li-ion batteries remains a problematic issue that requires research community attention.

The SC performance analysis shows that it can handle current peaks and address battery pack temperature.

The expense & weight of SC can be compensated if it minimizes the risk of thermal runaway.

2.3.1 Classification of LIB cooling systems:

In a previous lesson, we went through the processes which require place in the BTMS of an electric vehicle. Now that we've got that out of the way, let's talk about the several methods of cooling that can bring down the operating temperature of the batteries caused by the generation of heat. The following techniques, which are discussed in **Fig. 4**, can be utilized in the LIB cooling classification process.

They are based on-

1. Power usage, which includes both active and passive

The term "active cooling" refers to several cooling methods that rely on an external device to facilitate better heat transfer. The intensity of fluid flow can be increased by active cooling methods, which in turn can further increase the amount of heat transferred via convection. Active cooling techniques such as air being pushed using a fan as well as blower, direct liquid cooling, jacket cooling, and cold plate cooling are all options that can be employed to optimize a thermal management system.

The passive cooling technique requires very little in the way of energy and relies on the surrounding environment to act as a heat sink. Indirect cooling solutions are an appropriate choice for the temperature control of both electric vehicles (EVs) and electronic gadgets because of their higher functionality and lower cost compared to other cooling methods. Techniques that fall under the category of passive cooling include phase change material (PCM) cooling and heat pipe cooling. Passive cooling is able to achieve a great deal of natural convection and heat dissipation by utilizing a heat spreader or a heat sink to maximize the convection and radiation heat transfer modes.

2. The working fluid, which can be any of the following: cooling by air, liquid cooling, PCM cooling, or a mix of these two. When two or more ways (or working fluids) of cooling are utilized in tandem, this type of cooling is referred to as hybrid cooling.

3. Arrangement, which means that it will depend on where the cooling system is positioned in the array. They are able to take on one of three possible forms: direct-indirect, series-parallel, or internal-external.

A good example of an internal cooling system would be one that uses electrolyte as a cooling agent and circulates it through microchannels, as well as an internal cooling path that moves water throughout the battery cells. The most common type of cooling media is an external one. It is accomplished by cooling the battery with an external coolant such as air or liquid, and it can happen either way.

The classification of a cooling system as direct or indirect is determined by whether or not the cooling fluid is in contact directly with the LIB. Direct cooling is defined as having a direct contact with the object being cooled; otherwise, it is referred to as indirect cooling.

The terms "series" and "parallel" refer to two distinct types of cooling circuits that can be found in LIB cooling. The kinds of cooling circuits that are used are decided based on the circumstances.

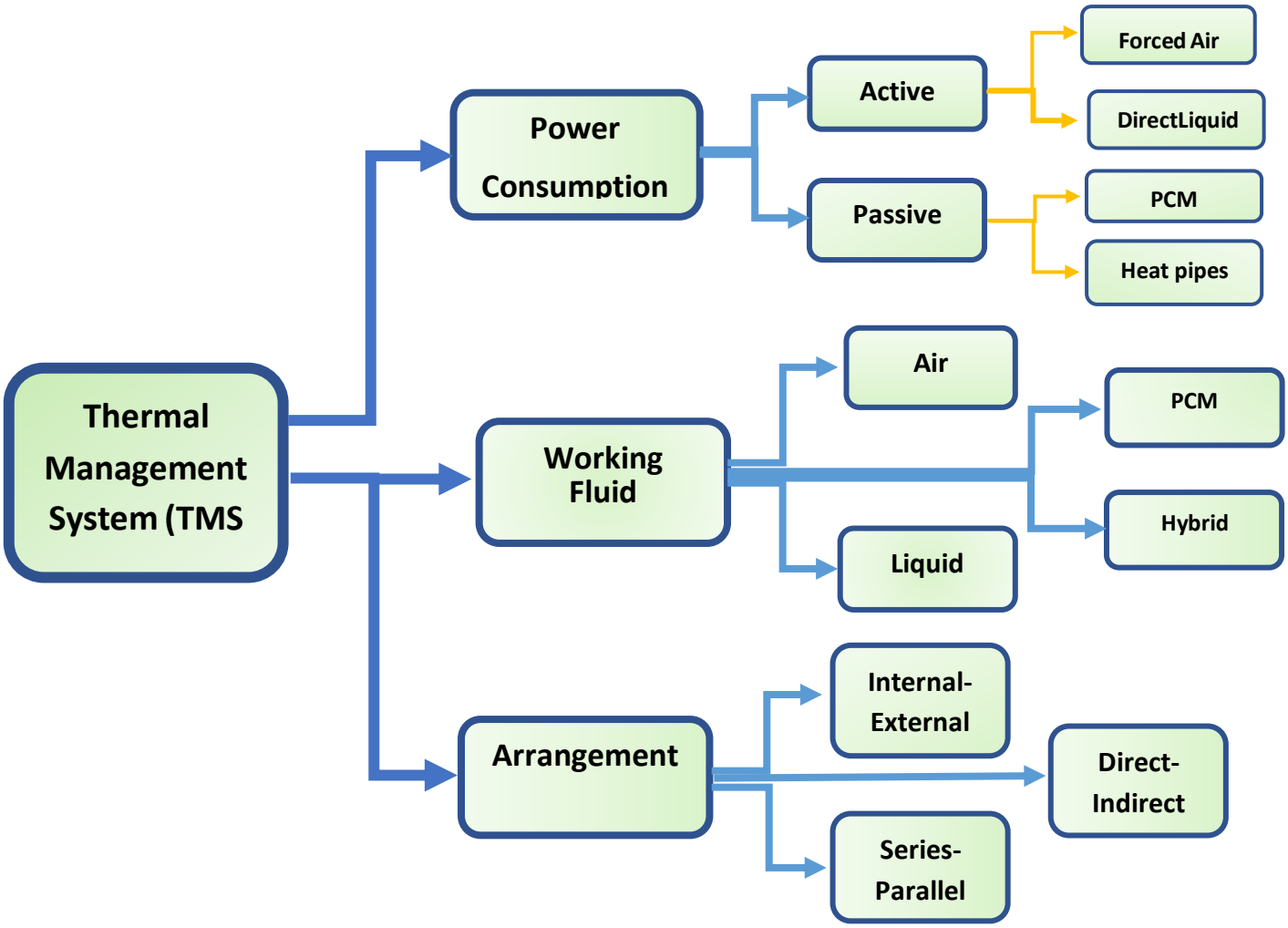

Figure 4: Classification of BTMS

2.3.1.1 BTMS cooled by air

The BTMS makes use of an air coolant system due to the ease of its construction and the low amount of maintenance it requires. As a potential source of cooling, options include the air drawn from the evaporator, the air drawn from the cabin after it has been preconditioned, and the air drawn from the surrounding environment. The driving propensity, the surrounding conditions, and the amount of heat generated all go into the decision of the air source. Because air has a low heat capacity and poor thermal conductivity, air-cooled systems are not as effective as other types of cooling systems. Due to the necessity of preserving an adequate air space between individual batteries, this method has a restricted capacity for the storage of batteries, which is another one of its downsides. Because it relies on a coordinated network of duct and fans to move a substantial quantity of air for efficient cooling, the system is complex, cumbersome, and noisy. Research is being carried out in order to improve the efficiency of the cooling system. Alterations are introduced to the system's cell arrangement, airflow paths, and the architecture of the air channel in order to raise the system's overall efficiency.

The exact design of an air-cooled battery system that Park et al [12] analyses from a theoretical perspective and then models numerically in order to achieve the required thermal characteristics. Because a traditional HEV battery system is formed up of several battery cells which are piled one on above the other, the cooling performance of the system is determined by the even spread of air flow cycling in the coolant channel. This circulation helps to dissipate the heat that is generated by the battery cells. It has been demonstrated that it is possible to achieve the needed cooling performance even though the current layout and design of the battery system has not been altered by making use of a tapered manifold and pressure relief ventilation. In order to evaluate the effectiveness of the cooling system, the temperature resistance model is applied. This model is able to classify the various heat transport methods. In order to achieve the required level of cooling performance while simultaneously taking into account the

limits imposed by the air flow arrangement, a suggested tapered manifold and pressure relief ventilation are being put to use. Additionally, the amount of electricity required for operating a fan is decreased when the air pressure is released.

Cho et al. [13] constructed a transient numerical model of a LIB pack for electric vehicle applications. This model included a thermal management system that was air-cooled. Both the experimentally determined map of the battery's internal resistance and the voltage measured across an open circuit are incorporated into the battery model. When attempting to calculate the amount of activation voltage that has been lost, the Butler-Volmer equation is given direct attention. In order to represent the effects of the module setup, various environmental conditions are used. In every possible configuration of the battery pack, the differential in temperature between the modules was larger when the surrounding air temperature was cooler, while it shrank when the surrounding air temperature was higher. In addition, the configuration of the module has a substantial impact on temperature deviation, and this is true regardless of the surrounding environment. The variance in temperature between sections within a battery pack can be greatly reduced when the modules are organized in such a way that greater numbers of cells are located adjacent to the entry point for air. This effect is seen regardless of the temperature of the surrounding environment.

The purpose of the research carried out by Lu et al. [14] is to evaluate the effect that air cooling has on the temperature uniformity of a little battery pack as well as the mitigation of hotspots under a variety of air flow paths and airflow rates. The numerical results reveal that an increase in the effective heat transfer zones among the battery faces and the air-coolant can result in a drop in the maximum temperature as well as an increase in the highest temperature variance in a densely packed battery box. This can be done by improving the maximum temperature difference. The findings imply that an eventual reduction in the maximum temperature will occur when the size of the cooling channels is increased. This method of decreasing the highest possible temperature is not

the most effective one since the maximum temperature decrease degree gradually decreases as the diameter of the cooling channels increases. This is more evidence that this method is not the most effective one.

The research conducted by Chen et al. [15] optimizes the design of the LIB pack alongside the air-cooled BTMS by using the organization of the cells in the battery separation for improved cooling performance. This is done in order to improve the cooling performance of the system. Combining the flow impedance network model with the heat transfer model and maintaining an even battery heat generation rate is recommended as a method for developing an optimization plan for the battery pack. The BTMS's cooling performance has been significantly improved as a result of the modification. Following optimization, there is a 42% reduction in the maximum temperature differential, and there is also a slight reduction in the peak temperature of the battery pack; however, the overall pressure loss of the system does not change. In addition, the performance of the updated BTMS is superior to that of the first version even when the flow rates of the inputs are changed and when there is an unstable rate of heat generation. The approach of optimization suggests that the distance between LIBs should be modified such that it is larger around the one that has the greatest temperature and that it is less around the one that has the lowest temperature.

In the work of Xie et al [16], experimental and computational fluid dynamics (CFD) computations are used to investigate the impacts of three factors (the air-inlet angle, the air-outlet angle, and the width of the air circulation lane among LIBs) on the dissipated heat of a LIB pack. These parameters are the air-inlet angle, the air-outlet direction, and the dimension of the air flow channel between LIBs. After that, an orthogonal test technique and a single factor analysis are utilized to find the optimal values for the three layout parameters. The optimal circumstances for cooling performance are an air-inlet angle of 2.50 degrees, an air-outlet angle of 2.50 degrees, and a channel width of 2.50

degrees. Using the optimization method results in a reduction of 12.82% in the maximum temperature as well as a reduction of 29.72% in the temperature differential.

2.3.1.2 BTMS cooled by liquid

Both direct and indirect methods of cooling can be utilized to accomplish liquid cooling of the LIB. When compared to air cooling, the cooling efficiency of liquid cooling is significantly higher. It ensures that the temperature is distributed evenly throughout the LIB pack. In general, liquid cooling provides a performance that is both consistent and continuous. These are the benefits that come with using a system that uses liquid to cool. The expense of a liquid cooling system is one of the drawbacks connected with using it. A significant amount of money and resources are needed to purchase the necessary pieces of equipment in order to design a system that uses liquid cooling. Additionally, it has a significant cost of upkeep.

In the direct kind of liquid cooling, the battery is put into the coolant itself and cooled that way. In this kind of cooling, the conductivity of the coolant must be extremely low or nonexistent for the sake of the safety of the vehicle. Despite the fact that it has tremendous cooling potential, it has not yet been commercialized for use with EVs because research and development on the technology is ongoing.

Through the pipes of an indirect cooling system, the coolant makes its way through the system. Additionally, it is comparable as the cooling system which we see in internal combustion engines. For this kind of cooling, the coolant needs to have a high heat capacity in addition to corrosion inhibitors. On the current market, no other cooling system compares to it in terms of potential.

Tong et al. [17] solved a transient mathematical model for a lithium-ion bipolar battery pack, taking into account the preservation of charge, species, and energy. This model was solved for a variety of galvanostatic drain rates of the battery pack. After determining two limiting circumstances, one with cooling and one without, the temperature range where the pack will run with various discharge rates may be

calculated. It has been observed that 45, 22 and 7 stacks on the level of the modules of the pack may be positioned within the coolant plates with a median temperature that is lower than 313 Kelvin if an adequate cooling temperature of 1 C, 2 C, and 5 C-rates are applied, respectively. This is possible if the coolant plates have a rate of 1 C, 2 C, or 5 C. Because raising the coolant speed and coolant plate thickness allows to manage the maximum temperature and temperature non-uniformity, but doing the same raises the mechanical load and contributes to the pack's size and weight, a compromise among these variables should be made. Increasing the coolant speed and coolant plate thickness allows to manage the maximum temperature and temperature non-uniformity.

To explore the thermal properties of LIB packs, the researchers Qian et al [18] developed a numerical model in three dimensions with the use of a type of liquid cooling approach that is based on mini-channel cold-plates. This model was constructed using a computer program. The effects of the variety of channels, the inlet mass transfer rate, the flow direction, and the channel width were investigated as they related to the thermal behaviors of the battery pack. According to the findings, the mini-channel cold-plate thermal management technique was efficient in lowering the temperature of the battery during a **5C** discharge by providing a high level of cooling efficiency. This was demonstrated by the findings. It was adequate to employ a cold plate with five channels, and it was obvious that increasing the pace at which mass was being introduced into the system would result in a decrease in temperature.

Experimental and computational investigations are carried out in this paper by Li et al [19] to investigate the thermal properties of water cooling-based BTMS in LIBs rapid cycling. The goal of this research is to better understand how water cooling affects thermal performance. In numerical simulation, an electrochemical-thermal concept is applied in order to provide predictions regarding the thermal behavior. The voltage, current, as well as temperature distribution within each individual battery as well as the battery pack are provided according to both practical and simulated research outcomes.

In addition, when it comes to improving the thermal efficiency with the battery pack under low cycle rates, a circulating water-cooled system is the method that stands head and shoulders above the competition. In addition, a combination system needs to be created as part of the real battery pack system in order to accommodate the scenario in which battery packs are used for a variety of methods and at varying rates.

The method presented by Chen et al. [20] provides a complete approach to quantitatively measuring the cooling performance of a liquid-cooled battery module. CFD is used to develop a model of fluid-solid coupled heat dissipation, and the thermal parameter values for this model are obtained by experimentation. The Latin Hypercubes method is utilized in order to generate variable mixture samples of and sensitivity analysis is applied in order to ascertain the manner in which structural factors influence heat dissipation performance. The process of multi-objective optimization is then used to accomplish the construction of a cooling system that has a lower operating temperature with lesser energy consumption. It shouldn't be difficult to put into practice the method that was described for the manufacturing of industrial battery packs. The findings show that the temperature decrease will be bigger given identical input power, 1.87 degrees Celsius, and that temperature variance can also be adjusted within a tight range, 0.35 degrees Celsius. Additionally, the results suggest that the reduction in temperature will be greater than 1.87 degrees Celsius.

2.3.1.3 BTMS cooled by PCM

PCM is an acronym for phase change material, which refers to any substance that has the ability to either store latent heat or release it in order to keep its temperature relatively stable. Traditional air-cooling-based BTMS not only consumes more power, but it also is unable to meet the requirement of contemporary LIB packs that have a high energy density. Liquid cooling BTMS, on the other hand, necessitates the use of complex equipment in order to achieve the desired effect. As a direct consequence of this, PCM-based BTMS is gaining in popularity. Utilizing PCM as a heat sink would

enable a battery pack's temperature to be kept within the normal operating range for an extended period of time without the need for any additional power from an external source. PCMs have the potential to dramatically boost the efficiency with which BTMS dissipates heat if they are combined using fillers which possess high thermal conductivity, such as expandable graphite & metal foam, or if they are combined with fins. In comparison to the more traditional methods of cooling, such as cooling via air, cooling by liquids, and heat pipe cooling, the PCM cooling method is often thought of as the one that is most suited for BTMS because of its low cost, simple equipment requirements, and high cooling efficiency.

2.3.1.3.1 The PCM classification system

There is a wide variety of PCM classification criteria to choose from. PCMs can be roughly categorized as Solid-Solid PCMs (SSPCMs), Solid-Liquid PCMs (SLPCMs), Solid-Gas PCMs (SGPCMs) and Liquid-Gas PCMs (LGPCMs) according to the phase of the substances before and after the changing process. These categories are referred to as solid-solid PCMs, solid-liquid PCMs, solid-gas PCMs, and liquid-gas PCMs, respectively. SLPCMs belong to the most prevalent application field among them because of their enormous latent heat capacity, little variation in volume throughout the phase switching process, and simplicity of getting raw materials. This makes them an ideal candidate for use in a variety of industries. **Figure 5** contains a discussion of them.

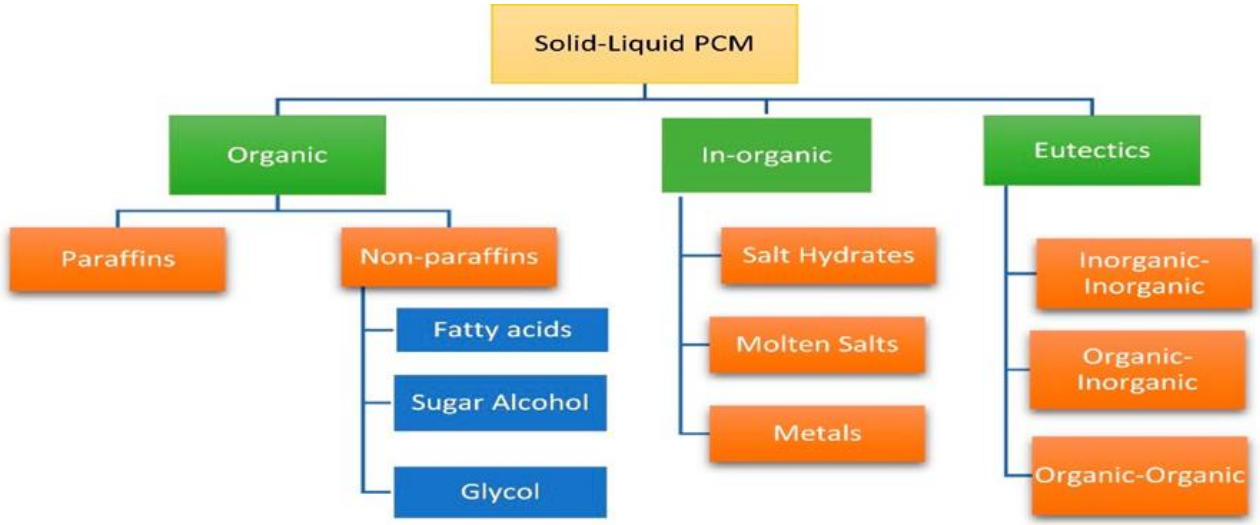

Figure 5: Classifications of PCM [21]

Lieu et al [21] provided the basis for this overly-generalized category of PCM. Organic PCMs most often refer to paraffin and non-paraffin compounds, the latter of which can consist of stearic acid, polyols, long-chain alkanes, plus a variety of other non-paraffin substances. Because of their superior corrosion-resistant properties, safety, nontoxicity, high chemical durability, and nearly no super cooling, organic PCMs have traditionally served as the principal source for PCM raw materials. This is due to the fact that organic PCMs almost never experience super cooling. However, in addition to their benefits, they also have certain downsides, such as a low heat conductivity and an ease in phase change leakage.

The main ingredients of inorganic PCMs are water, salts in hydrate form, salts that have melted, and metal. Salts that are hydrated and metal are among the most sought-after commodities. In addition to being non-combustible and leak-proof, these materials possess an elevated latent heat capacity and are very affordable. Because of the caustic character of hydrated salts, the simple means of phase separation they provide, and the supercooling they exhibit, their use in general applications is severely limited.

Crystal mixes of many soluble components can be defined as eutectic phase change materials (PCMs), and this can be done by simultaneously melting and solidifying the combination. The temperature at which they melt and the temperature at which they freeze are often smaller compared to those of substance that is pure. The preparation of eutectic PCMs often involves the combination of two or more chemicals that have low melting temperatures. These substances can be organic compounds, inorganic compounds, or a combination of both types of compounds.

2.3.1.3.2 PCMs selection methods

The selections are basically done on the following aspects.

1. Thermodynamic properties, including good thermal conductivity, an elevated latent heat in fusion per unit volume, an excellent specific heat, a low degree of supercooling, and a high density. In addition to this, their volume should not change much when they change phase, and they should have a strong capacity of absorbing heat and obtain latent heat.

2. It ought to have some kinetic features, such as an increased nucleation rate and a high crystal growth rate.

3. They should be chemically stable, resistant to corrosion, non-toxic, and combustible, among other desirable characteristics.

4. The temperature at which the PCM changes phase is well within the range of temperatures considered normal for operation.

5. It should be readily available on a big scale, have a reasonable price, and not have a tendency to leak.

2.3.1.3.3 Improvement of PCMs Using Various Improving Techniques

1. Fins added: Battery cooling system can be improved by adding fins with PCM.

Advantages-

a. Make the operational process as easy as possible.
b. The materials can be acquired without much difficulty.
c. Excellent capacity for removing heat from the environment.

Disadvantages-

a. Large contact's barrier to heat flow.
b. expensive with limited ability to refill.
c. a significant high volume

2. Fillers added: Battery cooling system can be improved by adding fillers material with PCM.

Advantages-

a. Reduced expenses and enhanced latent heat.
b. Simple accessibility of the resources needed

Disadvantages-

a. It is straightforward to form aggregates and precipitate.
b. BTMS does not have sufficient thermal uniformity.

3. Encapsulation: Battery cooling system can be improved by capsulating the PCM.

Advantages-

a. Strong in all the right places and quite flexible.
b. Excellent resistance to corrosion and excellent performance while sealing.
c. Maximum protection

Disadvantages-

a. Demand that is high in terms of technology.
b. Demanding standards for the materials used in packaging.

At present, pure PCMs have not been able to fully meet all application requirements because to various limitations such as super cooling, low thermal conductivity, and chemical instability. As a consequence of this, researchers' principal concern regarding the performance and applications of PCMs is in finding ways to boost their thermal conductivity. In order to meet the ever-higher expectations set by the industry, the thermal conductivity of PCMs has had to be improved in a variety of ways during the course of their development.

Currently, the addition of fins, advancements in packaging technology, and the use of high-temperature-conductive fillers are the three methods that are considered to be the most essential. The concept of including fillers has emerged as the dominant way of modification due to the ease with which it can be implemented and the cheap cost involved. The table that can be seen above discusses a variety of methods for enhancing thermal conductivity, highlighting the benefits and drawbacks associated with each approach [21].

A unique PCM-based temperature control system for electric vehicle (EV) batteries was presented and analyzed in the work that was done by Hallaj and colleagues [22]. According to the results from the simulations, the temperature increase of the module that utilized the PCM was significantly lower in comparison to that of the equivalent cell under similar cooling settings. It is anticipated which the temperature rise will be lower for the 100 Ah cell that has heat-transfer coefficients ranging from medium to high than it will be for the cells in the module that have a PCM thermal management system. However, with elevated cooling rates (for example, h=100 W W m^2 K^{-1}), the temperature differential between the core of the cell and the surface of the cell in 100 Ah cells is significant.

Khateeb et al. [23] discovered findings concerning a LIB sub-module that had a point of melting of between 41 and 44 degrees Celsius and had nine 18650 Li-ion batteries encased in PCM. Examining the Aluminium foam that is included within the PCM and the fins that are linked to the battery module were done so in order to solve the PCM's low thermal conductivity as well as its small natural convection heat transfer coefficient. According to the simulation findings of the LIB module utilizing PCM alone, the PCM has a low thermal conductivity, which makes it useless at removing heat from the system. The rise in temperature within the battery was reduced by 250 degrees Celsius due to the use of Aluminium foam in addition to the PCM. The LIB module showed a temperature elevation of 25 degrees Celsius during summer operation, with a starting temperature of 40 degrees Celsius. This temperature rise occurred within the LIB module's safe temperature range. The PCM failed to melt even though the winter working circumstances included a start temperature of 0 degrees Celsius.

A passive thermal management system for LIBs that uses PCM was put through its paces by Kizilel et al [24], who subjected it to extreme circumstances that included a rate of discharge of 2.08C-rate (10A) and a surrounding temperature of 450C. PCM allows high energy packs to be reliably discharged at elevated currents and results in a capacity depletion rate that is approximately half that with LIB packs that do not include thermal management devices. In addition, the packs' compactness helps to minimize the total weight of applications that require a great deal of power.

Rao et al. [25] addresses the thermal energy management capabilities of aging commercial rectangular LiFePO4 power batteries utilizing PCM as well as the thermal behavior connected to the thermal conductivity between the PCM and the cell. In addition, the authors examine the thermal energy management capabilities of the PCM. In accordance with the results of the experiments, the cells released at a current of 35 A (**5C**). Separate processes are used for the formulation of each individual cell and the 3-D modules that make up the battery pack. The research clearly demonstrates that a difference in temperature is invariably brought about through the thermal resistance that exists within the cell. It is essential to raise the thermal conductivity of the PCM and

lower its melting point if one wants to see an increase in the rate of heat transfer. The PCM having a melting point that is lower than 45 degrees Celsius will be more effective in removing heat if the maximum temperature that is wanted is less than 50 degrees Celsius. Before the PCM melts, there will be a temperature differential that is far less extreme over the entirety of the unit. In addition to this, a well-designed BTMS has to have a k_{pcm}:k_c ratio that is appropriate.

PCMs of varied thicknesses are used to enclose the cells in the research conducted by Javani et al. [26]. Despite the restricted periphery surface of the LIB, the orthotropic characteristic of Li-ion cells helps increase the horizontal transmission of heat along with the effectiveness of the PCM surround the cell.

The results show that making use of PCM brings both the maximum temperature and the temperature fluctuation within the cell down to lower levels. A PCM which is 12 mm thick has the effect of reducing the temperature by 3.0 kelvin. It is then discovered that the comparable values for layers with thicknesses of 3 mm, 6 mm, and 9 mm are 2.8 K, 2.9 K, and 3.0 K, respectively. In addition, the influence of the PCM upon the cell's temperature is magnified while the cooling system works in a transient situation. When a PCM that is three mm thick is utilized for the Li-ion cell, the temperature distribution turns around ten percent more uniform. This is an important effect regarding thermal management systems of electric cars.

Goli et al. [27] provide evidence that hybrid PCM using graphene fillers has the potential to greatly improve heat control and LIB dependability. The addition of graphene to a PCM based on hydrocarbons has the potential to improve the material's thermal conductivity from over two orders of scale while maintaining the material's capability to latent heat storage. The both latent and sensible heat storage together with

the improved heat conduction external to the battery pack contribute to a considerable reduction in the rise in temperature that occurs inside of a conventional LIB pack.

The thermal management for a cylindrical battery cell is investigated by Greco et al. [28], who focus on PCM-compressed expanded natural graphite (CENG). In addition, the highest temperature that can be reached with the PCM/CENG cooled strategy is significantly lower than the maximum temperature that can be reached with the forced convection cooling strategy when applied to the same setup. Throughout the process of melting, the PCM cooling may maintain the maximum temperature at a lower level while simultaneously lengthening the time it takes for the temperature to rise during the transient.

R. Bias [29] examined the effectiveness of RT-42 paraffin in controlling battery temperature at thicknesses from 1 to 7 mm surrounding the cell. Maximum temperature control is achieved with RT-42 paraffin up to 4 mm thick. Pure RT-42's poor thermal conductivity affects heat transmission. Therefore, Al2O3/RT-42 paraffin nano PCM (NePCM) with % weight fractions of 0.5, 1, 2, and 5 was tested at 4 mm critical thickness. NePCM maintained a maximum battery temperature of 42.77 °C and remained partly liquefied after a 1200 s discharge cycle. A lumped 3.7 V 1.5 Ah 18,650 Li-Ion battery was quantitatively analyzed for 1200 s of discharge at **3C** rate. Recorded temperature data was validated experimentally. Further investigation determined the necessary thickness of RT-42 (base PCM) around the battery cell to ensure safety and operating limits. For BTMS safety and effectiveness, RT 42 paraffin must be 4 mm thick. At a discharge rate of **3C**, the highest battery temperature was 42.92 °C, and the PCM was largely liquefied after 1200 s.

The use of Al_2O_3/RT 42 paraffin increases the liquid fraction as the weight fraction increases. By increasing the weight percentage of Al_2O_3 nanoparticles, the maximum battery temperature rises owing to reduced latent heat. The maximum measured temperature was 42.88 °C for 5 wt.% and 42.77 °C for 0.5 wt.%.

B.E. Lebrouhi [30] says Adding cooling pipes enhances system performance, with an optimal number of up to 9 pipes. The maximum battery cell temperature drops from 31°C to 20°C, while the liquid coolant inlet temperature drops from 25°C to 10°C. Finally, the proposed low-cost lumped model is effective for simulating, constructing, and optimizing battery packs with heat management systems in real-world settings. The proposed model for a low-cost Li-ion battery pack system includes a hybrid liquid coolant-phase change material (PCM) thermal management system. Passive thermal management (PCM) and hybrid thermal management (Liquid coolant-PCM) are better than natural convection (air) at maintaining battery temperature by absorbing and dissipating heat from cell cells.

Lowering the liquid coolant input temperature in battery pack systems helps absorb accumulated heat in PCM and maintain lower battery levels. The battery cells' maximum temperature drops from 31°C to 20°C, while the liquid coolant input temperature drops from 25°C to 10°C. Increasing coolant velocity is advised for heat dissipation after fully charging the PCM. To optimize coolant pump energy usage, a controlling strategy must be implemented for the system. Nine cooling tubes are recommended for the examined battery pack design. Adding tubes above this amount does not appreciably enhance system performance.

In the work of Seunghoon Lee [31] a compact BTMS with great space utilization in a continuous cycle of **3C** charging and **5C** discharging, a battery thermal model and PCM model were created through an experiment and parametric study. The cycle has a maximum temperature of 38.4 °C and a maximum temperature difference of 3.9 °C, both within the recommended range. A PCM with a melting temperature of 44 °C has a maximum temperature 45.6 °C higher than the appropriate temperature. Melting at 27.7 °C rapidly enters the phase change section in 105 s. Therefore, a melting temperature of 36.1 °C suitable. A thickness of 2 mm is chosen as the upper section of PCM did not fully liquidate right away following **3C** charging. With an inlet

temperature of 31 °C and velocity of 0.2 m/s, the suggested BTMS reduces operating time by 12.4% and returns the liquid fraction of the PCM to zero at the conclusion of the cycle, making it suitable for continuous use.

In Murali's study [32], a PCM-based BTMS design was improved to provide optimal cooling performance by integrating different cooling methodologies. The hybrid BTMS, combining PCM and heat pipe, is the most effective, minimizing temperature rise and maintaining uniform cell temperature without external power, even at high discharge rates. Consider factors such as low-reactivity PCM/Heat pipe material selection, number, layout, and configuration. Compared to adding high thermal conductive particles to PCM, CPCM with porous foams has higher conductivity. While expanded graphite in CPCM offers better machinability and chemical stability, metallic foams are preferred for their uniform inner structure, which improves thermal conductivity over EG. Despite strong thermal conductivity, PCM/foam contributes similarly to PCM/high thermal conductive particles in thermal management, with a slight reduction in maximum temperature rise and temperature differential.

The effectiveness of PCM cooling depends on factors such as melting temperature, thermal conductivity, mass, cell spacing, and thickness. Design and thermal parameters should be optimized for optimal cooling performance.

Al Hallaj [22] suggests that passive cooling systems using phase-change materials (PCM) can simplify thermal management for battery systems. The PCM thermal management system transfers latent heat from discharge to the cell component during relaxation, maintaining its temperature beyond the outside temperature for extended periods, enhancing battery energy efficiency.

This can be beneficial in cold EV applications with intermittent battery operation. Keeping the battery temperature higher with the PCM allows for increased effective capacity. Another example is the usage of Li-ion batteries in satellites. When a satellite

orbits the planet, it experiences a dramatic temperature change from the light to dark sides.

The quick change in temperature affects battery performance.

The heat preserved within the battery pack via a PCM can mitigate the impact of rapid temperature changes.

Weng [33] found that Phase change material (PCM) cooling, which balances heat distribution and ensures safety, is widely employed in lithium-ion battery thermal management. Experimental results indicate that a PCM module with a thickness of ~10 mm provides optimal cooling performance, aligning with theoretical calculations. However, the decreased heat dissipation capabilities at the battery bottom should be considered while constructing the module. Increasing laying aside time improves cooling efficiency, but selecting the PCT depends on specific applications and requirements, notably those aiming for increased battery capacity. Proposed PCM filling methods use gradient thickness or conductivity to account for heat dissipation capabilities at different points on the module. A PCM module with a thickness of ~10 mm exhibits ideal cooling performance, corresponding with theoretical calculations, due to its heat resistance. By increasing laying-aside time, cooling efficiency can be improved. Selecting the phase transition temperature depends on the application and requirements, notably for larger battery capacity retention.

2.3.1.4 BTMS Cooling System by Heat Pipes

A device known as a heat pipe is a kind that is capable of spontaneously transferring heat and does not require any extra power sources to do so. A wick, an adiabatic, an evaporator, and a condenser are the components that make up this system.

Evaporator section is attached to the heat point (heat source) in which the liquid acts as the working fluid of the heat pipe absorbs sand and evaporates it. Following its evaporation, the working fluid then makes its way towards the condenser section by

way of the adiabatic part, which is caused by the pressure differential inside the system. Prior to the condensation process, heat is transferred from the working fluid to the heat exchanger of the condenser. Following its transformation into a liquid state, the working fluid is again transported through the evaporator using the capillary action generated by the wick. This is how the operation of a heat pipe goes. The system is, on the whole, not very bulky, it has a relatively rigid geometry, and it has a minimal maintenance burden. However, the lithium-ion battery thermal management technique of EVs does not make use of this technology because of its restricted contact area, weak capacity, and therefore low efficacy. This is because of the three reasons listed above.

Rao et al. [45] developed a thermal management system using heat pipes in response to the heat-generating nature of batteries in order to lengthen the cycle period of batteries and reduce the overall cost of EVs. Their goal was to comply with the heat-generating nature of batteries. The results of the experiment indicated that it was possible to maintain a maximum temperature that was lower than 50 degrees Celsius even when the rate of heat generation was lower than 50 watts. When paired with the temperature differential that is wanted, the rate of heat creation shouldn't be more than 30 W.

In the research carried out by Li et al [46], a TR model is combined to a Volume of Fluid (VOF) model of heat pipe cooling and then solved in ANSYS FLUENT. This allows the researchers to model the transfer of heat and mass that occurs among heat pipes and batteries. The heat and mass transfer within a VOF model are calculated utilizing a user-defined function (UDF) program which involves both a mass source and an energy source. This code is used throughout the TR process. The use of numerical simulations allows for the investigation of the TR processes that occur within an individual battery under a variety of different operating conditions, as well as the TR propagation that occurs from one cell to adjacent batteries. The TR of an individual battery is not something that can be stopped using the heat pipe cooling system,

although it is possible to stop it from spreading from one cell to the batteries that are close.

2.3.1.5 BTMS Cooling System Using Thermoelectric Current

The optimal operating temperature for LIBs lies within a certain temperature range. When batteries are heated, their performance suffers in equatorial and subtropical locations; on the other hand, batteries cannot function properly in climates that are below freezing. Thermoelectric elements utilized by BTMS make it possible to heat and cool LIB in accordance with the specifications.

There are two broad categories that can be used to classify applications for thermoelectric elements. The Seeback effect, that converts heat in to electricity, is the fundamental principle behind the first one (also known as a thermo electric generator, or TEG). The second approach, known as the thermo electric cooler or TEC, is predicated on an action known as the Peltier effect. This effect converts the energy from an electric current into a useful impact that may either cool or heat a space. Before this point in history, TEC was employed in a variety of vehicle industries for functions including heating and cooling, as well as providing passengers with comfort. Following the discovery of this fact, BTMS promptly began utilizing it. TEC is composed of both p-type and n-type semiconductors. Through air or a cooling liquid, the hot end of the TEC is attached to the heat sink, which is normally in the form of a cold plate, while the cold end of the TEC is attached to the LIB for the purposes of BTMS. Direct current (DC) must be supplied in order for TEC to perform its intended function. As DC is provided to the warmer side, heat flows from the heat origin side (LIB) and passes to the colder plate side. This cools the LIB. The transformation of electrical potential into thermal energy results in an increase in temperature. Because of this, the same TEC can produce either a cooling or heating effect depending on what the requirements for LIB operation are at any given time. Furthermore, the total amount of DC power that is provided can be altered in order to control the amount of cooling and heating that is produced. Above discussed methods are the widely used cooling strategies that are used

and also some of them are under research. In addition to this, researchers have also looked into other methods for improving BTMS design.

In order to improve the safety characteristics of 18650 LIB while it is being stored or transported, the TR expansion experiment on nine-palace grid glass fiber partition packaging was explored by experimental and computational modelling by Qin et al [47]. This was done in order to boost the performance of TR. According to the findings, the glass fiber barrier has the potential to successfully restrict the TR expanding LIB when there's a predetermined distance among the batteries & the partition that surrounds them. The thickness of the barrier is 1.2 mm, and the recommended distance among the battery & the partition is 2.2 mm. Under perfect circumstances, the highest temperature that may be reached on the surface of the battery is only about 130 degrees. A LIB's capacity for safety and protection can be significantly improved by employing the most effective packing configuration for its glass fiber partitions.

Because water mist is a more natural and efficient way of cooling, it was chosen as the subject of this investigation by Liu et al. [48] to investigate the effects of water mist (WM) upon TR through a series of studies. The batteries at various SoCs were heated using an electric heater in order to induce TR, and the surface temperatures of the batteries were monitored during the testing process. It was found that delaying the onset of TR by applying WM prior to approaching the threshold temperature may have this effect. WM must begin to appear when the temperature is between 20 and 30 degrees Celsius or lower than the temperature at which the SoC's threshold temperature is reached. On the other hand, it was demonstrated that WM is unable to halt TR when the temperature is getting close to the critical level.

2.3.1.6. BTMS Cooling System with PCM and FIN Coupled

Jie Mei [38] found that a PA-based thermal management system for lithium-ion batteries performs well and reliably under various optimization strategies. Two optimization strategies, EG and fin, were chosen. Next, charge and discharge experiments were conducted at various ambient temperatures. The surface morphology and DSC of PCMs were recorded individually before and after cycling, with the following key conclusions:

The Tt and ΔH of PA/EG were marginally lower than PA because to the thermal conductivity network of EG and a lower mass fraction of PA. Both PCMs showed some thermal performance loss after multiple cycles, but still qualified as a thermal management material.

EG created a superior thermal conductivity network in PA, resulting in better thermal management than PA/Fin. The combined effect of EG and Fin improved thermal management in the PA, resulting in a 35.5 % drop in battery temperature.

PCM thermal management performance was impacted by ambient temperature, with higher temperatures resulting in lower performance. The optimization impact of EG and Fin decreased with rising temperature. Although the PCM failed at 60 °C, the effective thermal conduction of PA/EG/Fin allowed for further battery temperature management. Next, we will study thermal management solutions for lithium-ion batteries in greater ambient temperatures.

According to studies by Zhiqiang Sun [39], the PCM-Fin system outperforms both the pure battery and PCM systems. Model validation with experimental data is used to conduct numerical simulations to discover the underlying mechanisms. Fin structures improve battery thermal performance by increasing heat transfer area and creating a thermal conductive network within the PCM. New fin configurations, including longitudinal fins and cylindrical rings, were proposed to improve heat transport in PCM-based BTMS. The impact of fin structure dimensions, such as cylindrical ring position,

number of rings and longitudinal fins, and heat generation rate, on the thermal management performance of the PCM-Fin BTMS was assessed. The proposed fin structures provide a thermal conductive network within the PCM, transferring heat from the battery to it fast and extending its lifespan.

(The radial distance between the cylinder ring and battery significantly impacts the thermal management performance of the BTMS. The dimensionless distance of 0.2 is recommended for applications.

The usage of many rings boosts heat transfer between the battery and PCM, but significantly impacts thermal management performance of the BTMS by reducing the PCM within the device.

Increasing the number of longitudinal fins from 0 to 8 extends the battery's working time by expanding the heat conductive network. Increasing the number of fins reduces the working time by reducing the PCM in the BTMS. The PCM-Fin system described in this study reduces battery temperature rise even at 20W heat generation and outperforms the pure PCM system in thermal management.

The battery module is tested with and without PCM at **1C**, **2C**, and **3C**. Then, the PCM module's application fin structure is tested using rectangular, triangular, trapezoidal, I-shape, and T-shape fins and increasing fin number for heat transfer. Additionally, convection effects at the PCM module's outer shell are examined. Finally, an optimized PCM module is proposed and compared to Choudhari's PCM module [40]. The thermal management system using PCM cooling kept Lithium-ion battery temperatures within safe limits at lower current rates **1C/2C**. Due to poor heat storage and low conductivity, this PCM technique fails to control lithium-ion battery temperature at higher current rates. High current rate also causes a rapid rise in Lithium-ion battery temperature, which may shorten its lifespan. Fin structure intercalation in the PCM module lowers battery temperature by 2 °C and 6.4 °C at **2C** and **3C**. Due to improved PCM conduction, it also reduces the battery-PCM temperature difference from 3.36 °C to 1.78 °C. Most fin structures behave similarly to battery temperature. In terms of

temperature difference, I-shape fins are most efficient and triangular fins are least efficient. When convection effects surround the PCM module, heat dissipation may increase. Increasing air circulation reduces battery temperature mostly. Low thermal conductivity of PCM is a major heat transfer issue. PCM thermal conductivity can be increased by adding expanded graphite, metal foam, or carbon fiber. Fins can help improve PCM heat conduction. This fin structure boosts PCM thermal conductivity and lowers melting time.

Rajesh Akula's paper [41] introduces a fin-PCM-EG composite for improved thermal management of Panasonic NCR18650BD batteries at discharge rates above **2C**. Fins and EG are enhanced with PCM for thermal conductivity. A computational technique, the Newman P2D model, was used to estimate heat generation from batteries at discharge rates over **2C** (**2**, **3**, and **4C**), validated using in-house experiments at 0.5, 1, and **2C**. Three heat sinks, one without fins and two with 130 and 260 fins, were compared to provide a better thermal management strategy for higher C-rate battery discharge. The impact of adding 10, 20, 25, and 30% weight fractions of EG to PCM is thoroughly examined. The heat sink with 260 pure Eicosane fins achieves 14.2, 17.6, and 19.1 °C lower temperatures than a plain HS with Eicosane at discharge rates of **2**, **3**, and **4C**. Adding 30% EG by weight to Eicosane improves battery performance by reducing average temperatures and achieving temperature uniformity across all heat sink configurations. Heat sinks with 130 fins are preferable over those with 260 fins due to significant improvements in temperature management, thermal conductance, and thermal capacitance with 30% EG. Eliminates the complexity of 260 fin construction with no thermal performance impact.

In his study, Liu [42] explores the impact of Aluminium fin insertion on PCM heat management performance. We compared the performance of two fin structure shapes. Simulation results show that bifurcated fin structures have the lowest battery maximum temperature, reducing it by 6.16 K compared to pure PCM under **5C** discharge (**5C**

means battery discharges from full charge to 0% in 1/5 h). This study examines the numerical impact of adding Aluminium fin structures to PCM battery thermal management. The fin structure addition reduces battery maximum temperature while decreasing latent heat. Among fin shapes studied, bifurcated fin structures outperformed pure PCM, resulting in a 6.16 K reduction in battery maximum temperature during **5C** discharge. The fin structure with two branches can achieve a 0.50 K temperature drop compared to the single-branch bifurcated fin. The following sections examine the effects of various contributing factors. The thermal performance is significantly affected by fin numbers and thermal contact resistance. The number of fins should balance thermal performance and weight, while thermal interface materials should minimize contact resistance in real applications. No significant influence was detected on PCM width under current conditions.

Naresh [43] found that adding hexagonal fins to Phase Change Material (PCM) improves melting fraction and yields better results. The proposed fin structure uses hexagonal fins at 90-degree angles to maximize heat flow and PCM melting fraction. Increasing the number of fins in the Battery Thermal Management System reduces efficient heat dissipation for the PCM due to viscous Phase Change Material flow between fins. The PCM-fin structure employed in this study demonstrated higher thermal performance compared to non-accessible fins or PCM systems alone.

According to the analysis of the relevant literature, the majority of the earlier research on BTMS that combined PCM and the liquid cooling approach concentrated on inserting liquid cooling structures between battery cells together with PCM in order to dissipate the heat from the cell and recover the latent heat of the PCM well. This was done in order to accomplish both of these goals simultaneously. Although these designs demonstrate a high level of efficiency in regards to cooling performance, the total volume of the system becomes considerably enlarged. This creates crucial concerns due to the fact that low space utilization of BTMS degrades the overall battery performance, such as capacity. Additionally, the approach that is used to position the liquid cooling frameworks between the battery cells is difficult to employ in the bottom cooling

method, which is a way that is now being utilized in many electric vehicles. Even in those few designs in which the liquid cooling structures are located in a location other than between the cells, the constraints are evident and can be summarized as follows.

There are a very small number of research that look at the performance of BTMS under conditions of high current rate (>1.0C), however these studies are quite few. Extreme situations, such as rapid discharging, have to be taken into account, although recently there has been a tendency toward continuously increasing the range of the current-rate that occurs throughout the discharging process. In addition, it is difficult to locate studies in earlier research that validated the numerical model of double-layered PCM and double-layered PCM coupled with FIN on the battery cell with experimental data in consideration of the practical application. This type of validation is helpful for performing an in-depth examination of the BTMS.

2.4 Objectives of the present work

The research that has been published so far makes it abundantly clear that a substantial amount of work, both experimental and computational, has been done in the field of BTMS. Extensive research has previously been done on the topic of comparing and contrasting the benefits and drawbacks of different methods of cooling, including as liquid cooling, PCM cooling, and air cooling. A great number of studies have been done in order to cut down on the necessary amount of power and to make the battery pack smaller overall. We came to the conclusion that researchers are currently showing a significant amount of interest in PCM-assisted battery cooling.

This paper focuses its attention primarily on double-layered PCM cooling under a single battery (**Case-1**), double-layered PCM cooling paired with Fin under a single battery (**Case-2**), alternating the PCMs of both cases, and alternating the PCMs under two separate batteries. Altering the number of Fins in **Case-2**, along with capturing the intermittent behaviour of PCM with the help of the commercial program ANSYS FLUENT 16.2, are both on the agenda for this study. For the purpose of this simulation,

we have chosen to use an 18650 $LiCoO_2$ LIB, with Lauric Acid and Paraffin (RT-42) serving as the PCMs and Aluminium serving as the Fin.

The following objectives are fulfilled and presented in this thesis:

1. Validating the battery temperature and PCM with respect to different constant heat generation in a single cell battery (18650).

2. Temperature characteristic with respect to time of a single cell lithium-ion battery of constant heat generation without both PCM and fin in 2D model.

3. To investigate the cooling effects of double layer of different PCMs on a single battery structure in 2D model.

4. To investigate the cooling effects of double layer of different PCMs (alternating the position of PCMs) on a single battery structure in 2D model.

5. To investigate the cooling effects of battery 2D model covered by fins.

6. To investigate the cooling effects of fins inserting into double layer of different PCMs on a single battery structure in 2D model.

7. To investigate the cooling effects of fins inserting into double layer of different PCMs by alternating their position on a single battery structure in 2D model.

8. Taking the best result from previous, investigate the cooling effect by changing geometry of battery model maintaining constant volume in 2D model

9. Investigate the cooling effect of single battery by increasing the number of fins without changing the total volume and weight inserting into double layered PCMs.

Chapter 3

3. Numerical modelling

3.1 Geometric modelling

The 18,650 Li-ion battery (LiCoO2, 2.4Ah) is tested in this study for evaluation purposes. Paraffin [RT42] and lauric acid are used as PCMs and aluminium is used as Fin in this project. In order to get the most effective cooling effect for the battery, we put it through total of **eight tests**, moving from the most fundamental to the most sophisticated shape, utilizing both PCMs and Fins, as well as without using either of these, and experimenting with other strategies.

- **Case-1:** Battery cooling without any PCM and fin with constant heat generation.
- **Case-2:** Battery cooling by double layered PCMs (inner layer paraffin [RT42] and outer layer lauric acid) with constant heat generation within battery.
- **Case-3:** Battery cooling by double layered PCMs (inner layer lauric acid and outer layer paraffin [RT42]) with constant heat generation within battery.
- **Case-4:** Battery cooling by single layer of Fin with constant heat generation within battery.
- **Case-5:** Battery cooling by double layered PCMs (inner layer paraffin [RT42] and outer layer lauric acid) with symmetric fins (embedded within PCMs) with constant heat generation within battery.
- **Case-6:** Battery cooling by double layered PCMs (inner layer lauric acid and outer layer paraffin [RT42]) with symmetric fins (embedded within PCMs) with constant heat generation within battery.
- **Case-7:** Battery cooling by double layered PCMs (inner layer lauric acid and outer layer paraffin [RT42]) with asymmetric Fins (Embedded within PCMs) with constant heat generation within battery.
- **Case-8:** Battery cooling by double layered PCMs (inner layer lauric acid and outer layer paraffin [RT42]) with increasing the number symmetric fins with

constant volume (embedded within PCMs) with constant heat generation within battery.

Detailed modelling of these cases is explained below,

3.1.1 Case-1: Battery cooling without any PCM and fin with constant heat generation.

Figure 6 depicts the computational domain that is utilized for this numerical simulation of battery. One 18650 $LiCoO_2$ LIB is contained within the module that is shown. The battery has a height of 65 mm and a diameter of 18 mm, however, because we are running a 2-D numerical axisymmetric (about longitudinal side of battery) simulation here, it is displayed as a rectangle instead of its actual dimensions. In this Battery is used with any PCM layer and fins.

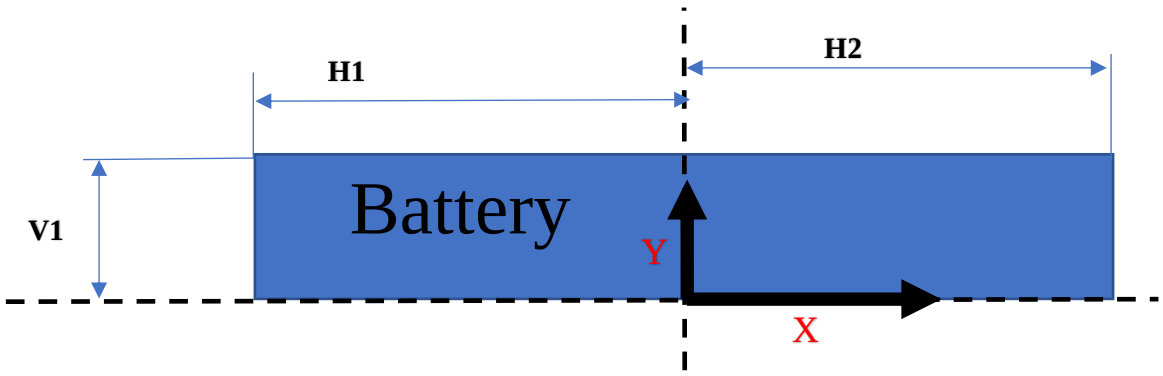

Figure 6: Geometry of physical model (**Case-1)**

Table 1: Properties and dimensions of **case-1**

Battery	**$LiCoO_2$ (18650)**
Dimension	**Value**
H1	32.5 mm
H2	32.5 mm
V1	9 mm

3.1.2 Case-2: Battery cooling by double layered PCMs (inner layer paraffin [RT42] and outer layer lauric acid) with constant heat generation within battery.

Figure 7 depicts the computational domain and meshing that were utilized for this numerical simulation of battery cell heat transfer utilizing Two different layers of PCMs cooling. One 18650 $LiCoO_2$ LIB is contained within the module that is shown. The battery has a height of 65 mm and a diameter of 18 mm, however, because we are running a 2-D numerical axisymmetric (about longitudinal side of battery) simulation here, it is displayed as a rectangle instead of its actual dimensions. The PCM, which is adjacent side of battery, named Paraffin [RT42] and the PCM which is outer side of battery is Lauric Acid. Both PCMs are merged with each other. Both the PCM has taken 4 mm of thickness.

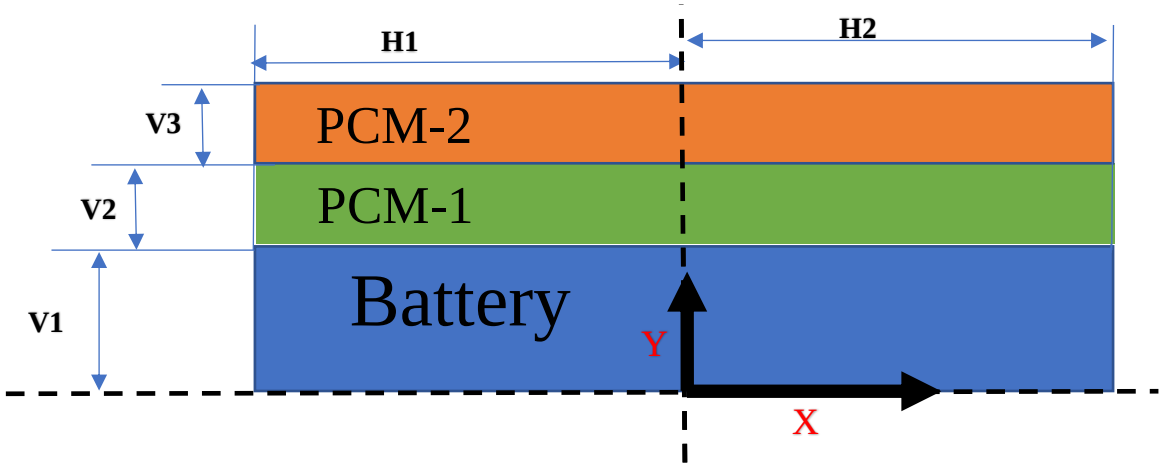

Figure 7: Geometry of physical model (**Case-2)**

Table 2: Properties and dimensions of **case-2**

PCM 1	**Paraffin [RT42]**
PCM 2	**Lauric Acid**
Battery	**$LiCoO_2$ (18650)**

Dimension	Value
H1	32.5 mm
H2	32.5 mm
V3	9 mm
V4	4 mm
V6	4 mm

3.1.3 Case-3: Battery cooling by double layered PCMs (inner layer lauric acid and outer layer paraffin [RT42]) with constant heat generation within battery.

Figure 8 shows the computational domain and meshing used for this numerical simulation of battery cell heat transfer using two PCM cooling layers. The displayed module has one 18650 $LiCoO_2$ LIB. The battery is 65 mm tall and 18 mm wide, but because we are performing a 2-D numerical axisymmetric (longitudinal side) simulation, it is shown as a rectangle of half size width of 9 mm. The battery's outer PCM is Paraffin [RT42] while the neighbouring PCM is Lauric Acid. Both PCMs are merged. Both PCMs are of 4 mm thickness.

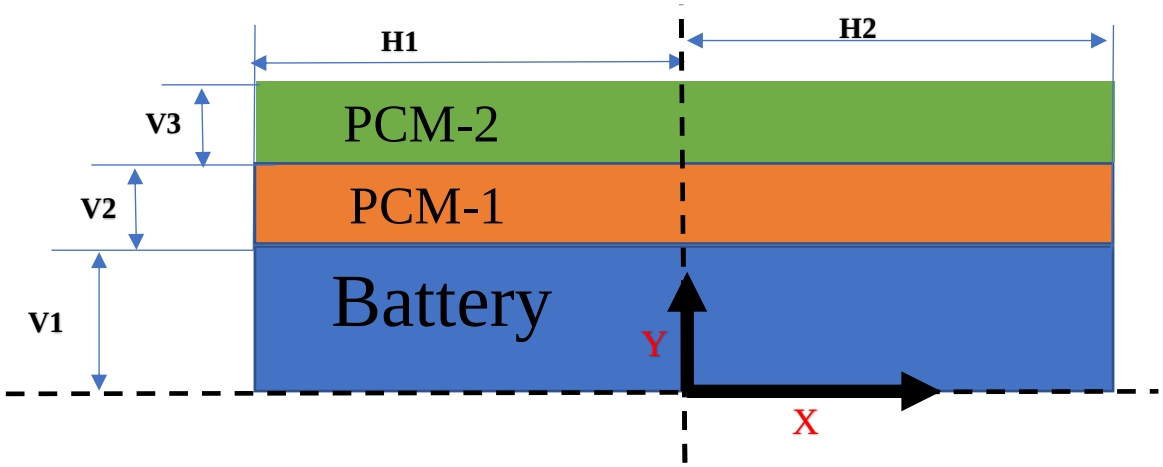

Figure 8: Geometry of physical model (**Case-3)**

Table 3: Properties and dimensions of **case-3**

PCM 1	**Lauric Acid**
PCM 2	Paraffin [RT42]
Battery	**$LiCoO_2$ (18650)**

Dimension	Value
H1	32.5 mm
H2	32.5 mm
V3	9 mm
V4	4 mm
V6	4 mm

3.1.4 Case-4: Battery cooling by single layer of Fin with constant heat generation within battery.

Figure 9 represents s the computational domain and meshing used for this numerical simulation of battery cell heat transfer using only a single layer of fin. One 18650 $LiCoO_2$ LIB is contained within the module that is being presented. The battery has dimensions of 65 millimeters in height and 18 millimeters in width; however, because we are running a two-dimensional numerical axisymmetric simulation (on the longitudinal side), it is displayed as a rectangle with a width of just 9 millimeters. The battery's outer wall is covered by an 8 mm thickness of fin, which is made of aluminium.

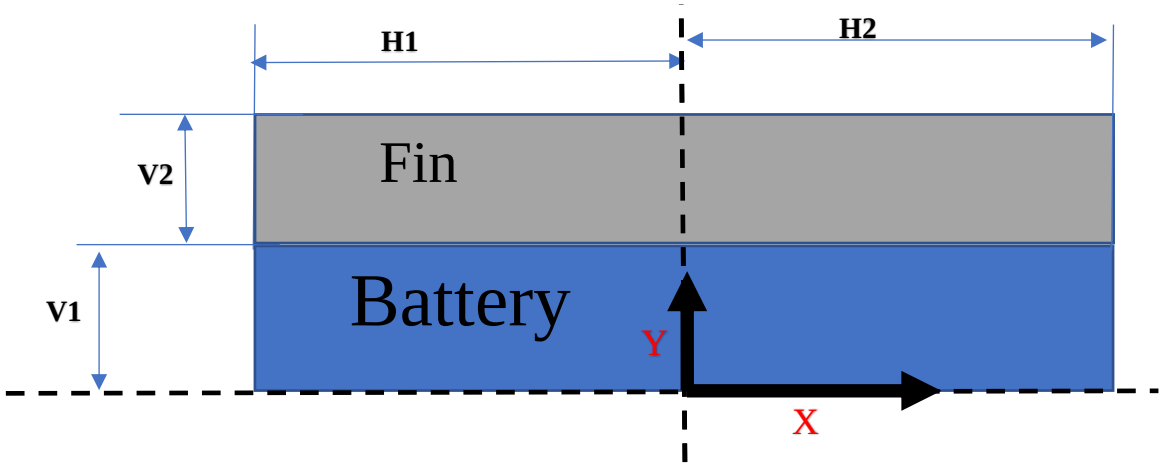

Figure 9: Geometry of physical model (**Case-4)**

Table 4: Properties and dimensions of **case-4**

Fin	Aluminium
Battery	$LiCoO_2$ (18650)

Dimension	Value
H1	32.5 mm
H2	32.5 mm
V3	9 mm
V4	4 mm
V6	4 mm

3.1.5 Case-5: Battery cooling by double layered PCMs (inner layer paraffin [RT42] and outer layer lauric acid) with symmetric fins (embedded within PCMs) with constant heat generation within battery.

Figure 10 depicts the computational domain and meshing that was utilized for this numerical simulation of heat transport within a battery cell using two distinct PCMs cooling layers along with fins inserted within the PCMs. The item being presented is a module that contains one 18650 $LiCoO_2$ LIB. The height of the battery is 65 mm, and its width is 18 mm; however, because we are running a 2-D numerical axisymmetric simulation (longitudinal side), it is depicted as a rectangle. The PCM of the battery's outer layer is Lauric Acid, while the PCM of its neighbour is Paraffin [RT42]. Both PCMs are combined into one. The thickness of both PCMs is 4 mm. with a length of 8 mm and a width of 4 mm, four fins are inserted vertically into both PCMs so that they touch the battery wall and outer faces were opened to outside.

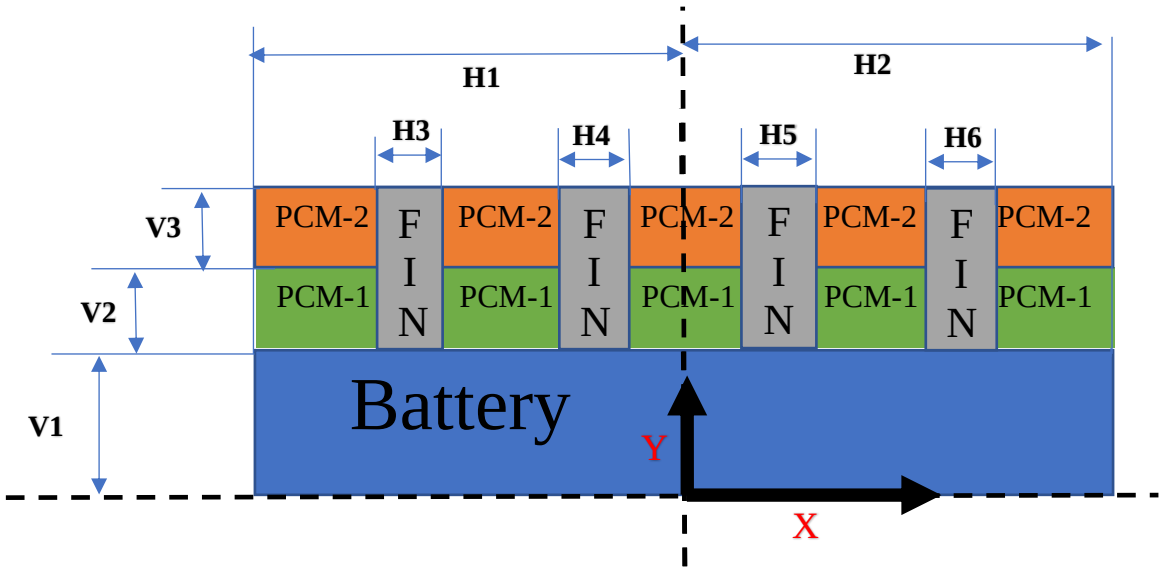

Figure 10: Geometry of physical model (**Case-5)**

Table 5: Properties and dimensions of **case-5**

PCM 1	**Paraffin [RT42]**
PCM 2	**Lauric Acid**
Battery	**$LiCoO_2$ (18650)**
Fin	**Aluminium**

Dimension	Value
H1	32.5 mm
H2	32.5 mm
H7	4 mm
H8	4 mm
H9	4 mm
H10	4 mm
V3	9 mm
V4	4 mm
V6	4 mm

3.1.6 Case-6: Battery cooling by double layered PCMs (inner layer lauric acid and outer layer paraffin [RT42]) with symmetric fins (embedded within PCMs) with constant heat generation within battery.

Figure 11 shows the computational domain and meshing used to simulate heat transport in a battery cell with two PCM cooling layers and fins. The module comprises one 18650 $LiCoO_2$ LIB. The battery is 65 mm tall and 18 mm wide, yet a 2-D numerical axisymmetric simulation (longitudinal side) depicts it as a rectangle. The battery's exterior layer has Paraffin [RT42] (PCM-2), whereas its neighbour has Lauric Acid (PCM-1). Both PCMs are merged. Both PCMs are 4mm thick. With an 8-mm length and 4-mm breadth, four fins are vertically put into both PCMs to touch the battery wall and open their outside edges.

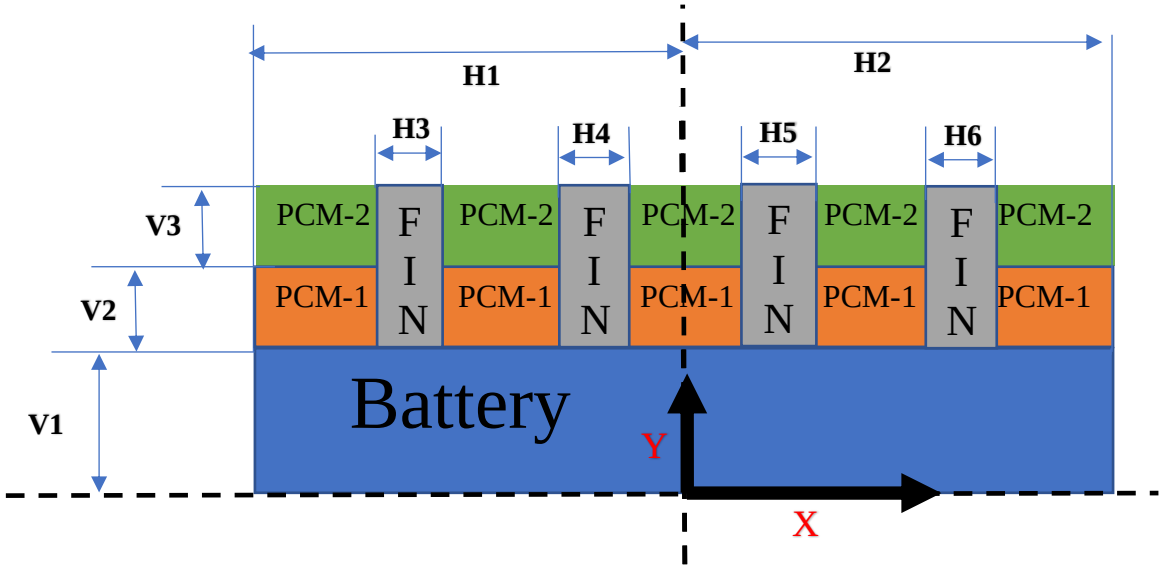

Figure 11: Geometry of physical model (**Case-6)**

Table 6: Properties and dimensions of **case-6**

PCM 1	**Lauric Acid**
PCM 2	**Paraffin [RT42]**
Battery	**$LiCoO_2$ (18650)**
Fin	**Aluminium**

Dimension	Value
H1	32.5 mm
H2	32.5 mm
H3	4 mm
H4	4 mm
H5	4 mm
H6	4 mm
V1	9 mm
V2	4 mm
V3	4 mm

3.1.7 Case-7: Battery cooling by double layered PCMs (inner layer lauric acid and outer layer paraffin [RT42]) of asymmetric geometry with Fins (Embedded within PCMs) with constant heat generation within battery.

The computational domain and meshing that were utilized to simulate heat transport in a battery cell with two PCM cooling layers and fins are displayed in **Fig. 12**. There is one 18650 $LiCoO_2$ LIB contained within the module. A two-dimensional numerical axisymmetric simulation (on the longitudinal side) portrays the battery as a rectangle, despite the fact that its height is 65 mm and its width is 18 mm. The outermost layer of the battery contains Paraffin [RT42] PCM, but the one next to it contains Lauric Acid. The two PCMs have been combined. In this scenario, the width of both PCMs is asymmetrical, with one half measuring 5 mm and the other measuring 3 mm. Both PCMs each receive a vertical insertion of four fins, which are designed to make contact with the battery wall while remaining open to the atmosphere. Two of the fins measure 10 mm in length, and the other two measure 6 mm in length each. Each of the fins has a width of 4 mm.

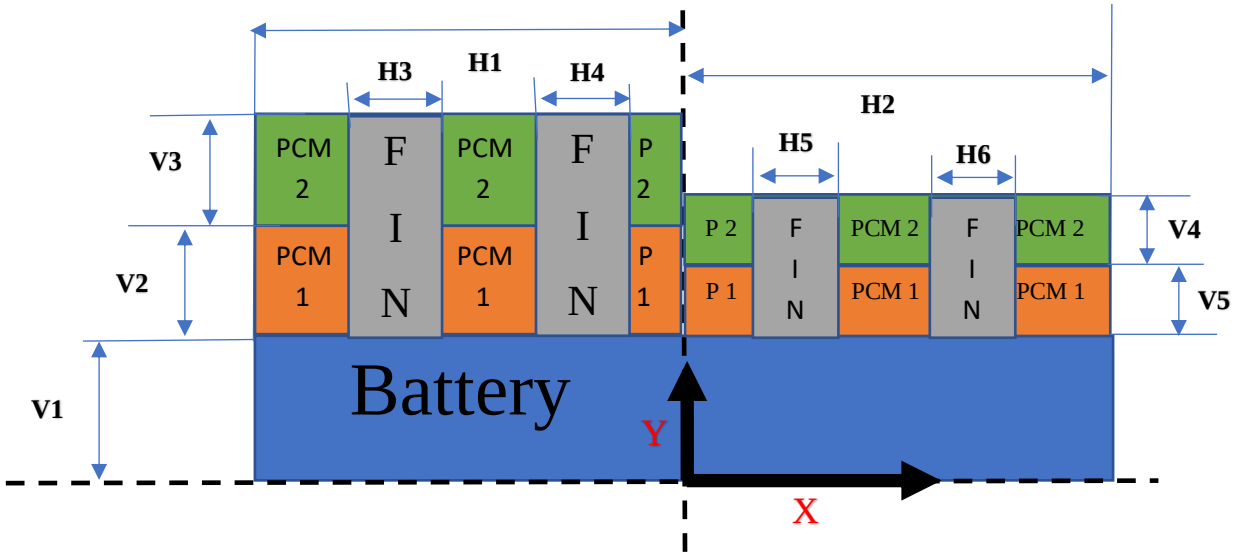

Figure 12: Geometry of physical model (**Case-7)**

Table 7: Properties and dimensions of **case-7**

PCM 1	**Lauric Acid**
PCM 2	**Paraffin [RT42]**
Battery	**$LiCoO_2$ (18650)**
Fin	**Aluminium**

Dimension	Value
H1	32.5 mm
H2	32.5 mm
H3	4 mm
H4	4 mm
H5	4 mm
H6	4 mm
V1	9 mm
V2	5 mm
V3	5 mm
V4	3 mm
V5	3 mm

3.1.8 Case-8: Battery cooling by double layered PCMs (inner layer lauric acid and outer layer paraffin [RT42]) with increasing the number symmetric fins with constant volume (embedded within PCMs) with constant heat generation within battery.

The computational domain and meshing used for this numerical simulation of heat transfer within a battery cell, which included fins inserted within the PCMs and two different PCM cooling layers, are shown in **Fig. 13**. The thing being displayed is a module with a single 18650 $LiCoO_2$ LIB in it. The battery has dimensions of 65 mm in height and 18 mm in breadth, but as we are performing a 2-D numerical axisymmetric simulation (longitudinal side), it is shown as a rectangle. Lauric Acid is the PCM of the neighbouring layer while Paraffin [RT42] is the PCM of the battery's outer layer. Each PCM measures 4 millimeters thick. Eight fins, each 8 mm long and 2 mm wide, are put vertically into both PCMs, touching the battery wall and having their exterior faces opened to the outside.

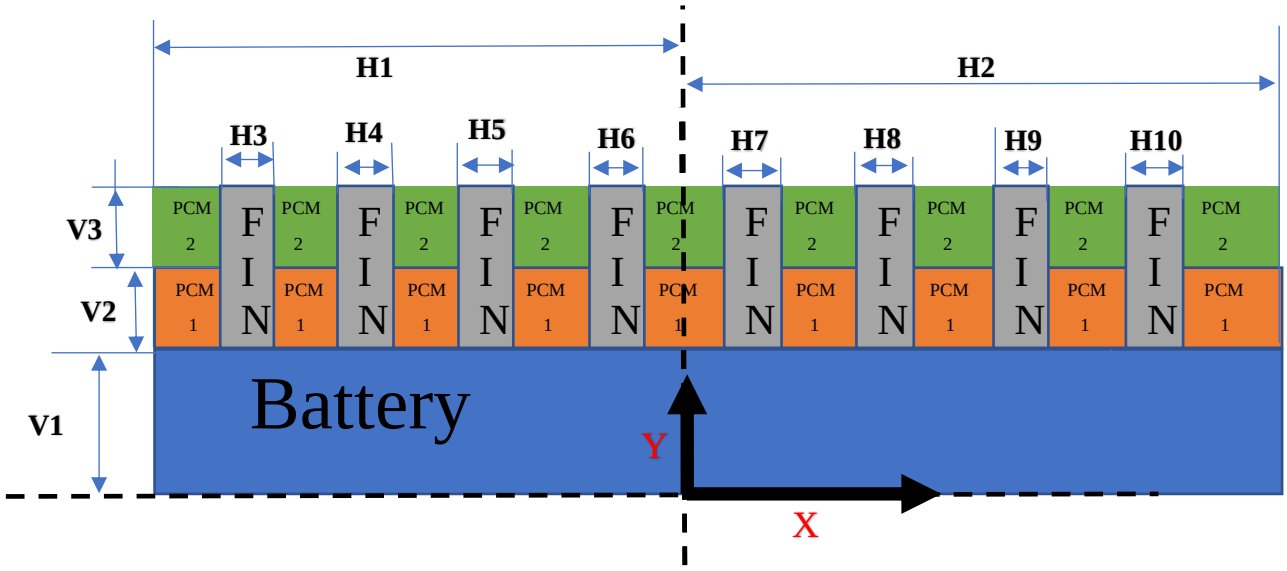

Figure 13: Geometry of physical model (**Case-8)**

Table 8: Properties and dimensions of **case-8**

PCM 1	**Lauric Acid**
PCM 2	**Paraffin [RT42]**
Battery	**$LiCoO_2$ (18650)**
Fin	**Aluminium**

Dimension	Value
H1	32.5 mm
H2	32.5 mm
H3	4 mm
H4	4 mm
H5	4 mm
H6	4 mm
H7	4 mm
H8	4 mm
H9	4 mm
H10	4 mm
V1	9 mm
V2	9 mm
V3	9 mm

3.2 General properties of material

In this case we were assuming that the battery was placed horizontally. The properties of the battery are listed in **table 9**.

3.2.1 Table 9: Properties of $LICoO_2$ battery [40]

Sl no	Parameters	Value
1	Density (kg/m^3)	2720
2	Specific heat (J/kg-k)	300
3	Thermal conductivity (W/m-K)	3

A user-defined function, abbreviated as UDF, was put to use to handle the development of heat on the inside of the battery. This topic is going to be covered later on in the section on battery modelling. The modelling of the battery is performed in the same way as during the validation of the battery, with the exception that the ISC component has been eliminated from the UDF.

Outside wall is surrounded by the acrylic shell. The right wall is consisted of battery positive end, PCM 1 right end and PCM 2. At the left wall is consisted of Battery Negative end, PCM 1 left end and PCM 2 left end.

In this particular instance, Two PCM of different properties (Lauric Acid and Paraffin [RT42]) are used. The properties of Lauric Acid and Paraffin [RT42] are listed in the **table 10** and **table 11** below respectively.

3.2.2 Table 10: Thermo-physical properties of the lauric acid as the PCM [44]

Sl no	Property	Solid	Liquid
1	Liquidus temperature, T_l (K)	-	321.35
2	Solidus temperature, T_s (K)	316.65	-
3	Melting temperature, T_m (K)	319	
4	Density, ρ (kg/m^3)	940	885
5	Specific heat, C_p (J/kg-K)	2180	2390
6	Thermal conductivity, k (W/m-K)	0.16	0.14
7	Viscosity, μ (kg/m-s)	-	0.008
8	Thermal expansion co-efficient, β (1/K)	0.0008	
9	Latent heat of fusion, L_f (J/kg)	187210	-

3.2.3 Table 11: Thermo-physical properties of Paraffin [RT42] acid as the PCM [40]

Sl no	Property	Solid	Liquid
1	Liquidus temperature, T_l (K)	-	316.15
2	Solidus temperature, T_s (K)	311.15	-
3	Melting temperature, T_m (K)	314	
4	Density, ρ (kg/m^3)	830	790
5	Specific heat, C_p (J/kg-K)	1950	2190
6	Thermal conductivity, k (W/m-K)	0.21	0.19
7	Viscosity, μ (kg/m-s)	-	0.02
8	Thermal expansion co-efficient, β (1/K)	0.0001	
9	Latent heat of fusion, L_f (J/kg)	165000	-

The fins can be in the following shapes: rectangular, trapezoidal, triangular, I-shape, and T-shape. In order to compare different fin types, the area of each fin type should remain constant. Due to an increase in heating sensitivity, there is a significant difference between PCM modules with and without fins. In comparison to non-finned

geometry, fins reduce the overall thermal resistance and provide two extra routes for heat to travel. In comparison to a series arrangement of the non-finned geometry, this finned design offers a parallel arrangement that divides the heat flow and lowers total resistance. Lower temperature gradients result in more uniform heat transfer along the length of the fins. As a result, finned geometry exhibits a homogeneous temperature contour. This is caused by the passage of hot conventional currents through the length of the fin from one end that is connected to the battery module. Rectangular and I-shaped fins can be used to detect the distinct fin types, which exhibit minimal variation with low temperature.

In this study rectangular fin has been used, which is made of aluminium. Fins, are of same thickness, are put in between the PCMs separating each PCM with several parts. The Properties of aluminium fin are listed in **table 12**.

Table 12: Properties of Aluminium Fin [40]

Sl no	Parameters	Value
1	Density (kg/m^3)	2719
2	Specific heat (J/kg-k)	871
3	Thermal conductivity (W/m-K)	202.4

3.2.4 Battery Governing Equations

When it comes to modelling TR in LIB, LIB modelling is where the majority of the attention is placed. In the preceding sections 1.1 and 1.2, we went over the fact that in order to model the LIB, one must have a solid understanding of both the chemical and heat transport aspects of the process. As a result, we require a multidisciplinary engineering approach in order to model LIBs and find solutions to their challenges.

In the case of a 2-D simulation, the temperature within the LIB will fluctuate both spatially and over the course of time. ANSYS's primary focus is on solving the generalized two-dimensional heat transfer equation because this is the equation that must be satisfied for temperature variation to be obtained. The equation for the transport of heat can be expressed as

$$\frac{\delta}{\delta x}\left(k\frac{\delta T}{\delta x}\right) + \frac{\delta}{\delta y}\left(k\frac{\delta T}{\delta y}\right) + Q_{gen} = \rho_{jr} * C_{P_{jr}} * \frac{dT}{dt} \quad \ldots\ldots\ldots\ldots\ldots (1)$$

3.4 Numerical Modelling Of PCM

The enthalpy-porosity technique [46] was utilized in order to do PCM simulation. This approach does not make an explicit attempt to follow the solid-liquid interface. The mushy zone, on the other hand, is handled as if it were porous, whose porosity having equivalent to the melt percentage (or volume fraction) that corresponds to every single cell within the computational area. During the melting process, a phase-shifted material goes through a region that is known called the **mushy zone** on its way from the solid state to the liquid state. A semi-solid region that is regarded to be situated between both liquid and solid states is referred to as a **mushy zone**. The melt fraction gives an indication of the percentage of the cell volume that is present in liquid form. The "**enthalpy-porosity approach"**, that represents an important update of the enthalpy formulation, also has connections to the liquid fraction, f. This connection was made in order to better understand the relationship between the two concepts. The latter is based on an apparent similarity between the flow of fluid throughout a porous medium as well as the partially liquid material found in the mushy zone. This similarity was discovered by accident. It is obvious that it is used in the situation in which the medium of liquid is managed properly and permitted to flow. The primary advantage of using this method is that it eliminates the need for variable transformations while simultaneously solving linked equations for momentum and energy on a constant grid. In order to keep the amount of complexity at a level that is more approachable, the following set of relevant assumptions has been made.

3.4.1 Assumptions

- The PCM that is melting exhibits the behaviour of a Newtonian fluid.
- PCM's characteristics are distinct depending on whether it is in the solid or liquid phase.
- The effects of viscous dissipation as well as thermal radiation are essentially non-existent.
- The flow is described as being two-dimensional, laminar, and incompressible, with the exception of the body force term.
- The **Boussinesq approximation**, which is written as $\boldsymbol{\rho_l - \rho = \rho_l \beta (T - T_m)}$, where $\boldsymbol{\beta}$ is the thermal expansion coefficient of PCM and Tm is the average melting temperature of PCM. It gives an accurate representation of the density stratification that occurs within the fluid constituents.
- The liquid and solid states, when brought into touch with one another, are found to be homogenous, isotropic, and in a state of thermal equilibrium.

The viscosity is the only thermo-physical property of the PCM that is not a function of temperature. This is because all of the other thermo-physical properties, such as the density, thermal conductivity and even particular heat capacity, depend on the melt fraction.

3.4.2 PCM Governing Equation

The equations for energy, momentum, and continuity that rely on time are represented as follows. They are the ones responsible for regulating the combined velocity and temperature fields, as long as the presumptions described earlier are true. The governing conservation equations for the PCM system are as follows:

Continuity equation:

$$\frac{\partial \rho}{\partial t} + \nabla . (\rho V) = 0 \ldots\ldots\ldots\ldots\ldots (2)$$

Momentum equation:

$$\frac{\partial(\rho V)}{\partial t} + \nabla.(\rho V) = -\nabla p + \mu\nabla^2 V + \rho g + S_m \text{ ..... (3)}$$

Energy equation:

$$\frac{\partial(\rho H)}{\partial t} + \nabla.(\rho V H) = k\nabla^2 T + S_h \text{ ..... (4)}$$

Where ρ represents the density, V represents the velocity vector, p represents the pressure, T represents the temperature, S_m represents the momentum source term, H represents the specific enthalpy, k represents the thermal conductivity, represents the dynamic viscosity, and g represents the acceleration due to gravity. It is also referred to as the specific enthalpy (H), and it is equal to the sum of the sensible enthalpy (h) and the latent enthalpy ((ΔH).

$$\mathbf{H = h + \Delta H} \text{.....(5)}$$

In this context, the equation for the sensible enthalpy is where:

$$\mathbf{h = h_{ref} + \int_{T_{ref}}^{T} C_p \ dT} \text{ ..... (6)}$$

Where h_{ref} stands for the enthalpy of reference at the temperature of reference Tref, the value of Cp represents the specific heat. The latent heat content of a solid can be zero, while the latent heat content of a liquid can be one.

$$\Delta H = \beta L_f \text{ ..... (7)}$$

In this case, the latent heat of fusion is denoted by L_f, and the liquid fraction is denoted by β, which can be defined as follows:

$$\beta = \begin{cases} 0 \ if \ T < T_s \\ \frac{T - T_s}{T_l - T_s} \ if \ T_s < T < T_l \\ 1 \ if \ T > T_l \end{cases} \text{ ..... (8)}$$

The temperature at the solidus is denoted by T_s, while the temperature at the liquidus is denoted by T_l. The expression for the energy source term S_h, which is used in equation (14), is as follows:

$$\mathbf{S_h} = \frac{\boldsymbol{\partial(\rho \Delta H)}}{\boldsymbol{\partial t}} + \boldsymbol{\nabla}.(\boldsymbol{\rho V \Delta H}) \ldots\ldots\ldots\ldots (9)$$

The momentum source term S_m that is used in equation (13) to explain flow in a porous media can be represented as a function of melt fraction in the way that is described in the following.

$$\mathbf{S_m = A(\beta)\ V} \ldots\ldots\ldots\ldots\ldots\ldots (10)$$

The porosity function, denoted by the notation A(β), was given by Brent et al. [47]. The source term, which was utilized to denote what flows in the porous medium in the equation for momentum, needs a value of zero in the liquid phase in order to allow for free motion, but it has to be big in the phase of solids to force the velocity values to be near zero values [48]. This is because the source term had been used to illustrate the flow within the porous medium in the equation of momentum. The following is the most common use of a modified version of the Carman-Kozeny equation, and that is derived from the Darcy law for describing fluid flow in porous media:

$$\mathbf{A(\beta)} = \frac{\boldsymbol{A_{mush}(1-\beta^2)}}{\boldsymbol{\beta^3 + \varepsilon}} \ldots\ldots\ldots\ldots\ldots (11)$$

where A_{mush} is usually the mushy zone constant, that specifies how rapidly the fluid velocity reaches 0 as it solidifies, and ε is a very small computational constant that is used to prevent zero from being included in the denominator (which is, in this case, = 0.001).

In the previously given formula (21), the function A(β) is responsible for taking into account the velocity switch-off that occurs in solid PCM. When all of the PCM melting (T > Tl), the source term (S_m) within the momentum equation approaching 0

and the melt fraction approaches $\beta \rightarrow 1$, getting closer to the generic equation for momentum conservation that applies for a Newtonian fluid flow. This happens when the temperature rises above Tl. However, the entire PCM is solid and hence $\beta \rightarrow 0$ whenever the temperature inside the PCM is lesser compared to the solidus temperature ($T < Ts$), the entire PCM turns into a solid, and as a result, becomes less than 0. As a result of the flow velocity being so close to zero in this scenario, the contributions made by the source term are not very significant. As a consequence of this, the source term will not make a significant impact during the melting process until the mushy zone (also known as the melting regime) has been reached.

In this regime, the mushy zone parameter A_{mush} is responsible for the majority of the regulation of the PCM melting characteristics and heat transmission. The values that are set associated with this parameter, which are determined by the layout of the PCM, have a significant impact on the position of the interface between the solid and liquid phases of melting as well as how the interface moves as the melting process progresses. Values of A_{mush} that are sufficiently large can properly anticipate the solid-liquid interface because they suppress flowing through the PCM's solid regions. This allows for more accurate predictions. When attempting to define the movement of the solid-liquid interface, A_{mush} values with low values provide erroneous predictions, while A_{mush} levels with high values produce oscillating outcomes. Alternately, excessively high values of A_{mush} suggest that there is a greater quantity of the PCM within the mushy area, indicating that it's predominantly static. The real behavior of the PCM in natural convection is underestimated as a result of this, whereas extremely low values of A_{mush} exaggerate the level of melting that occurs. As a result, it is absolutely necessary to give careful consideration to the selection of the A_{mush} parameter when one is planning the numerical modelling of the melting process. For the majority of computations, it is recommended that values fall among 104 kg/m^3s and 107 kg/m^3s [44].

3.5 Boundary Conditions

In this instance, we have presumed that the battery is set in a horizontal orientation. Therefore, gravity is not taken into account in this particular scenario. The value that was calculated before for the amount of heat generated is used. Aside from that, all of the other settings are exactly the same, and we will go over the approach for setting up PCM cooling in the following section.

The initial and boundary conditions used in Numerical simulation are described below**.**

A. Initial condition at t = 0, T (t = 0) = Ti = 300 K.
B. Internal constant heat generation of 94,023.84 W/m^3 as a heat source is applied in Li-ion battery, which is designated as **3C** current rate.
C. Acrylic shell as outer shell with a natural convection heat transfer coefficient 5.7 W/m^2K is selected.
D. Fin outer wall, with a natural convection heat transfer coefficient 6 W/m^2K is selected.
E. Bottom layer of battery is used as axisymmetric axis.
F. Right end of battery along with PCMs is used as positive end with a natural convection heat transfer coefficient 5.7 W/m^2K is selected.
G. Left end of battery along with PCMs is used as negative end with adiabatic situation.

3.6 Computational procedure

The whole domain was initialized to 300 K and the user scalars used are from the battery validation literature [5]. Time step size of 0.5 seconds, maximum iteration of 300 and number of step size 30,000 were used.

The Boussinesq approximation provides a description of the difference in density that exists between the various fluid constituents. In the field of fluid dynamics, the study of buoyancy-driven flow, commonly known as natural convection,

makes use of the Boussinesq approximation as an analytical tool. It does not take into consideration variations in density unless those variations are stated in terms that are multiplied by g, which stands for gravitational acceleration. The essential tenet of the Boussinesq approximation is that despite the fact that there is just a negligible variation in inertia, gravity is strong enough to manifest itself as a discernible difference in specific weight. The Boussinesq approximation is utilized in situations in which the temperature of a fluid changes from one area to another, leading to the movement of fluid and the transfer of heat.

In the instance of the PCM simulation, the solidification and melting model was used in addition to the energy and viscous models. The value of the mushy zone parameter, A_{mush}, was taken as a constant (2 x 105), the same as it was in the PCM paper work done by Fadl et al [44], which was validated. In the section titled "Computational set-up of PCM," the specifics of the mushy zone parameter are explored in detail. In this particular instance, the PCM domain is considered to be a fluid medium.

This study takes into account a transition temperature range of approximately 4.7 K, which is equal to $2\Delta T$. This range is also known as the melting range. The "solidus" temperature is considered to be $(Tm - \Delta T)$, while the "liquidus" temperature is thought of as $(Tm + \Delta T)$.

The battery's characteristics were the same as those listed in **table 9**. The circumstances of the UDF and the cell zone were the same as those of the air flow run. In contrast to the modelling of the flow of air, boundary conditions were enforced in each of the four corners (walls) of the square cavity. At the walls, a convective boundary condition was utilized, with h equal to 5.7 W/m^2-K and T equal to 300 K.

For the pressure-velocity coupling, the semi-implicit technique for the pressure linked equations (SIMPLEC) was used. For the pressure terms' spatial

discretization and interpolation, the PRESTO (Pressure Staggering Option) scheme [45] was utilized. Using a second order upwind technique, the advection component was discretized, the diffusion term was discretized using central differencing, and the transient term was discretized using a first order implicit discretization scheme. Gradient used as least squared cell based. For density, momentum, pressure correction, thermal energy, and melt fraction, the under-relaxation factors that were used were 1, 0.7, 0.3, 1, and 0.9, respectively.

In order to satisfy the convergence conditions of 10-6 for the continuity and velocity components and 10-11 for the energy equations, the maximum number of iterations for each time step was set at 300. This decision was made in order to ensure that all of the equations were solved correctly. The volume monitor was used to plot the volume average liquid fraction of the PCM zone against time and temperature average also, and the surface monitor was used to determine the facet average value of the internal battery as well as both PCMs. The vertex monitor was used to determine the point temperature of both positive and negative end of battery. The problem was solved by beginning with a time step size of 0.5 seconds and a starting value of 300 K for the user scalars. At a temperature of 300 K, both the PCM domain and the battery domain were patched.

Axisymmetric model has taken into this analysis, where battery's longitudinal side has taken as X-axis and battery along with both PCMs thickness has taken as y axis. In order to discretize the geometry, the ANSYS 16.2 meshing tool was utilized. Edge scaling was applied to the batteries, PCMs, and fins in order to further enhance the mesh. This is because there is contact or interaction between solids and fluids close to the PCMs' walls, solids and fluids close to the battery wall zone or interface zone, and solids and solids close to the zone between the fins and the battery wall in various cases in this project. In that region, a boundary layer is created as a result of conjugate heat transfer. Therefore, we will need to create a mesh interface zone between all surfaces (PCM to PCM, PCM to battery,

PCM to fin, and fin to battery) in order to more accurately capture the effect of heat transmission. In order to capture the rapid movement of attributes at the interface, we will also need to design a finer mesh.

Different meshing techniques have been used in each of 8 cases. Edge meshing and face meshing have been made on model in different way in different cases. There are various number of nodes and elements in different cases with different orthogonal quality and skewness. **Table 13** shows the meshing quality of all cases below.

Table 13: Computational meshing quality of all cases.

Case No	Meshing Quality			
	Nodes	**Elements**	**Orthogonal Quality**	**Skewness**
1	17720	16580	0.96197	.020759
2	37480	34933	0.9627	.20307
3	37480	34933	0.9627	.20307
4	58922	55277	0.96323	0.20214
5	102535	95789	0.96351	0.2005
6	102535	95789	0.96351	0.2005
7	154238	144188	0.9626	0.20383
8	178062	166226	0.9632	0.20103

3.7 Battery validation

A study done by Choudhari [40] that comprises of a battery surrounding by Paraffin [RT42] (PCM) has been shown to be legitimate by the work that we have shown here. In this particular instance, we will be looking at three different scenarios. The first thing that we did was try to determine the effect that PCM has by comparing two different cases: one with PCM cooling and one without. Second, we have observed how the changes in constant heat generation (W), one of which is in **1C** and another of which is in **3C**, affect the heat dissipation of the battery into the environment as well as the melting time of the PCM. Last but not least, by studying the process of melting and solidifying, we have attempted to recreate the intermittent nature of PCM's activity. We have utilized an 18650 LIB that has been covered by a PCM that is 9 millimeters thick for each of the three operations.

3.7.1 Numerical modelling of validation

In this case, the diameter of the battery is measured to be 18 millimeters, and there is a PCM with a thickness of 9 millimeters surrounding it. In this instance, Paraffin [RT-42] served as the PCM. The ANSYS 16.2 design modeller was used in order to generate the geometry.

In order to discretize the geometry, the ANSYS meshing tool was utilized. This simulation required a total of 35213 nodes and 27785 elements in order to be carried out. It may be deduced from the fact that the average skewness was 0.08 and the average orthogonal quality was 0.98 that the meshing is of a satisfactory quality. The face-sizing algorithm was employed throughout the entirety of the domain. The meshing elements have a size of 0.2 millimeters each.

As demonstrated in **Fig**.**14a** and **Fig.14b**, a time step size of 0.5s, 10000 step-size, and a maximum of 300 iterations are sufficient to provide a satisfactory agreement between our current study and the work of Choudhari [40].

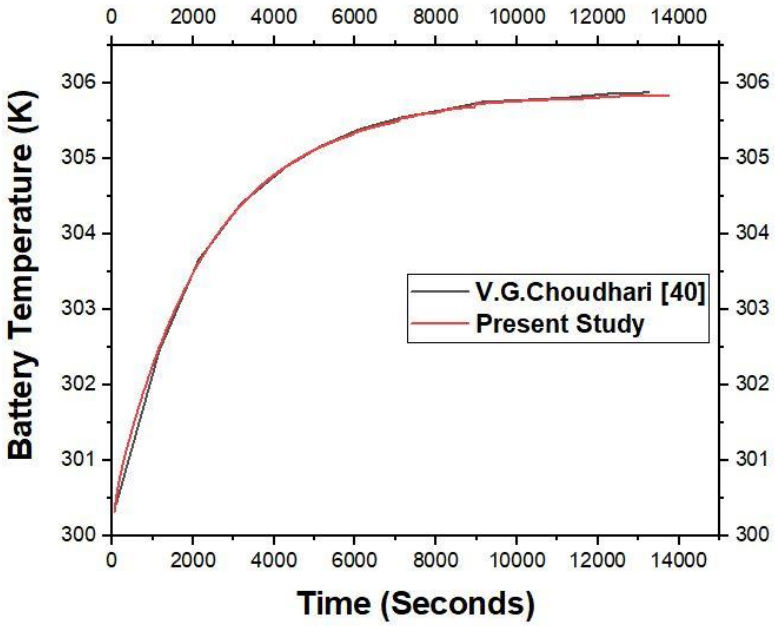

Figure 14a: Validation of Temperature vs. Time graph in **1C** (10,447 W/m^3) heat generation

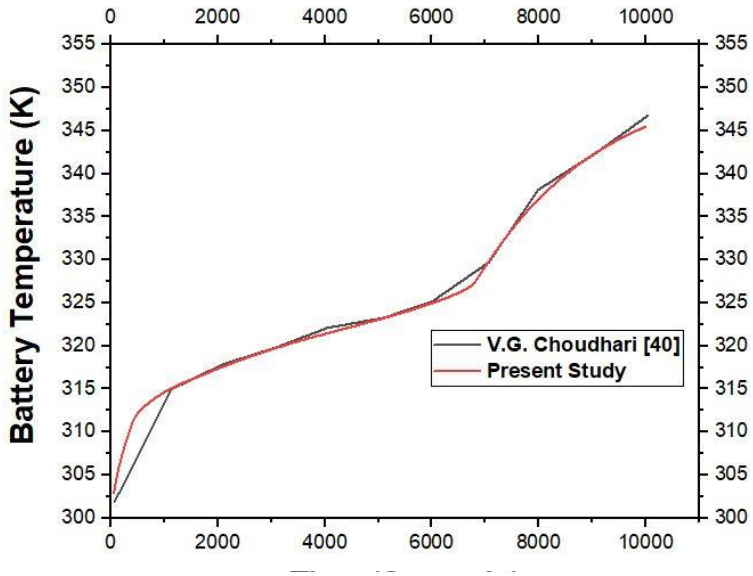

Figure 14b: Validation of Temperature vs. Time graph in **3C** (94,023 W/m^3) heat generation

3.8 PCM Validation

A study done by Fadl et al. [33] that comprises of a container that has lauric acid (PCM) in it has been shown to be legitimate by the work that we have shown here. They modelled the system using the data obtained from the experiment that had been carried out by Kamkari et al [39]. Within the context of that work, the measurement of PCM

melting involved recording the geometry of the melting interface in relation to time. The interior of the container has dimensions of 0.05 meters in width, 0.12 meters in height, and 0.12 meters in depth. The wall of the container maintained a temperature of 700 degrees Celsius throughout the experiment. The remaining three walls of the enclosure had a thermal conductivity of 0.043 W/m-K, and they were joined to a sheet of plexiglass with a thickness of 0.025 meters.

3.8.1 Numerical modelling of validation

Here, we have validated the particular instance of a horizontal enclosure with a value of 2 x 105 for the mushy zone parameter (A_{mush}). The mesh size and the time step size that were employed for the simulation were the optimal ones that were used in the study [33], which are (50 x120) and 0.2 seconds respectively. Through the use of the ANSYS FLUENT 16.2 program, the simulations were carried out as code with a 2-D double precision (2ddp) format. The pressure-based coupled approach was utilized in order to find solutions for the momentum and continuity equations. During the simulation, the gravity vector was adjusted to a value of -9.8 m/s^2 in the y-direction. This adjustment was made in order to better predict the natural convection that would occur in the PCM.

For the pressure-velocity coupling, the semi-implicit technique for the pressure linked equations (SIMPLE) was used. For the pressure terms' spatial discretization and interpolation, the PRESTO (Pressure Staggering Option) scheme [34] was utilized. Using a first order upwind technique, the advection component was discretized, the diffusion term was discretized using central differencing, and the transient term was discretized using a second order implicit discretization scheme. For density, momentum, pressure correction, thermal energy, and melt fraction, the under-relaxation factors that were used were 1, 0.7, 0.3, 1, and 0.9, respectively.

In order to satisfy the convergence conditions of 10-6 for the continuity and velocity components and 10-11 for the energy equations, the maximum number of iterations for each time step was set at 300. This decision was made in order to ensure that the simulation would run smoothly.

The foregoing computational approach was utilized in order to achieve a satisfactory level of congruence between the results of our current investigation and the work done by Fadl et al [33]. The contrast between our recent findings and previous research can be seen in **Fig. 15**.

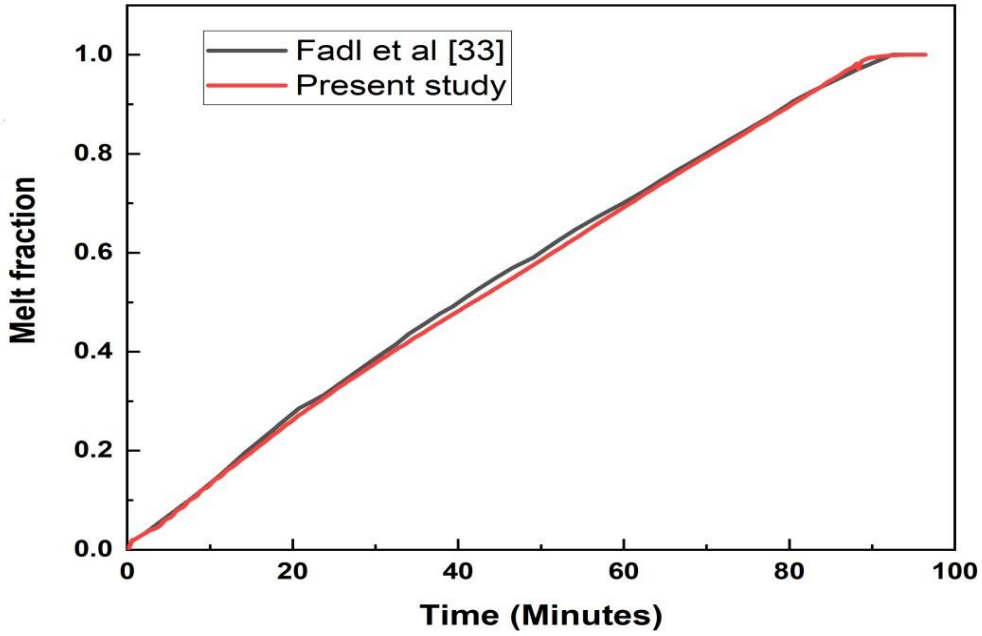

Figure 15: Comparison of Melt fraction vs. Time

Chapter 4

4. Results and discussion

4.1 Battery without PCM and fin.

In the **first case** we have taken only a lithium-ion 18650 battery with constant heat generation of **3C** (94,023.84 Watt/m^3) inside the battery (**figure 6**). We have evaluated all the cases in this project taking the high heat generation value of **3C** for better safety purpose. We have mentioned earlier that we have performed this simulation to know how the temperature of the battery varies with time and come to the saturation temp with the surrounding, where the battery temperature become same or changing minor instead of increasing time. We took h = 5.7 W/m^2-K and T = 300 K in natural convection situation for the study. **Figure 16** shows the variation of temperature vs. time.

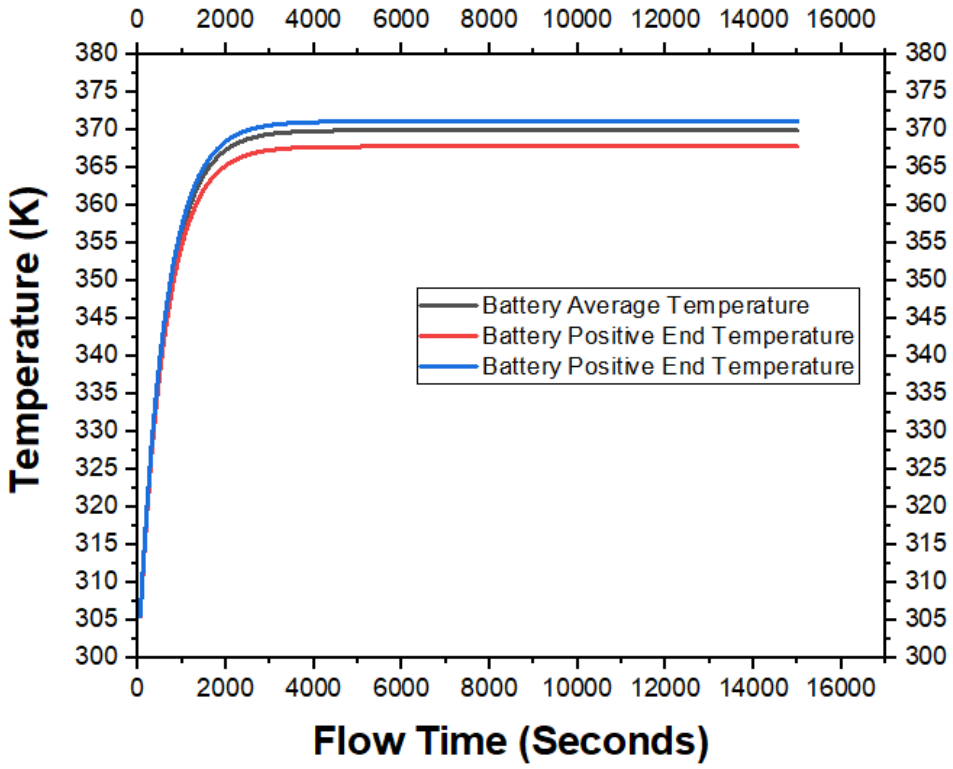

Figure 16: Temperature vs. Flow Time

As we can see from the graph that without PCM and fin the temperature inside the battery increases at a much faster rate. We can see from the graph that battery negative end temp is higher and battery positive end temp is lower than the average temp as battery negative end is in adiabatic condition and battery positive end is in natural convection situation. The average temperature reaches a steady value (369.96 K) after some time. This is because after sometime a situation happens when the heat generation by battery equals the heat taken by convection.

4.2 Double Layered PCM Cooling (Inner Layer Paraffin [RT42] and outer Layer Lauric Acid)

In our next study **case-2** we chose double layer of different PCMs with different properties. One is Paraffin [RT-42] and another is Lauric Acid. Same lithium-ion battery (18650) is used with constant heat generation of **3C** (94,023.84 Watt/m^3) inside the battery. Paraffin [RT-42] is used as PCM-1 which is adjacent with battery outer layer and Lauric Acid is used as PCM-2 which is adjacent to PCM-1 but far away from battery outer layer **(Fig. 7)**. Here we have taken axisymmetric model of battery about x-axis which is battery's longitudinal side. **Figure 17** shows the variation of temperature of battery with respect to time.

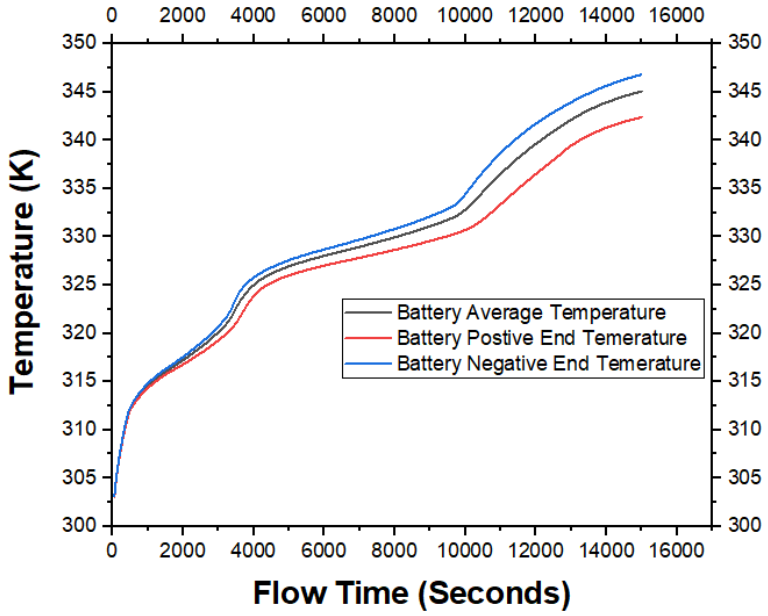

Figure 17: Temperature vs. Flow Time

If we focus on both PCMs temp during analysis in **case-2** with flow time that will depict in **figure 18**

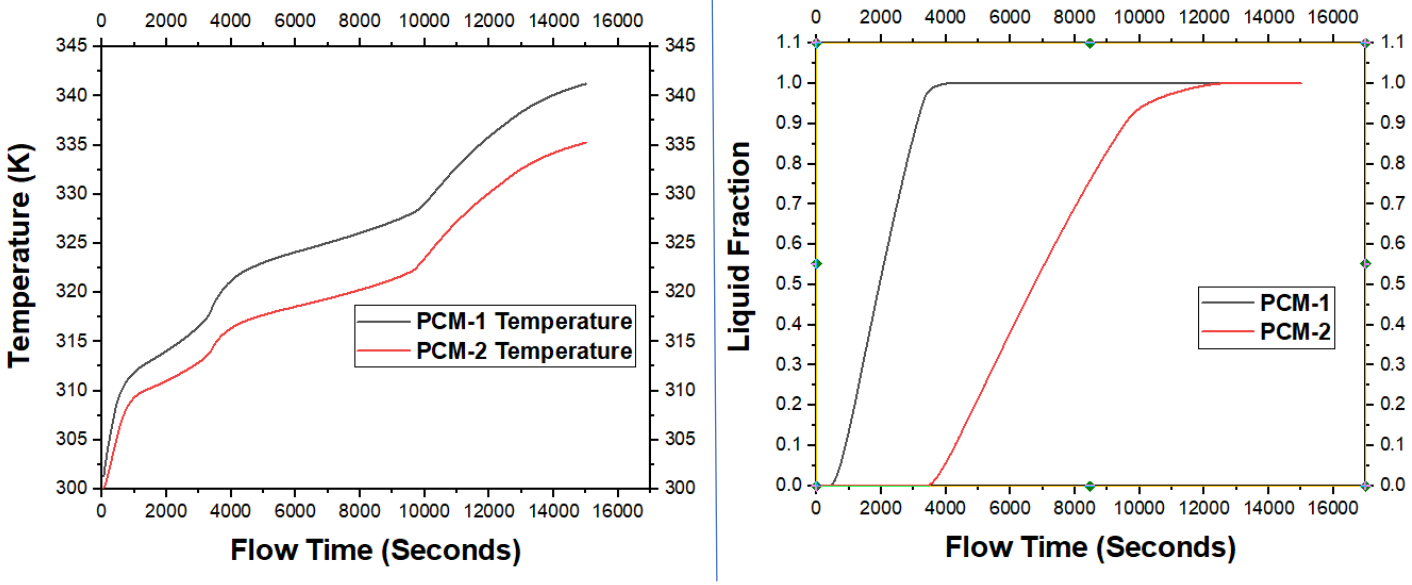

Comparison of Temperature (**Figure 18)** and Liquid Fraction (**Figure 19**) between PCM-1 and PCM-2

Figure 18 shows that PCM-1's temperature is higher than PCM-2's because PCM-1 is closer to the direct battery outer wall while PCM-2 is farther from the battery and closer to PCM-1's outer layer.

Let come to liquid fraction of both PCMs in this case, from where we can easily understand about the melting situation of each PCM within different battery temp with corresponding flow time.

Figure 19 is all about melting solidification of PCMs. It is clear from the **figure 19,** when PCM-1 has come to the point where it is about to melt completely then PCM-2 has been started to melt.

We can observe that with double layered PCMs, battery temperature become very much decreased. There are certain fluctuations in temperature vs flow time graph during the analysis. But still if we compare between **case-1** and **case-2**, there is vast

difference in battery temperature. In **Fig**. **20** we will show the temperature difference between **case-1** and **case-2**.

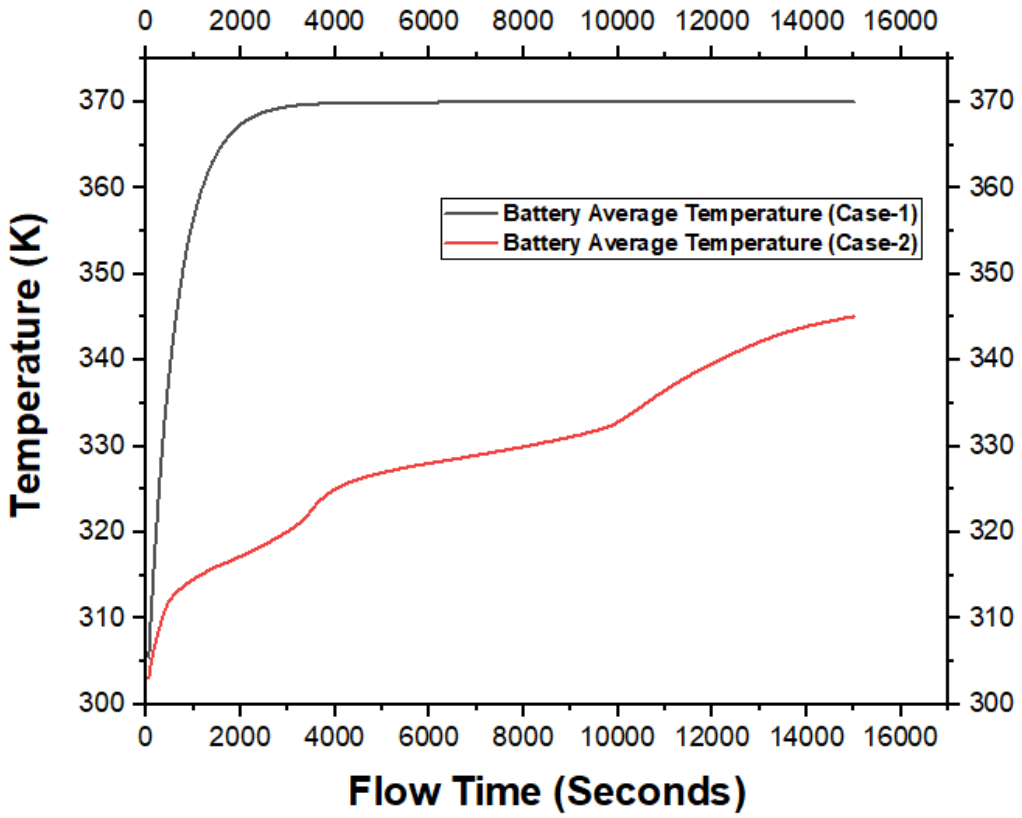

Figure 20: Comparison of Battery Temperature between **Case**-1 and **Case**-2

In **case-1** during 2000 seconds, battery temperature is about to touch 367 K whereas in **case-2** due to double layered PCM battery temperature is still at 316 K. If we watch the final result that we get from the analysis in 15000 seconds that 369.96 K is ultimate temperature where 345 K is ultimate temperature from **case-2** which is very much less and effective.

4.3 Double Layered PCM Cooling (Inner Layer Lauric Acid and outer Layer Paraffin [RT42])

In our subsequent investigation, **case-3**, we decided to use a double layer of various PCMs that had already been used in **case-2**. However, the PCMs layer has changed this time. Battery outer wall is near to lauric acid, which is designated by PCM-1, and paraffin [RT-42], which is adjacent to lauric acid and designated by PCM-2 (**Fig. 8)**. The same lithium-ion battery (18650) is utilized, and its internal temperature remains constant at **3C** (94,023.84 Watt/m^3). All of the analyses' dimensions and other steps are the same as before. The battery's temperature variation with regard to time is depicted in **Fig. 21**.

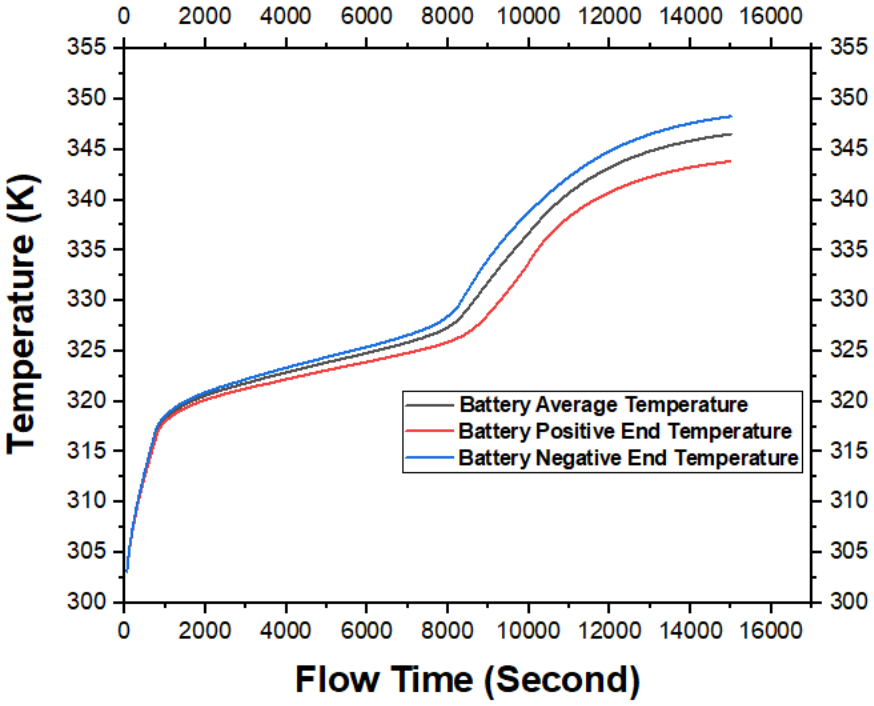

Figure 21: Temperature vs. Time

If we focus on both PCMs temp during analysis in **case-2** with flow time that will depict in **Fig. 22** and **Fig. 23.**

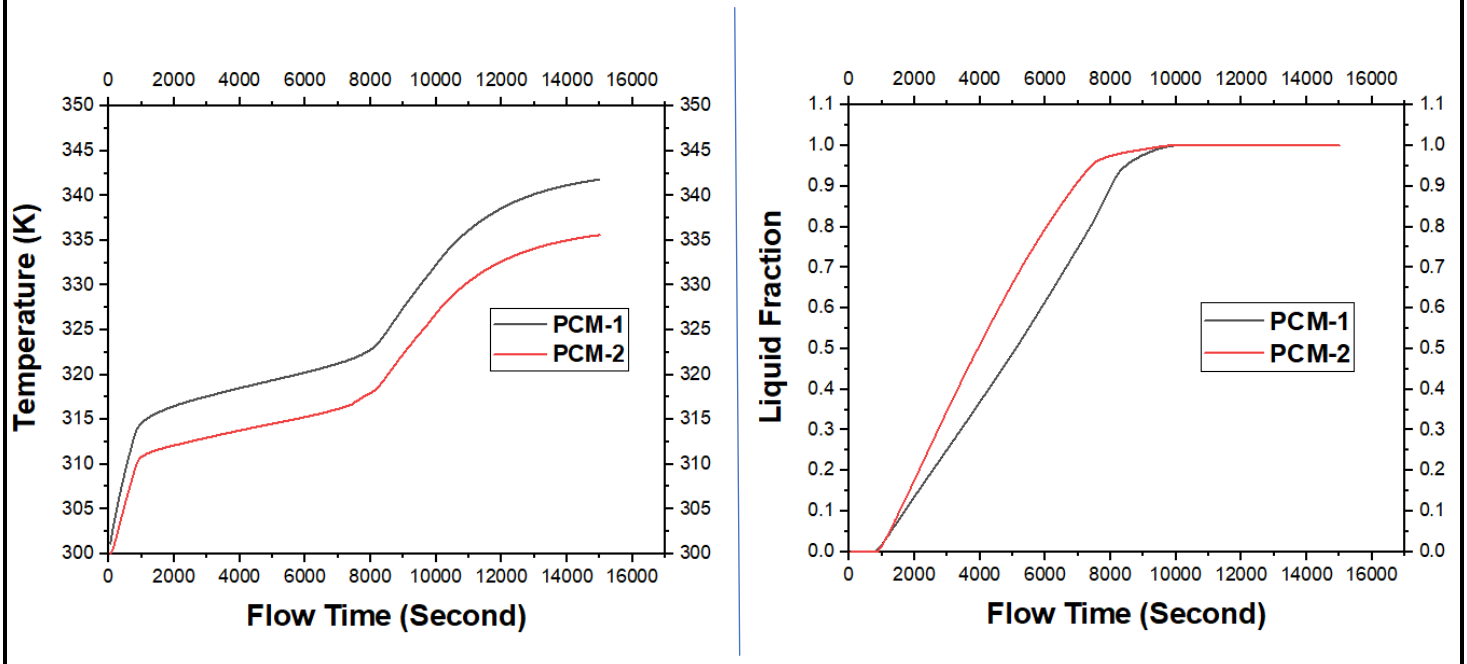

Comparison of Temperature (**Figure 22**) and Liquid Fraction (**Figure 23**) between PCM-1 and PCM-2

If we compare between **case-2** and **case-3**, we can observe that in **case-2** battery temperature is fluctuating than **case-3** and overall battery temperature of **case-3** with respect to flowing time is slightly less than the **case-2**. **Figure 24** depicts comparison of overall battery temperature between **case-2** and **case-3**.

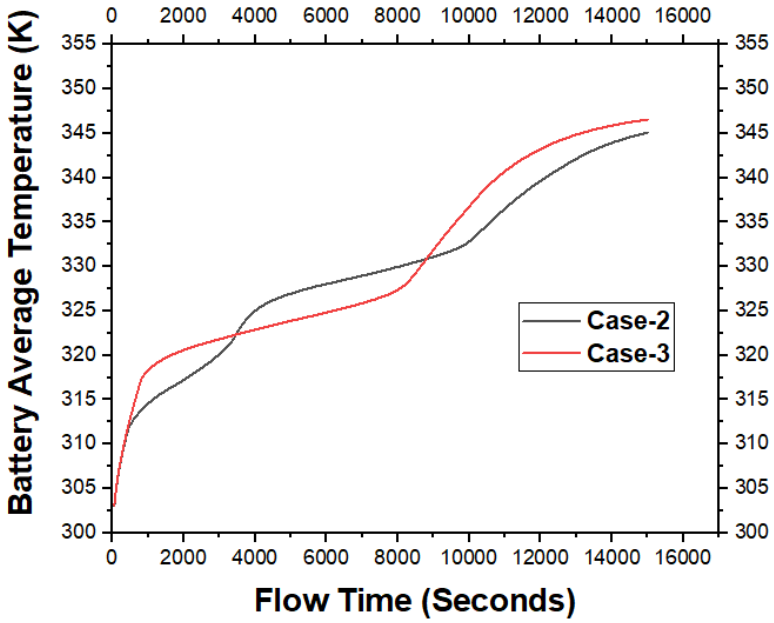

Figure 24: Comparison of Battery Temperature between **Case-2** and **Case-3**

4.4 Battery cooling only with fin

In our next study **case-4** we take a lithium-ion 18650 battery covered by a layer of Aluminium fin **(Fig. 9)**. Here also the constant heat generation inside the battery is taken as **3C** (94,023.84 Watt/m^3). **Figure 25** shows the variation of temperature of battery (average, positive end and negative end) vs. time.

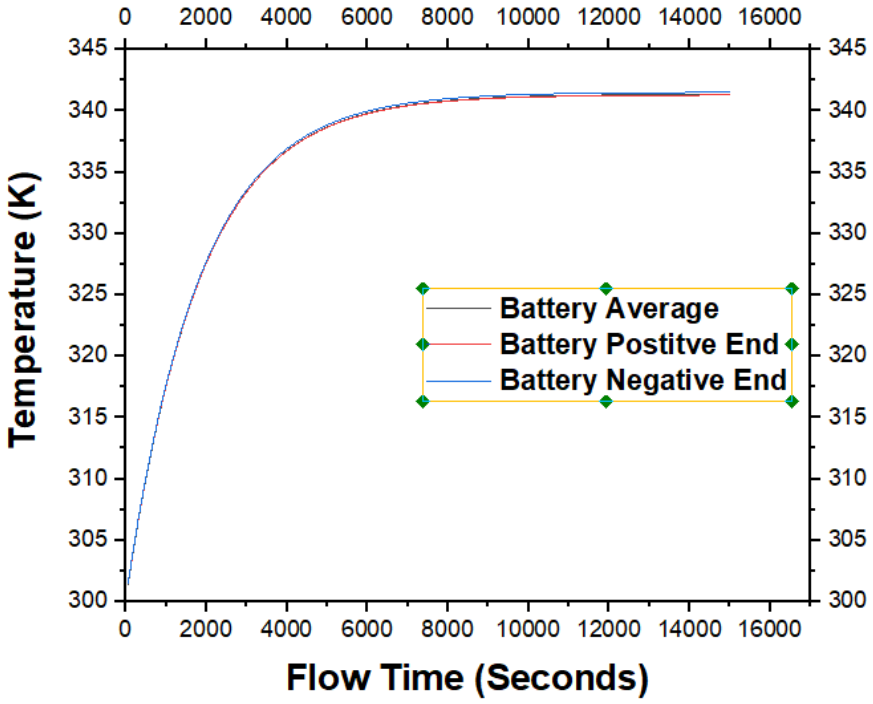

Figure 25: Temperature vs Flow Time (**Case-4**)

We have already done 4 different cases with different configurations. In every case there are certain battery temperature becomes up and down. With every test we want to lower the battery temperature. In **Fig. 26** we will make comparison between the cases analysed up to **case-4**.

From the **Fig. 26**, we can observe that lower temperature has been achieved by fin coupled battery up to a certain flow time (15000 seconds). But in this case if we observe carefully, it is very clear that in fin coupled battery temperature becomes very high at early stage and become almost constant after a certain time flow (5000 seconds). So, fin-coupled battery model (**case-4**) is not efficient not only average cooling temperature but also it makes the battery heavier because of high density of fin (Aluminium). For, efficient battery cooling we can consider **case-2** and **case-3**. Although **case-2** can minimize temperature of battery at final stage better than **case-3**, but overall **case-3** is slightly more efficient than **case-2** for overall battery cooling.

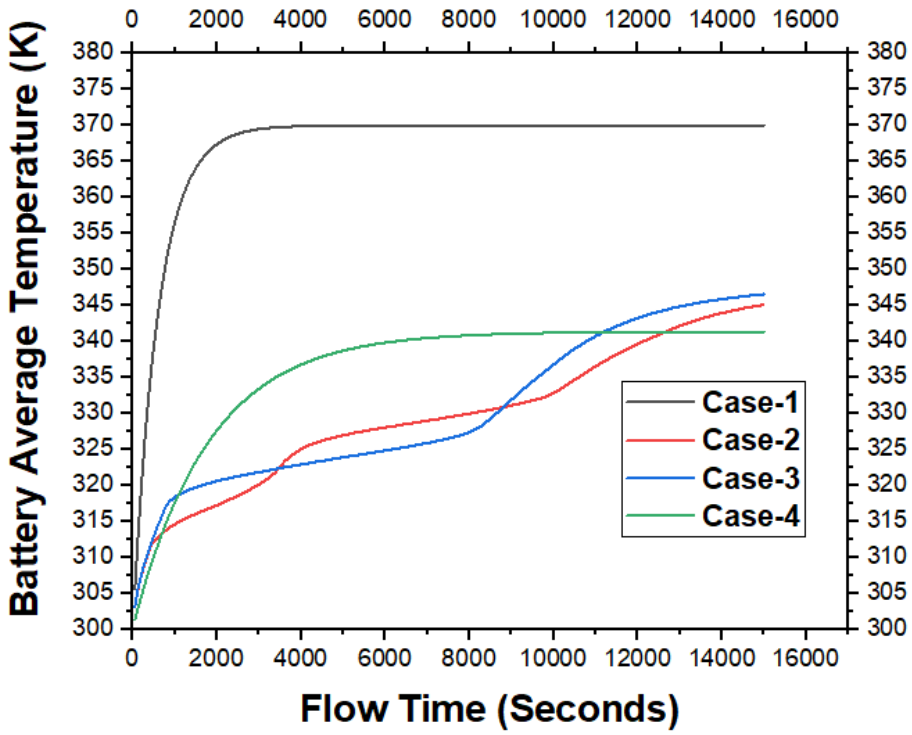

Figure 26: Comparison of Battery Average Temperature between **Case-1**, **Case-2**, **Case-3** and **Case-4**

To make more efficient battery cooling we will go for fin-coupled pcm cooling in next cases.

4.5 Double Layered PCM Cooling with symmetrical fins embedded (Inner Layer Paraffin [RT42] and outer Layer Lauric Acid)

In our next study **case-5** we chose double layer of different PCMs just like **case-2**, paraffin [RT-42] (PCM-1) is adjacent to battery outside wall and lauric acid is outer most pcm (PCM-2). But in this case fins of multiple number are inserted through the PCMs up to battery outer wall **(Fig. 10)**. Besides that, all the conditions are same as of **case-2**. **Figure 27** shows the variation of temperature of battery with respect to time.

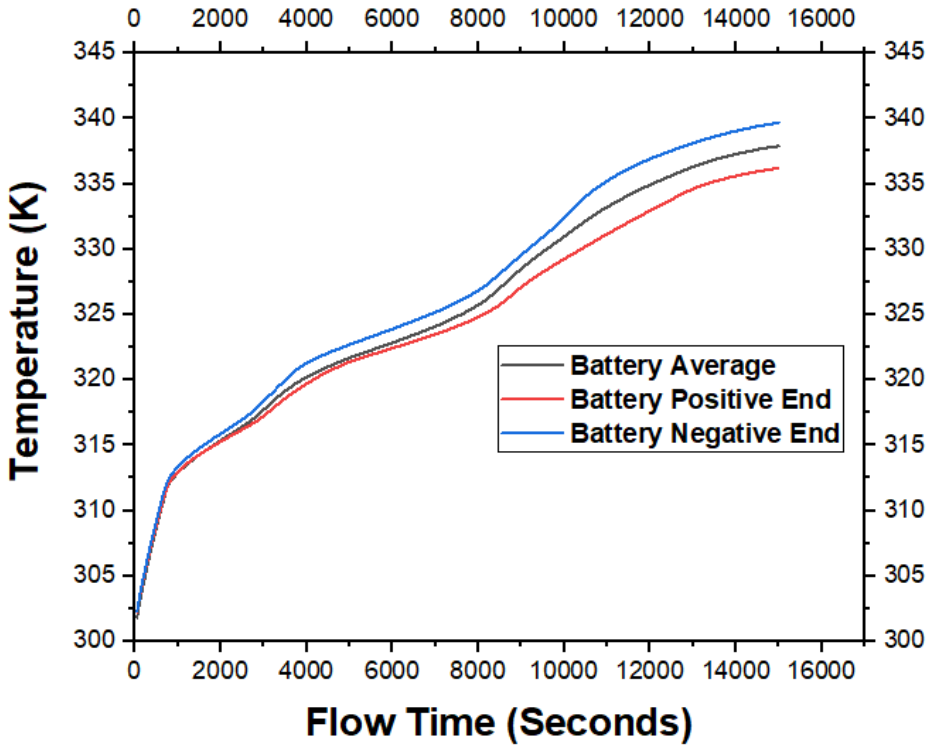

Figure 27: Temperature vs Flow Time

If we focus on both PCMs temp and liquid fraction during analysis in **case-5** with flow time that will depict in **Fig. 28** and **Fig. 29** respectively**.**

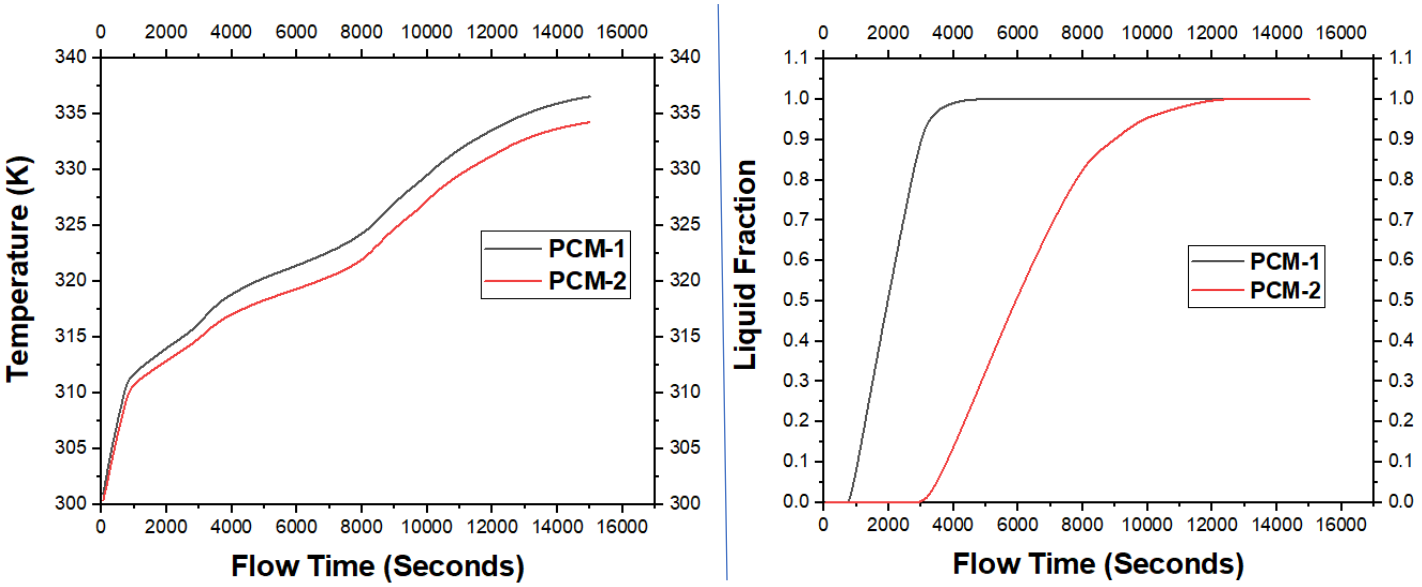

Comparison of Temperature (**Figure 28**) and Liquid Fraction (**Figure 29**) between PCM-1 and PCM-2

4.6 Double Layered PCM Cooling with symmetrical fins embedded (Inner Layer Lauric Acid and outer Layer Paraffin [RT42])

In our subsequent investigation, **case-6**, we chose a double layer of various PCMs, similar to **case-3**, with lauric acid close to the battery's outer wall and paraffin [RT-42] as the outermost PCM (PCM-2). However, in this instance, multiple-number fins are inserted through the PCMs and all the way up to the battery's exterior wall (**Fig. 11**). In addition, every circumstance is the same as in example 3. The battery's temperature variation with regard to time is depicted in **Fig. 30**.

If we pay attention to both the temperature of the PCMs and the liquid fraction when performing the analysis for **case-6** with flow time, the results will be depicted in **Fig. 31** and **Fig. 32** accordingly.

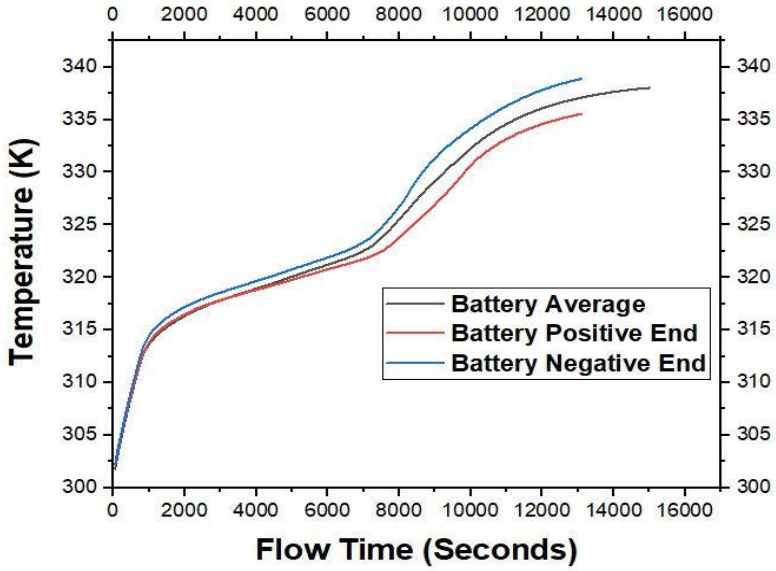

Figure 30: Temperature vs Flow Time

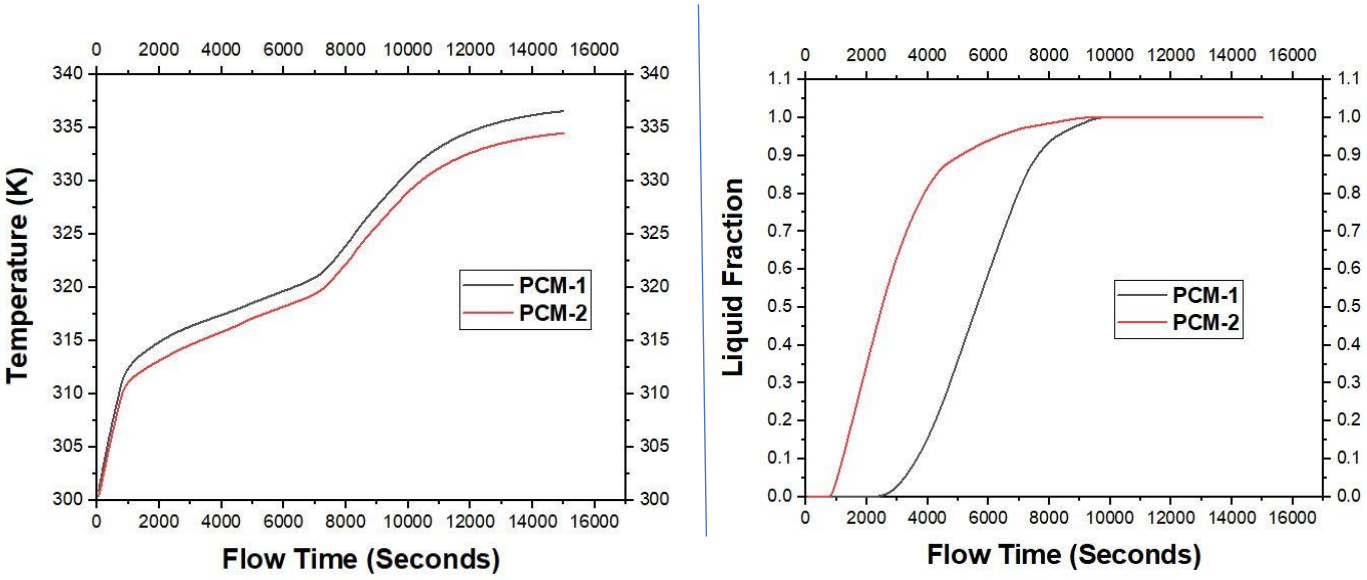

Comparison of Temperature (**Fig. 31**) and Liquid Fraction (**Fig. 32**) between PCM-1 and PCM-2

After **case-6**, we conduct a thorough analysis and contrast the battery cooling effects of **cases-5** and **case-6**. In the end, we determine that **case-6** is more effective than **case-5**. In **Fig. 33**, **case-5's** temperature is slightly lower than **case-6's** early on. At this stage, **case-6**'s outcome is successful. If we closely examine the end point, we find

that the temperatures in both scenarios are identical. We may conclude from a comparison of the two graphs that **case-6** is slightly more efficient because of the overall cooling impact and temperature variation.

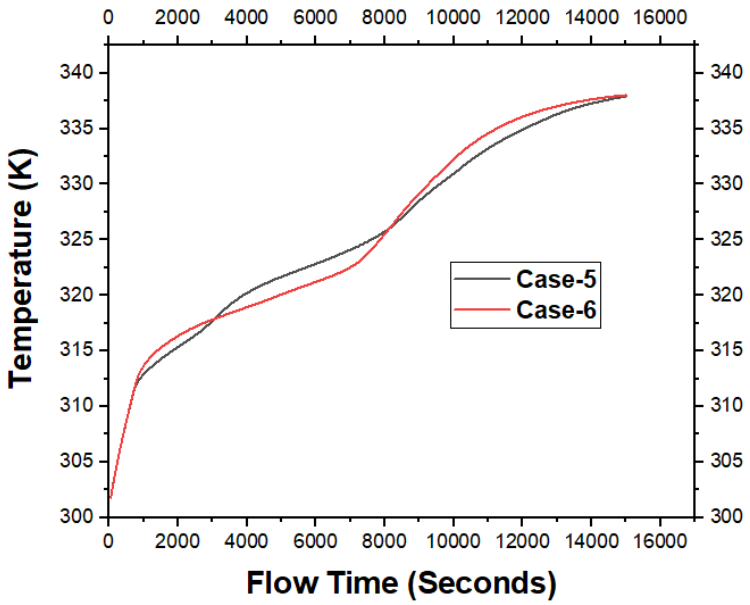

Figure 33: Comparison of Battery Temperature between **Case-5** and **Case-6**

The following cases are examined while using paraffin [RT-42] as the outer layer PCM and lauric acid as the inner layer PCM

4.7 Double Layered PCM Cooling of asymmetrical geometry with fins embedded (Inner Layer Lauric Acid and outer Layer Paraffin [RT42])

In the investigation that came after, **case 7**, we decided to use a double layer of different PCMs, identical to **case 6,** with lauric acid adjacent to the battery's outer wall and paraffin [RT-42] as the outermost PCM (PCM-2), with fins embedded with in PCMs touching the battery exterior wall. However, this case's geometry is asymmetric compared to other situations (**Fig. 12**). **Figure 34** shows the temperature changes of the battery throughout time.

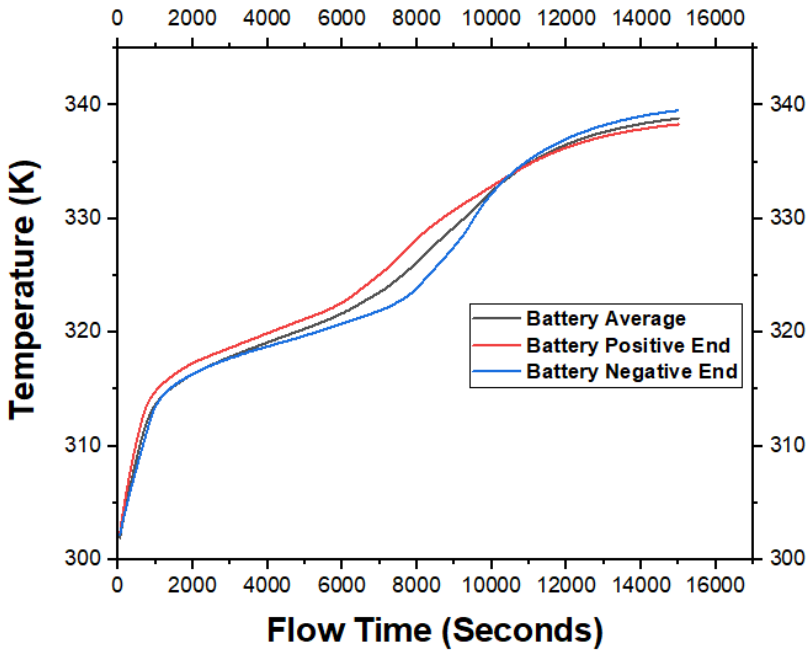

Figure 34: Temperature vs Flow Time

If we focus on both PCMs temp during analysis in **case-2** with flow time that will depict in **Fig. 35** and **Fig. 36.**

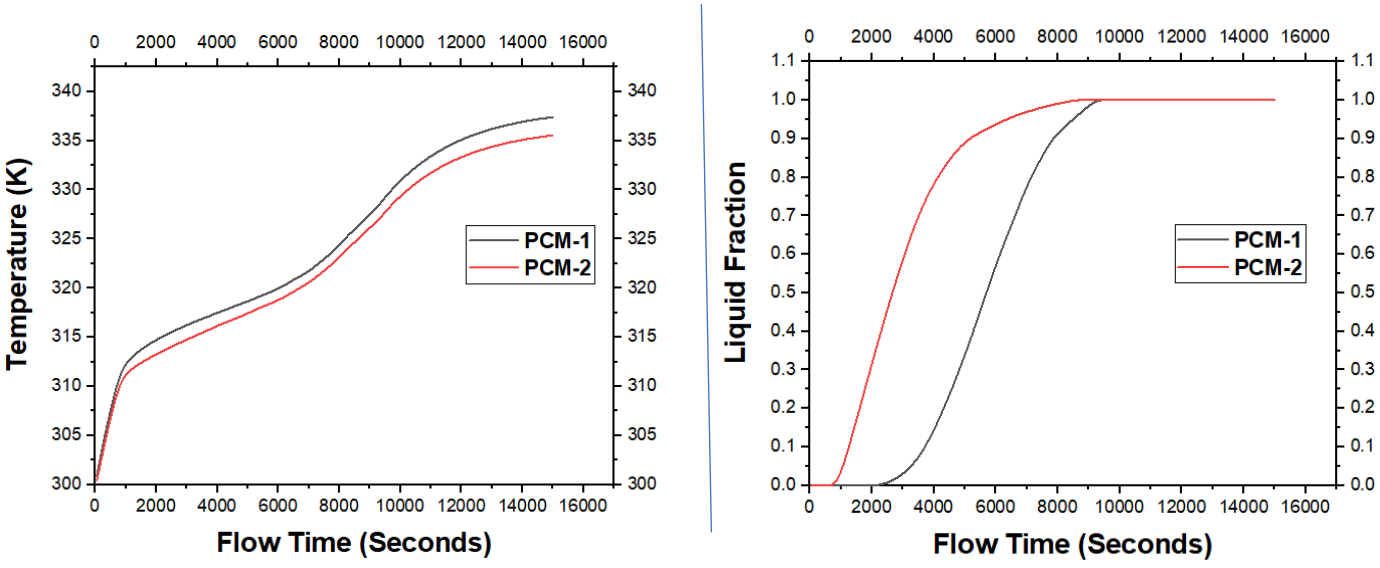

Comparison of Temperature (**Figure 35**) and Liquid Fraction (**Figure 36**) between PCM-1 and PCM-2

4.8 Double Layered PCM Cooling with symmetrical of multiple fins embedded (Inner Layer Lauric Acid and outer Layer Paraffin [RT42])

In our final test (**Case-8**), for getting comparatively good result from other cases we insert multiple number of fins (by splitting each fin into two, maintaining same volume and weight and having equal gap between them) in to a double layer of various PCMs, similar to **case-6**, with lauric acid close to the battery's outer wall and paraffin [RT-42] as the outermost PCM (PCM-2) **(Fig. 13)**. In addition, every circumstance is the same as in **case-6**. The battery's temperature variation with regard to time is depicted in **Fig. 37.**

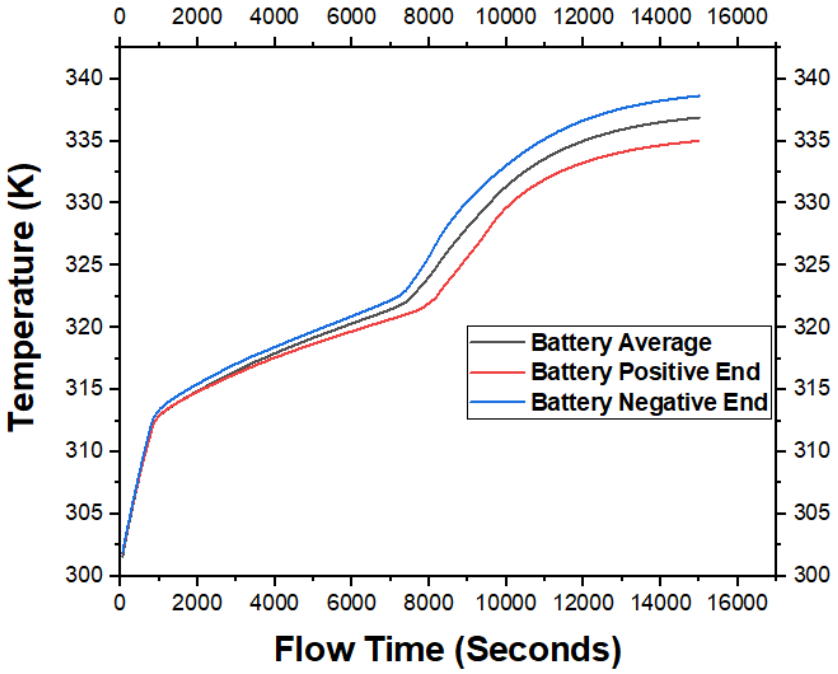

Figure 37: Temperature vs Flow Time

If we pay attention to both the temperature of the PCMs and the liquid fraction when performing the analysis for **case-6** with flow time, the results will be depicted in **Fig. 38** and **Fig. 39** respectively.

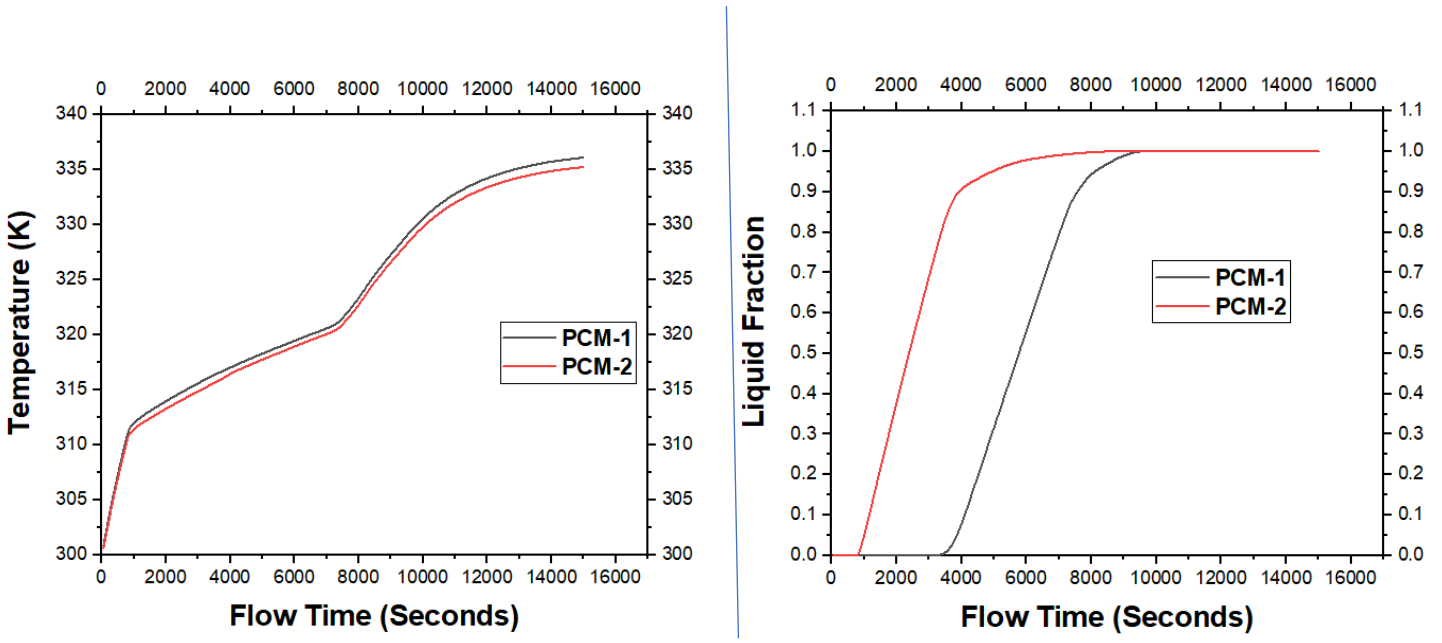

Comparison of Temperature (**Figure 38**) and Liquid Fraction (**Figure 39**) between PCM-1 and PCM-2

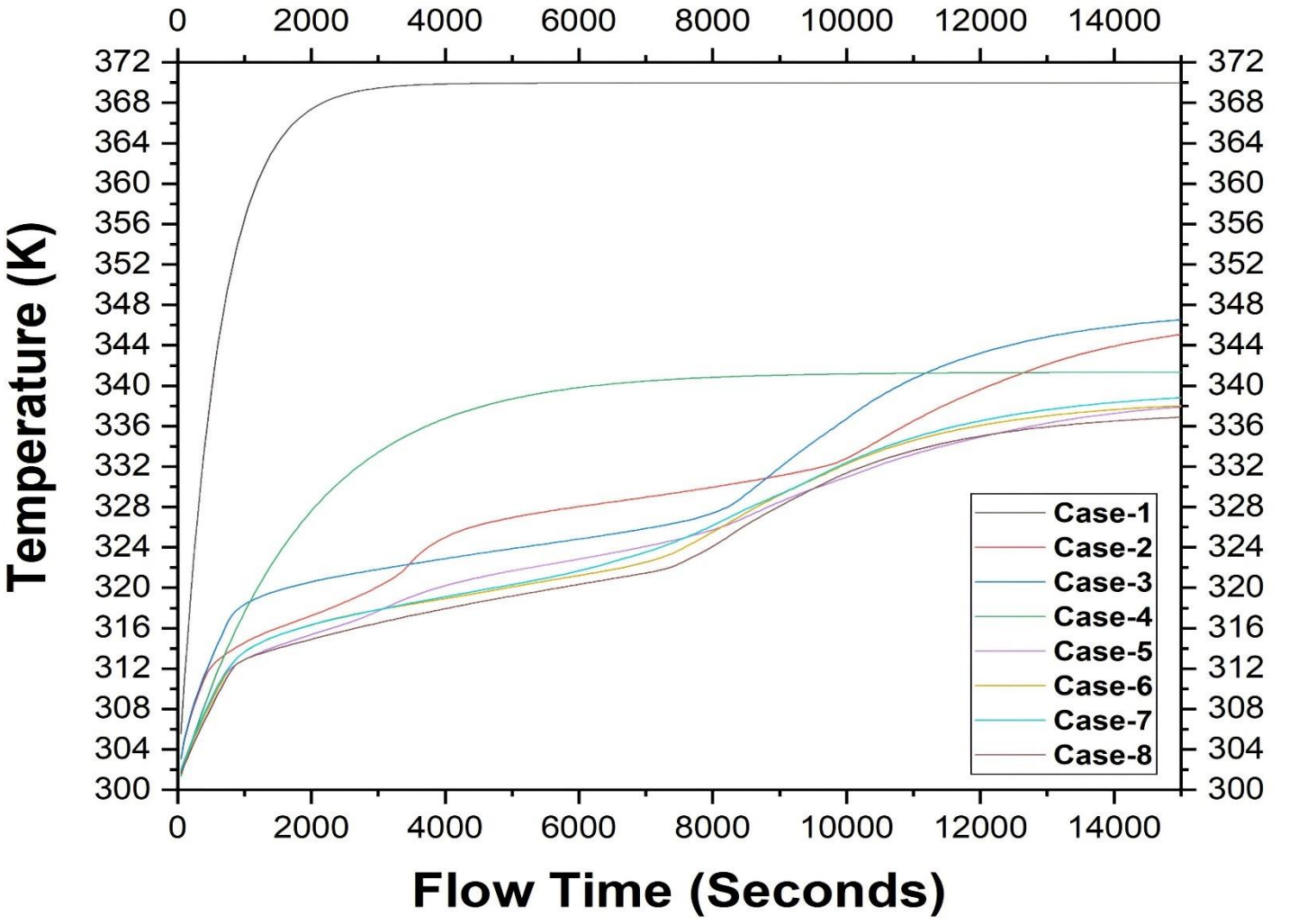

Figure 40: Comparison of Battery Average Temperature between All Cases

After completing final test, we have compared the average temperature of all cases. **Figure 40** depicts the accumulated result of all cases in to single diagram.

If we go for detailed analysis, the results and discussions are enlisted below. **(Fig. 41)**

1. Battery without any fin and PCM (**Case-1**) has highest temperature at the end, as also in over-all temperature.

2. Double layer of PCMs with a greater number of fins **(Case-8)** is providing best battery cooling effect and end temperature is also less compared to others.

3. Battery, covered with only fin **(Case-4)** is proving good cooling effect than battery, covered by only double layered of PCMs **(Case-2 & Case-3)**, at end point (15000 seconds) of test. But if we go for overall cooling effect, then PCM is providing good result, as fin-covered battery temperature rise upward slope is very much high compare to PCMs.

4. Each PCM has their own advantages and disadvantages during used as double layer. Paraffin is providing good result at early stage and end stage compared to lauric acid **(Case-2 | Case-3, Case-5 | Case-6)**. But at end point both alternating double-layered are providing almost same result. But, if we go for over-all (average) battery cooling effect, inner layer of lauric acid is providing comparatively good result than paraffin [RT-42].

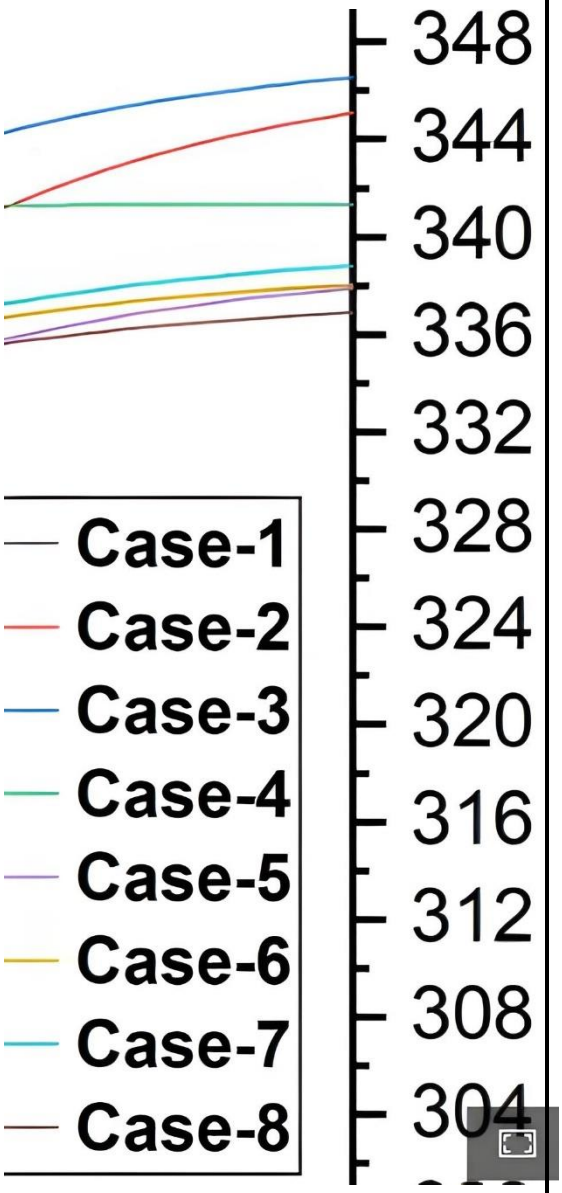

Figure 41: Temperature comparison of all cases (Zoomed)

5. Fins embedded double layered symmetric model **(Case-5 or Case-6)** is providing good result than not only double layered without fin symmetric model **(Case-2 or Case-3)** but also fin embedded double layer asymmetric model **(Case-7).**

4. Conclusion

Through the utilization of PCM and fin cooling, this study explores the dynamic behavior of the temperature of Lithium-ion batteries. A number of different numerical simulations have been carried out in double-layered PCM with and without fins in order to investigate the potential effects of PCM thickness, fin size, and fin number at a certain current rate. In order to achieve better PCM cooling, a complete understanding of those factors is required.

As a consequence of this, the culmination of this body of work can be summarized as follows:

1) The thermal management system that made use of a double layering of distinct PCMs cooling shown a quality performance in the process of bringing the temperature of the lithium-ion battery within a safe operating range at a higher current rate.
2) The thermal management of the battery will be dependent not only on the properties of the PCMs that are being used as double layers, but also on the orientation of those PCMs when various PCMs are being used as double layers. It is rather understable to predict the efficient thermal management from the orientation of PCMs in a double layer due to the fact that PCMs have varying heat capacities, thermal conductivities, and temperatures at which they transition from solid to liquid. In the course of our research, we have utilized two PCMs with distinct characteristics, namely lauric acid and paraffin (RT-42), to create a double layered that surrounds the battery. When compared to paraffin, the heat capacity, melting heat, and solidus-liquidus temperature of lauric acid are slightly higher. In the process of thermal management for double-layered PCMs, whenever lauric acid has been employed as an adjacent layer of the battery outer wall, it has been shown to compress the slope of the temperature curve at every portion more than paraffin has when used as an adjacent layer of the battery.

3) To better control the temperature of the battery over an extended period of time, a layer of fin that is the same thickness as a double layer of PCMs can sometimes be more effective than a double layer of PCMs.
4) When fins and PCMs are used together to reduce the temperature, heat dissipation is enhanced to a greater degree than it would be otherwise. There are three different ways that heat can be transferred through the fins when they are put into the double-layered PCMs that extend up to the battery's outside wall. One method is solid-solid conduction heat transfer, which occurs between the battery and the fin; the other two methods are solid-liquid convection heat transfer, which occur between the fin and PCM1 and PCM2, respectively.
5) The thickness of the PCMs and the fins is one of the most important factors in determining the cooling effect of the battery. It is not always the case that increasing the thickness of the PCMs and covering the relatively greater heat area (near the adiabatic area of the battery) with fins will result in a favourable cooling effect when considering the total thermal management.
6) The number of inserted fins and their position within double-layered PCMs have a significant impact on how quickly the temperature of the battery stabilizes. In the final scenario of our study, we have taken the same volume of fin, but we have split it up into several numbers that have been embedded into double-layered PCMs. These multiple numbers all have the same spacing between them. In comparison to the other tests, our cooling performance is the best.
7) Before concluding, it is important to point out that the scope of this research is limited to the thermal management system of a single lithium-ion battery and the thermal performance of that system employing PCM and fin structure. However, in a battery pack that is comprised of numerous cells, the cells that are located within the interior of the battery pack suffer a great deal due to the mutual heating of the other cells in comparison to the cells that are located on the exterior of the battery pack. In this way, the heat dissipation capability of the battery pack may be tested by inserting a double-layered PCMs structure that is embedded with fin into a high-heat affected zone.

Better temperature optimization is achieved by increasing the number of fins on the heat sink. Our research might be expanded to investigate the optimal number of multiple fins, as well as their shape, size, and thickness, with the purpose of achieving the best possible thermal management. Within double-layered PCMs, we are able to observe the effect of fin location. We also have the option of extending the study to include numerous batteries so that we may monitor the impacts of heat transfer and cooling as it occurs from one battery to another within a battery pack.

It is possible to draw the conclusion that the thermal management system in electric vehicles and hybrid vehicles that makes use of PCM material and applies the fin structure can be very effective in managing the temperature of Li-ion batteries. The optimal selection of the several PCMs, fins, and geometry discussed above is, However, necessary in order to obtain the highest possible performance.

References

[1] Hatchard, T.D., MacNeil, D.D., Basu, A. and Dahn, J.R., 2001. Thermal model of cylindrical and prismatic lithium-ion cells. *Journal of The Electrochemical Society*, *148*(7), p.A755.

[2] Kim, G.H., Pesaran, A. and Spotnitz, R., 2007. A three-dimensional thermal abuse model for lithium-ion cells. *Journal of power sources*, *170*(2), pp.476-489.

[3] Coman, P.T., Mátéfi-Tempfli, S., Veje, C.T. and White, R.E., 2017. Modelling vaporization, gas generation and venting in Li-ion battery cells with a dimethyl carbonate electrolyte. *Journal of The Electrochemical Society*, *164*(9), p.A1858.

[4] Panchal, S., Mathew, M., Fraser, R. and Fowler, M., 2018. Electrochemical thermal modelling and experimental measurements of 18650 cylindrical lithium-ion battery during discharge cycle for an EV. *Applied Thermal Engineering*, *135*, pp.123-132.

[5] Coman, P.T., Darcy, E.C., Veje, C.T. and White, R.E., 2017. Modelling Li-ion cell thermal runaway triggered by an internal short circuit device using an efficiency factor and Arrhenius formulations. *Journal of The Electrochemical Society*, *164*(4), p.A587.

[6] Lopez, C.F., Jeevarajan, J.A. and Mukherjee, P.P., 2015. Experimental analysis of thermal runaway and propagation in lithium-ion battery modules. *Journal of the electrochemical society*, *162*(9), p.A1905.

[7] Cai, T., Stefanopoulou, A.G. and Siegel, J.B., 2019. Early detection for li-ion batteries thermal runaway based on gas sensing. *ECS Transactions*, *89*(1), p.85.

[8] Feng, X., Ouyang, M., Liu, X., Lu, L., Xia, Y. and He, X., 2018. Thermal runaway mechanism of lithium ion battery for electric vehicles: A review. *Energy Storage Materials*, *10*, pp.246-267.

[9] Wang, Q., Ping, P., Zhao, X., Chu, G., Sun, J. and Chen, C., 2012. Thermal runaway caused fire and explosion of lithium ion battery. *Journal of power sources*, *208*, pp.210-224.

[10] Pesaran, A.A., 2001. Battery thermal management in EV and HEVs: issues and solutions. *Battery Man*, *43*(5), pp.34-49.

[11] Mali, V., Saxena, R., Kumar, K., Kalam, A. and Tripathi, B., 2021. Review on battery thermal management systems for energy-efficient electric vehicles. *Renewable and Sustainable Energy Reviews*, *151*, p.111611.

[12] Park, H., 2013. A design of air flow configuration for cooling lithium ion battery in hybrid electric vehicles. *Journal of power sources*, *239*, pp.30-36.

[13] Cho, G.Y., Choi, J.W., Park, J.H. and Cha, S.W., 2014. Transient modelling and validation of lithium ion battery pack with air cooled thermal management system for electric vehicles. *International journal of automotive technology*, *15*(5), pp.795-803.

[14] Lu, Z., Meng, X.Z., Wei, L.C., Hu, W.Y., Zhang, L.Y. and Jin, L.W., 2016. Thermal management of densely-packed EV battery with forced air cooling strategies. *Energy Procedia*, *88*, pp.682-688.

[15] Chen, K., Wang, S., Song, M. and Chen, L., 2017. Configuration optimization of battery pack in parallel air-cooled battery thermal management system using an optimization strategy. *Applied Thermal Engineering*, *123*, pp.177-186.

[16] Xie, J., Ge, Z., Zang, M. and Wang, S., 2017. Structural optimization of lithium-ion battery pack with forced air cooling system. *Applied Thermal Engineering*, *126*, pp.583-593.

[17] Tong, W., Somasundaram, K., Birgersson, E., Mujumdar, A.S. and Yap, C., 2015. Numerical investigation of water cooling for a lithium-ion bipolar battery pack. *International Journal of Thermal Sciences*, *94*, pp.259-269.

[18] Qian, Z., Li, Y. and Rao, Z., 2016. Thermal performance of lithium-ion battery thermal management system by using mini-channel cooling. *Energy Conversion and Management*, *126*, pp.622-631.

[19] Li, K., Yan, J., Chen, H. and Wang, Q., 2018. Water cooling based strategy for lithium ion battery pack dynamic cycling for thermal management system. *Applied Thermal Engineering*, *132*, pp.575-585.

[20] Chen, S., Peng, X., Bao, N. and Garg, A., 2019. A comprehensive analysis and optimization process for an integrated liquid cooling plate for a prismatic lithium-ion battery module. *Applied Thermal Engineering*, *156*, pp.324-339.

[21] Liu, C., Xu, D., Weng, J., Zhou, S., Li, W., Wan, Y., Jiang, S., Zhou, D., Wang, J. and Huang, Q., 2020. Phase change materials application in battery thermal management system: a review. *Materials*, *13*(20), p.4622.

[22] Al Hallaj, S. and Selman, J.R., 2000. A novel thermal management system for electric vehicle batteries using phase-change material. *Journal of the Electrochemical Society*, *147*(9), p.3231.

[23] Khateeb, S.A., Farid, M.M., Selman, J.R. and Al-Hallaj, S., 2004. Design and simulation of a lithium-ion battery with a phase change material thermal management system for an electric scooter. *Journal of Power Sources*, *128*(2), pp.292-307.

[24] Kizilel, R., Lateef, A., Sabbah, R., Farid, M.M., Selman, J.R. and Al-Hallaj, S., 2008. Passive control of temperature excursion and uniformity in high-energy Li-ion battery packs at high current and ambient temperature. *Journal of Power Sources*, *183*(1), pp.370-375.

[25] Rao, Z., Wang, S. and Zhang, G., 2011. Simulation and experiment of thermal energy management with phase change material for ageing LiFePO4 power battery. *Energy Conversion and Management*, *52*(12), pp.3408-3414.

[26] Javani, N., Dincer, I., Naterer, G.F. and Yilbas, B.S., 2014. Heat transfer and thermal management with PCMs in a Li-ion battery cell for electric vehicles. *International Journal of Heat and Mass Transfer*, *72*, pp.690-703.

[27] Goli, P., Legedza, S., Dhar, A., Salgado, R., Renteria, J. and Balandin, A.A., 2014. Graphene-enhanced hybrid phase change materials for thermal management of Li-ion batteries. *Journal of Power Sources*, *248*, pp.37-43.

[28] Greco, A., Jiang, X. and Cao, D., 2015. An investigation of lithium-ion battery thermal management using paraffin/porous-graphite-matrix composite. *Journal of Power Sources*, *278*, pp.50-68.

[29] Bais, A.R., Subhedar, D.G. and Panchal, S., 2022. Critical thickness of nano-enhanced RT-42 paraffin based battery thermal management system for electric vehicles: a numerical study. *Journal of Energy Storage*, *52*, p.104757.

[30] Lebrouhi, B.E., Lamrani, B., Ouassaid, M., Abd-Lefdil, M., Maaroufi, M. and Kousksou, T., 2022. Low-cost numerical lumped modelling of lithium-ion battery pack with phase change material and liquid cooling thermal management system. *Journal of Energy Storage*, *54*, p.105293.

[31] Lee, S., Han, U. and Lee, H., 2022. Development of a hybrid battery thermal management system coupled with phase change material under fast charging conditions. *Energy Conversion and Management*, *268*, p.116015.

[32] Murali, G., Sravya, G.S.N., Jaya, J. and Vamsi, V.N., 2021. A review on hybrid thermal management of battery packs and it's cooling performance by enhanced PCM. *Renewable and Sustainable Energy Reviews*, *150*, p.111513.

[33] Weng, J., Yang, X., Zhang, G., Ouyang, D., Chen, M. and Wang, J., 2019. Optimization of the detailed factors in a phase-change-material module for battery thermal management. *International Journal of Heat and Mass Transfer*, *138*, pp.126-134.

[34] Rao, Z., Wang, S., Wu, M., Lin, Z. and Li, F., 2013. Experimental investigation on thermal management of electric vehicle battery with heat pipe. *Energy Conversion and Management*, *65*, pp.92-97.

[35] Li, Y., Qi, F., Guo, H., Guo, Z., Xu, G. and Liu, J., 2019. Numerical investigation of thermal runaway propagation in a Li-ion battery module using the heat pipe cooling system. *Numerical Heat Transfer, Part A: Applications*, *75*(3), pp.183-199.

[36] Qin, J., Zhao, S., Liu, X. and Liu, Y., 2020. Simulation study on thermal runaway suppression of 18650 lithium battery. *Energy Sources, Part A: Recovery, Utilization, and Environmental Effects*, pp.1-13.

[37] Liu, T., Liu, Y., Wang, X., Kong, X. and Li, G., 2019. Cooling control of thermally-induced thermal runaway in 18,650 lithium ion battery with water mist. *Energy Conversion and Management*, *199*, p.111969.

[38] Mei, J., Shi, G., Liu, H., Wang, Z. and Chen, M., 2022. Investigation on the optimization strategy of phase change material thermal management system for lithium-ion battery. *Journal of Energy Storage*, *55*, p.105365.

[39] Sun, Z., Fan, R., Yan, F., Zhou, T. and Zheng, N., 2019. Thermal management of the lithium-ion battery by the composite PCM-Fin structures. *International Journal of Heat and Mass Transfer*, *145*, p.118739.

[40] Choudhari, V.G., Dhoble, A.S. and Panchal, S., 2020. Numerical analysis of different fin structures in phase change material module for battery thermal management system and its optimization. *International Journal of Heat and Mass Transfer*, *163*, p.120434.

[41] Akula, R. and Balaji, C., 2022. Thermal management of 18650 Li-ion battery using novel fins–PCM–EG composite heat sinks. *Applied Energy*, *316*, p.119048.

[42] Liu, H., Jin, C., Li, H. and Ji, Y., 2023. A numerical study of PCM battery thermal management performance enhancement with fin structures. *Energy Reports*, *9*, pp.1793-1802.

[43] Gajji Naresh, Kakarla Vidya Sagar, Lankala Sethuram Reddy, Eluri Nikhil Reddy, Nalamalapu Subba Reddy, Minesh Vohra. Battery thermal Management system using fin in PCM.

[44] Fadl, M. and Eames, P.C., 2019. Numerical investigation of the influence of mushy zone parameter A_{mush} on heat transfer characteristics in vertically and horizontally oriented thermal energy storage systems. *Applied Thermal Engineering*, *151*, pp.90-99.

[45] S.V. Patankar, Numerical Heat Transfer and Fluid Flow, Hemisphere, Washington DC, 1980.

[46] Brent, A.D., Voller, V.R. and Reid, K.T.J., 1988. Enthalpy-porosity technique for modelling convection-diffusion phase change: application to the melting of a pure metal. *Numerical Heat Transfer, Part A Applications*, *13*(3), pp.297-318.

[47] Vogel, J.J.F.M.J., Felbinger, J. and Johnson, M., 2016. Natural convection in high temperature flat plate latent heat thermal energy storage systems. *Applied Energy*, *184*, pp.184-196.

[48] M. Keyser, E. Darcy, D. Long, and A. Pesaran, Pat. No. US9142829 B2 (2015).

[49] Kamkari, B., Shokouhmand, H. and Bruno, F., 2014. Experimental investigation of the effect of inclination angle on convection-driven melting of phase change material in a rectangular enclosure. *International Journal of Heat and Mass Transfer*, *72*, pp.186-200.